UNIVERSITÉ de Liège

Département MSM
1, chemin des Chevreuils
B 4000 Liège
Belgium

Anne.Habraken@ulg.ac.be

CONTRIBUTIONS TO CONSTITUTIVE LAWS OF METALS: MICRO-MACRO AND DAMAGE MODELS

Parts A and B

Thèse présentée en vue de l'obtention du grade d'Agrégé de l'Enseignement Supérieur
par Anne-Marie HABRAKEN

Année académique 2000-2001

Membres du comité de Lecture

Université de Liège

Mme LECOMTE Jacqueline,
M. CESCOTTO Serge,
M. COHEUR Jean-Pierre,
M. FONDER Ghislain,
M. HOGGE Michel.

Membres extérieurs

Professeur Paul VAN HOUTTE
Departement Metaalkunde en Toegepaste Materiaalkunde
Katholieke Universiteit Leuven

Professeur Jean-Claude GELIN
Université de Franche Comté
Laboratoire de Mécanique Appliquée

Professeur Eric VAN DER GIESSEN
University of Groningen
Dept. of Applied Physics

A Jean-Luc, pour que chaque étape contribue à te renforcer face au caillou suivant et te laisse découvrir un fleuve tranquille.

To Jean Luc - that each step contribute to reinforcing you for the next stone you encounter, letting you discover a tranquil river.

A Tanguy, pour que tu trouves l'équilibre entre l'intelligence et la sensibilité qui t'habitent.

To Tanguy - that you find the balance between the intelligence and the sensitivity you possess.

A Maëlle, pour que tu exploites avec bonheur ta faculté d'adaptation, l'harmonie entre ton corps et ton esprit.

To Maëlle - that you successfully exploit your ability to adapt, the harmony between your body and mind.

A Yann, pour que ta joie de vivre continue à éclabousser ton entourage et te rende heureux.

To Yann - that your joy for life may always dazzle your entourage and bring you happiness.

A Aude, tu nous es arrivée avec beaucoup de racines, puissions nous t'aider à découvrir tes ailes.

To Aude - you came to us with many roots; with hopes that we can help you discover your wings.

Foreword

This thesis is the culmination of nearly four years of work, which began during a stay in Clermont-Ferrand in August 1997. It was interrupted many times and often delayed because of technical contingencies; among these, the departure and arrivals of team researchers, work on urgent contracts to be completed, personal matters, i.e., pregnancy, childcare and other family problems, including an untimely death. On a positive note, these delays enabled me to take some distance with regard to the subject matter.

Acknowledgements

I would like to thank all those who helped me to pursue my work in the face of professional and other difficulties.

I am grateful to my husband for his patience, his encouragement and time spent with the children, which allowed me to finish this work. If the children are right, their mother will have a bit more time and be calmer, now that the thesis is finished...

I also express my heartfelt thanks to:

- Professor Serge Cescotto, for his theoretical as well as moral assistance in the daily management of the team, for his friendship and for so often lending a needed ear;

- Ghislain Fonder, for his practical assistance in dealing with administrative tasks and his personal warmth;

- Philippe Boeraeve, Etienne Rondia, Michel Bechoux and Michel Basteyns, for their patience and efficiency in meeting my requests for experiments out of the usual context;

- the doctoral students and researchers who have contributed to my work; their scientific participation is defined more precisely in part A, but I acknowledge here the numerous chores that they carried out, which enabled me to concentrate on my thesis;

- Colette Verbist and Virginie Bertrand, for their help in the manuscript layout and corrections of the initial text;

- Gérard Franquet, for his precious assistance with a very large number of figures;

- Emile Lemaire for his good humor and ability to solve numerous computer related problems and Pierre Villers for his efficient help in managing the graphic post processors and the web;

- the members of the thesis committee who accepted to read this voluminous manuscript.

I also wish to thank the *Fonds National de la Recherche Scientifique* which has allowed me to pursue a professional career in research. Finally, I thank the academic authorities of the University of Liege for providing a pleasant work framework and a pluralistic environment that is as open as possible.

PART A

INTRODUCTION

Thèse présentée en vue de l'obtention du grade d'Agrégé de l'Enseignement Supérieur
par Anne Marie HABRAKEN

Année académique 2000-2001

CONTENTS

1. Objectives and thesis contents 1
   1.1. The general context of the thesis 1
   1.2. The historical context and the contents of the thesis 1

2. Scientific work 3
   2.1. Remeshing technique 3
   2.2. Phase transformation 5
   2.3. Contact modeling 5
   2.4. Continuous casting model 7
   2.5. Texture and plasticity models 8
   2.6. Damage models 10
   2.7. Forging models 11
   2.8. Recrystallization model 13

3. Activities as research associate 13

1. OBJECTIVES AND THESIS CONTENTS

1.1. The general context of the thesis

The researcher status differs depending on country, employer and time as new regulations and new requirements frequently appear to adjust to the society evolution.

In Belgium, the National Fund for Scientific Research (FNRS) offers jobs in scientific research. A Ph.D. thesis is required from candidates for the first permanent position, Research Associate. To access the next steps in the career, Senior Research Associate and Research Director, an "Aggregation in Higher Education" is necessary. This degree requires :

- a main thesis accompanied by three additional contributions;
- an oral presentation of this thesis in front of one's entire faculty and several foreign scientists;
- a public lecture on an imposed topic.

The format of the thesis was described in 1931 and has become quite obsolete. The most widely accepted interpretation is based on the probable subsequent career as Research Director and, eventually, University Professor. Contrarily to the Ph.D. Thesis which must demonstrate the ability to do research at the personal level, the Aggregation thesis must demonstrate the ability to conduct research, to take a broad view of a research subject and to diffuse one's experience in research; originality is, of course, not to be neglected.

1.2. The historical context and the contents of the thesis

My thesis is divided into four parts.

The first (part A), which is very short summarizes my work since March 1987, when I obtained my own Ph.D. Since that time, two Ph.D. theses have been completed under a shared supervision of professor Cescotto and myself. Four others Ph.D. theses are in progress. These four Ph.D students have already achieved their master theses. I have taken an active part in three additional theses and directed numerous final projects and research contracts leading to progress reports, final reports and publications. All the developments have been introduced in the Finite Element code LAGAMINE, set up in the MSM Department to simulate the forming of metals. More information about the work of my team can be found in section 2 of Part A. In fact, a collection of papers resulting from these researches could have been presented as the Aggregation thesis.

Part B of the thesis is devoted to micro-macro approaches. It is an extensive state-of-the art on the subject, presented in a unified way.

Part C is devoted to damage modeling. It also begins as a state of the art review but it is progressively focused towards the models that I have developed with my team.

As shown in section 2 of Part A, damage models and micro-macro approaches represent an important part of my contribution to the modeling of metal behavior modeling. Since Yongyi Zhu and Professor Cescotto had already developed the problematic of damage in the MSM Department, I have exploited and extended their work. I also had the opportunity to introduce micro-macro approaches in LAGAMINE thanks to a European project and a research project supported by the Région Wallonne. The development of this topic in the MSM Department results from my personal involvement.

As explained in the introductions of Parts B and C, research on micro-macro and damage approaches has been possible in the frame of different projects and thanks to the work of many different research engineers that I have supervised to the best of my ability. So, summarizing the behavior laws proposed by my team in one consistent text is of interest for researchers using them as code-users, or interested in implementing them into other codes. In order to choose the best orientations for further personal research, it is important to establish an extensive bibliographic review. This finally results in writing third cycle courses that could help future Ph.D. students of my team or other research groups worldwide. This goal was in itself an incitement to write this thesis. From this point of view, Part B is more complete, since I have already taught micro-macro approaches in February 2000 at the Graduate School in Computational and Experimental Mechanics. Part C, written for the most part in 1998 and 1999, already requires some updating.

Part D concerns the future : it concludes and offers perspectives for the continuation of the work.

The three papers joined as annex theses provide information about subjects not covered in the main text but to which I have significantly contributed. The first two present results of research performed with my co-workers using thermal-mechanical-metallurgical models. The last one is an article summarizing my contribution to contact between two bodies.

As much of my energy is devoted to metals at hot temperature, thermal-mechanical-metallurgical studies represent indeed another topic which should have been included in a consistent presentation and an up-dated literature review. When I began this thesis, I was confident that this would be summarized by two of my Ph.D. students. One of them, Jean-François Charles, left before completing a thesis; therefore the recrystallization model implemented in LAGAMINE is described only by articles in conference proceedings and internal reports. However, the developed macroscopic thermo-elasto-visco-plastic law has been extensively described by Frédéric Pascon in his DEA thesis (master's thesis). As the number of engineers having developed this field with me is limited, a coherent presentation seems less crucial than for damage and micro-macro approaches. Note that an Aggregation thesis would never end if one did

not decide to stop at a certain moment ! I am sure that my future work will be full of exciting new topics.

2. SCIENTIFIC WORK

My Ph.D. thesis (Habraken,1989) was entitled "Contribution à la modélisation du formage des métaux par la méthode des éléments finis", which, without surprise, can be translated as "Contribution to metal forming modeling by the Finite Element Method". This broad title was chosen for historical reasons; two very different topics were studied:

- The remeshing technique, adapted to a large displacement and deformation Lagrangian code and applied to simulations of forging processes.
- A thermal-mechanical-metallurgical model predicting phase volume fractions (austenite, cementite, ferrite, pearlite, bainite, martensite), stress, strain and temperature history during the cooling of steel parts. This work has been used by ARBED (Luxemburg steel industry) to study the Quenching-Self-Tempering of hot rolled steel beams.

Of course, since March 1989, I have developed the topics of this thesis but others as well (listed hereafter). These were chosen to fulfill industrial contracts or to develop new long-term research subjects that should help my department to continue its assistance mission for metal industries.

2.1. Remeshing technique

At the end of my Ph.D. thesis, a semi-automatic remeshing technique became available in LAGAMINE. The decision to remesh relies on geometric criteria or error criteria of the Zienkiewicz type. A semi-automatic mesh generator requiring some topological data from the user creates a new mesh. Then the stresses and internal variables are transferred from the old mesh to the new one and, finally, the simulation restarts. This approach is published in:

- An Automatic remeshing technique for finite element simulation of forming processes. Habraken, A.M., Cescotto, S., *Int. J. for Numerical Method. in Engineering*, (Dec. 1990), **30/8**, 1503-1525.

This remeshing technique became fully automatic with the help of Marek Dyduch, a Ph.D. student supervised by Professor Cescotto and myself. Error criteria are developed, based on the comparisons between the stress and strain rate fields directly computed by the code or the superconvergent ones. His research shows that an error criterion based on stresses can be applied to take the remeshing decision and an error criterion based on strain rates helps to define the variable nodal density in the new

mesh. Marek Dyduch adapts the evaluation of superconvergent meshes to get the stresses and internal values in the new mesh. The particular case of anti-hourglass stresses in mixed type elements is also studied. On the basis of these considerations, three research engineers, Zhou Ding Wu, Zhu Yongyi and André Godinas developed an automatic mesh generator starting from the old mesh data and the strain rate error indicator. A description of this work can be found in:

- Adaptive methods in finite element simulation of metal forming processes, Dyduch, M., Thèse de Doctorat en Sciences Appliquées, Université de Liège, (1995-1996).
- Automatic adaptive remeshing for numerical simulations of metalforming, Dyduch, M. Habraken, A.M., Cescotto, S. *Computer methods in applied mechanics and engineering*,**101**, (1992), 283-293.
- Error estimates and indicators for adaptive analysis of bulk forming, Dyduch, M., Cescotto, S., Habraken, A.M., *Computational Plasticity. Fundamentals and Applications*, edited by Owen, D.R.J. and Onate, E. at Pineridge Press, (1995), 1355-1367.
- Efficient Error Estimates for Adaptive Remeshing in 2D Metal Forming Modelling, Dyduch, M., Cescotto, S., Habraken A.M., NUMIFORM 95, *Simulation of Materials Processing: Theory, Methods and Applications*, edited by Shen & Dawson, at BALKEMA, (1995), 419-424.

Joëlle Pierry and Jean-Dominique Barnichon, from Professor Charlier's soil mechanics team, further improved the remeshing modules. This second group in the MSM department also works with the LAGAMINE code and maintains close ties with Professor Cescotto and myself. Jean-Dominique Barnichon implemented a classical method to interpolate the variables in the new mesh. For each new interpolation point, he localizes the old element where it belongs and uses the old element values to perform the interpolation. With the help of André Godinas for the mesh generator, Jean-Dominique Barnichon extended the whole remeshing method to multi-domain bodies. In soil mechanics, the different soil layers require such a tool. This research is summarized in Jean-Dominique Barnichon's thesis:

- Finite element modelling in structural and petroleum geology, Barnichon, J.D., Thèse de Doctorat en Sciences Appliquées, Université de Liège, (1998).

Finally, Sylvie Castagne, one of the research engineers whom I supervise, applied many of the above-described modules to study the surface layer of a rolled zinc sheet. Our goal was to investigate the 50μm surface layer, which shows one peak in texture intensity in industrial zinc sheets; this property can be correlated with the crack resistance of the sheet. A specialized mesh generator is developed and the final strain rate and temperature fields present maximums in the surface layer zone that could explain the experimental observations. These results are published at the 2nd ESAFORM (European Scientific Association in material FORMing) conference.

- Study of the Surface Layer of a Rolled Zinc Sheet, Castagne, S., Habraken, A.M, Wégria, J., 2nd *ESAFORM Conference on Metal Forming*, Guimaraes, Portugal, Covas J.A. Editor, (13-16 April 1999), 77-80.

2.2. Phase transformation

The model developed in my Ph.D. thesis was applied to optimize the Quenching-Self-Tempering process in ARBED (Luxemburg steel industry). Its description is published together with an application performed by ARBED in:

- Coupled thermo-mechanical-metallurgical analysis during the cooling of steel pieces, Habraken, A.M., Bourdouxhe, M., *"European Journal of Mechanics", A/Solids,* **11/3,** (1992), 381-402.

I did not have the opportunity to keep working in this direction until September 2000. However during conferences and as jury member of Ph.D. theses, I followed the developments of FEM models to simulate phase transformations. Thanks to one current project funded by the Région Wallonne, I can again apply my thermal-metallurgical model. As an industrial interest is clearly present, I soon hope to up-date and apply again this thermal-mechanical-metallurgical model.

2.3. Contact modeling

Whatever the forming process, forging, rolling, extrusion or deep drawing, the contact between the tools and the workpiece has to be simulated. During my research, I first had the opportunity to work with Professor Charlier on a two-dimensional contact element between a rigid tool called foundation and a deformable specimen. This research based on the penalty method is described by:

- Numerical modelisation of contact with friction phenomena by the finite element method, Charlier, R., Habraken, A.M., *Computers and Geotechnics*, **9**, (1990) 59-72.

I later extended the contact FEM element to the case of 2 deformable bodies, studying convergence according to the choice of weak or strong coupling between bodies in the stiffness matrix. This work, completed in 1992, was finally published in 1998:

- Contact between deformable solids, the fully coupled approach, Habraken, A.M., Cescotto, S., *Mathematical and Computer Modelling,* **28/4-8**, (1998), 153-169.

The efficiency of the method allows treating quite complex cases as, for instance, the swaging process during the installation of swaged bolts (see Figures 1-1 and 1-2).

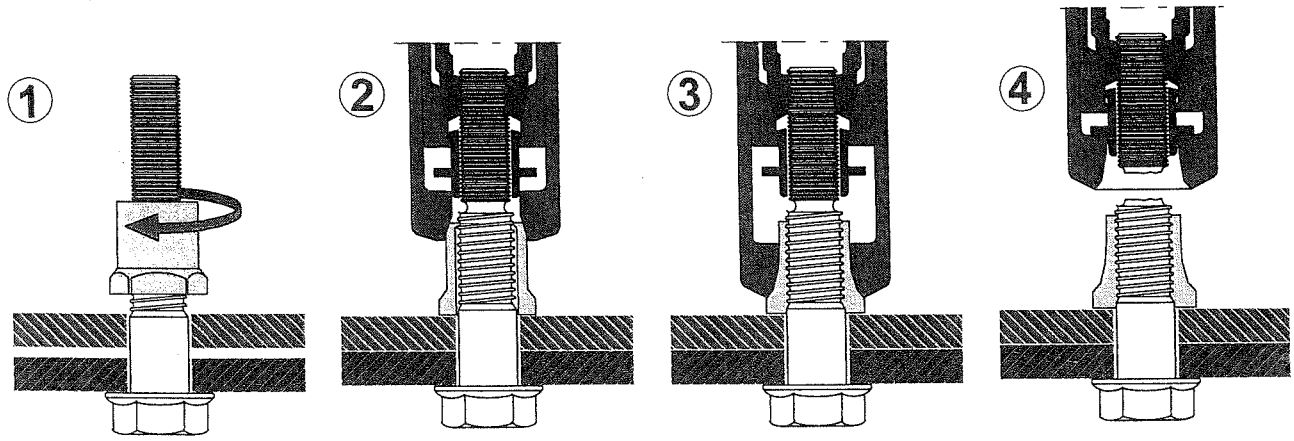

Figure 1-1 Installation of swaged bolts from "Swaged bolts: Modelling of the installation process and numerical analysis of the mechanical behaviour" by M. Dréan, A.-M. Habraken, A. Bouchaïr and J.-P. Muzeau, published in 5th International Conference on COMPUTATIONAL STRUCTURES TECHNOLOGY Leuven, Belgium, 6-8 September 2000

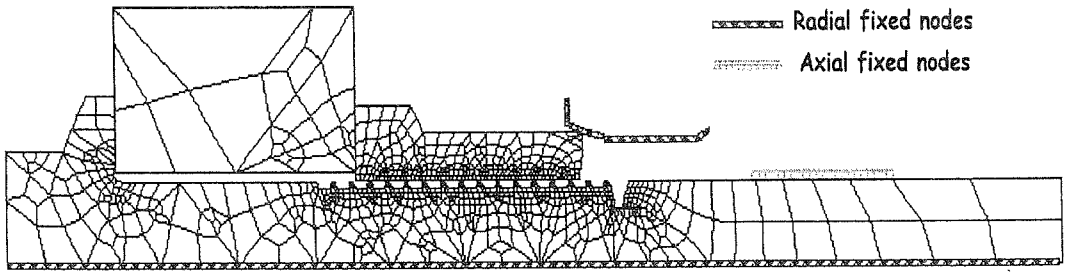

Figure 1-2 Axisymmetrical mesh used to model the second step of swaging process, from Dréan *et al.*, *Construction métallique,* **4**, (1999), 21-34.

Realized in collaboration with Michel Dréan, a Ph.D. student from CUST (Clermont-Ferrand, France), this application was published in a well-known French journal and presented at several conferences.

- Modélisation de la mise en œuvre des boulons sertis précontraints, Dréan, M., Habraken, A.M., Bouchair, A., Muzeau, J.P., *Construction métallique,* **4**, (1999), 21-34.

I have implemented the concept of "pilot nodes" in LAGAMINE. These nodes define the translational and/or rotational degrees of freedom of a rigid tool in contact with a workpiece. This approach is necessary to apply a blank holder force during a deep

drawing simulation. I have adapted this Pilot Node approach in three dimensions and implemented the analytical stiffness matrix to keep CPU time low. This is described in:

- Numerical approach of contact with friction between two bodies in large deformations, Habraken, A.M., Radu, J.P., Charlier, R., *Contact Mechanics, Int. Symposium,* edited by Curnier A., sponsored by Fondation LATSIS, Presses Polytechniques et Universitaires Romandes, (7-10 October 92), 391-408

The contact element used in LAGAMINE is a thermal-mechanical element where the thermal flow depends on the contact state. It is briefly described in:

- Dynamic Recrystallization during Zinc Rolling, Habraken, A.M., Charles, J.F., Wégria, J., Cescotto, S., *Int. J. of Forming Processes*, **1**, (1998), 53-73.

Some limited investigation has been conducted on an augmented Lagrangian approach, in collaboration with Professor Charlier and Jean-Philippe Bille.

- Numerical Approach of Contact Using an Augmented Lagrangian Method. Bille, J.P., Habraken, A.M., Charlier R., *3e Congrès National belge de mécanique théorique et appliquée,* (30-31 May 1994), Liège.

2.4. Continuous casting model

In collaboration with ARBED, two research projects have been conducted to simulate the continuous casting process with the LAGAMINE code. The first approach, which I performed in 1989, included 2 different behavior models for liquid and solid states. A mixture law was applied in the mushy zone. The experiments performed were not sufficient at that time to identify the model parameters; besides the model stability and convergence were quite poor. However this model has helped ARBED to optimize the mold taper, but no publication describes it.

Nearly 10 years later, a second project on continuous casting was initiated with a Ph.D. student, Frédéric Pascon. This time, an important experimental part of the research (performed at SIDMAR the research center, North Belgian steel industry) allows us to adjust our behavior law. The constitutive model adopted to simulate solid, mushy or liquid states is a thermal-elasto-visco-plastic law of the Norton type. First developed with Jean-François Charles to model zinc and steel rolling, this law has been greatly improved during this research. The convergence difficulties of the continuous casting model stimulated us to study all the details. Finally, the integration scheme as well as the loading-unloading criterion have been improved, and we have reached a quite stable and robust law. This research is described in Frédéric Pascon's DEA (master thesis) presented in September 2000, and published in international conference proceeding or journal:

- Finite element modeling of contact between the strand and the mould in continuous casting, Pascon, F., Diplôme d'études approfondies en Sciences Appliquées, Université de Liège, (September 2000).
- Thermo-mechanical model of a strand in the mould of a continuous casting plant, Pascon, F., Habraken, A.M., Bourdouxhe, M., Labory, F., *European Congress on Computational Methods in Applied Sciences and Engineering,* ECCOMAS 2000, Barcelona, 11-14 September 2000. CD-Rom with 979 papers. Our article is in section Computational Solid and Structural Mechanics, alphabetic classification on article title, (15 pages).
- Modélisation des phénomènes thermomécaniques dans une lingotière de coulée continue. Pascon, F., Habraken, A.M., Bourdouxhe, M., Labory, F., Mécanique & Industrie, **1**, (2000), 61-70.

2.5. Texture and plasticity models

This research began in 1994, thanks to a European COST project. Exchanges between our team and Professor van Houtte of Katholieke Universiteit of Leuven afforded us the possibility to implement a first yield locus based on texture data in LAGAMINE. Serge Munhoven and I tested this first plastic surface based on 4-dimensional spline functions. It shows bad convergence and continuity problems. A second method, developed by Jan Winter and based on a 6^{th} order series expansion in deviatoric stress space, gives satisfaction, enabling both teams to present FEM simulations on sheet behavior at the international conference, NUMIFORM 95.

- Anisotropic finite element simulation of plane strain tests. Winters, J., Van Bael, A., Munhoven, S., Habraken, A.M., Mols, K., Van Houtte, P., NUMIFORM, *Simulation of Materials Processing: Theory, Methods and Applications,* Shen & Dawson editors, BALKEMA (18-21 June, 1995), 357-362.
- Application of an anisotropic yield locus based on texture to a deep drawing simulation, Munhoven, S., Habraken, A.M., Winters, J., Schouwenaars, R., Van Houtte, P., NUMIFORM, *Simulation of Materials Processing: Theory, Methods and Applications*, , Shen & Dawson editors, BALKEMA (18-21 June, 1995), 767-772.

The Leuven Taylor's module to predict texture evolution was implemented in Liège and applied on aluminum extrusion by our team. Our results are close to those computed by a Norwegian team partner in the COST project:

- Texture prediction and aluminum extrusion, Degueldre, A., Habraken, A.M., Munhoven, S., Aukrust, T., Van Bael, A., Karhausen, K., *General Workshop COST 512, MMSP 96 Davos: Modelling in Materials Science and Processing,* edited by Rappaz M. and Kadro M. for the COST 512, Action Management

Committee. Published by the European Commission Directorate General XII Science Research Development, B-1048 Brussels, 260-265.

A project funded by the Région Wallonne partly devoted to the effect of texture evolution on yield locus shape started in September 1996. The fitting of a 6th order series, thanks to texture information, was considered too expensive (both in CPU time and memory storage requirement) to take into account texture evolution. It requires about 70000 calls to Taylor's module. Thus, it was decided to develop a description of a part of the yield locus requiring only 5 or 6 calls to Taylor's module. A so-called hyperplane approach was implemented in LAGAMINE and presented at NUMIFORM 98 conference:

- Comparison of Anisotropic Elastoplastic Laws Applied to Steel Sheet, Habraken, A.M., Radu, J.P., Duchêne, L., Wauters, M., Munhoven, S., NUMIFORM 98, *Simulation of Materials Processing: Theory, Methods and Applications,* edited by Huetink, Baaijens at Balkema, Enschede, The Netherlands, (22-25 June 1998), 769-774.

At that time, the lack of long-term involvement of engineers in this project severely slowed down the project but my long-term position allowed me to safeguard the information. Recently, the research could go on with the help of a Ph.D. student, Laurent Duchêne. Poor continuity of the hyperplane development is responsible for poor convergence; an improved approach called the interpolation method was proposed with André Godinas, Laurent Duchêne and myself and published in January 1999:

- Elastoplastic Anisotropic Model Based on Texture Analysis to Simulate Steel Sheet Behaviour, Duchêne, L., Habraken, A.M., Cescotto, S., *7th Int. Symp. on Plasticity*, Cancun, Mexico, edited by Akthar S. Khan at Neat Press, (5-13 January 1999), 325-328.

Our progress with this method has also been presented in the well-known ICOTOM and NUMISHEET conferences:

- Texture effects on steel sheet behaviour under large strain simulations, Duchêne, L., Godinas, A., Habraken, A.M., *12th Int. Conf. on Textures of Materials (ICOTOM-12),* Montreal, Canada, edited by Szpunar, J.A., at NRC Research Press Ottawa, (9-13 August 1999), 286-291.
- Metal Plastic Behaviour linked to Texture Analysis and FEM Method. Duchêne, L., Godinas, A., Habraken, A.M., NUMISHEET '99, *4th Int. Conf. and Workshop on Numerical Simulation of 3D Sheet* Forming Processes, Besançon, France, edited by Gélin, J.C., Picart, P., Université de Franche-Comté et ENSMM, (13-17 September 1999), 97-102.

It has been extensively described in Laurent Duchêne's DEA final paper:

- Implementation of a yield locus interpolation method in the finite element code Lagamine, Duchêne, L., Diplôme d'études approfondies en Sciences Appliquées, Université de Liège, (September 2000).

This method is now in its validation phase as Laurent Duchêne's Ph.D. thesis should soon lead to more comparisons between experiments and simulations. At the ESAFORM 2001 conference that I organized in Liège, I proposed a further study of a NUMISHEET 99 benchmark in order to compare different anisotropic constitutive laws for steel sheet behavior.

2.6. Damage models

The models developed by my team belong to the Lemaître & Chaboche French school of ductile rupture (Lemaître, J., Chaboche, J.L. 1985 *Mécanique des matériaux solides*, Dunod, Paris). They are macroscopic approaches of damage, where damage evolution is measured by the decreasing value of the apparent Young's modulus and, possibly, of Poisson's ratio.

I have supervised the implementation of a coupled isotropic elastoplastic damage model in the LAGAMINE code by Yongyi Zhu, a Ph.D. student with Professor Cescotto:

- Contribution to the local approach of fracture in solid dynamics, Zhu, Y., Thèse de Doctorat en Sciences Appliquées, Université de Liège, (1992).

This model has been applied on zinc sheets and aluminum rods in the graduation works written by Anne-France Cambron and Sylvie Castagne to get their Physician Engineer Degree.

With Wang Xiao Chuan, I have extended Zhu Yongyi's formulation to an elasto-visco-plastic model. For an aluminum alloy, the identification of the model was performed in our laboratory. So, accurate measurements of Young's modulus were developed; different experiments for the model validation were created. As the available geometry of the material was limited, we had to imagine non-classical experiments. Finally, the model has been applied to a rotative forging process for aluminum rods.

- An Elastic-visco-plastic Damage Model: from Theory to Application, Wang, X.C., Habraken, A.M., *Local Approach to Fracture* Fontainebleau (9-11 September 1996), *Supplément au Journal de Physique C*, **6**, (October 1996), 86-96.

As a large set of experiments on these aluminum rods were performed in our laboratory, with Li Hong Zhang, I have tried to go further in their exploitation. Additional comparisons of the elasto-visco-plastic damage model with experimental results were thus performed:

- A new elastic-visco-plastic damage model for annealed aluminum: theory, calibration and validation, Habraken, A.M., Zhang, L.H., Wang, X.C., Cescotto, S., *Symposium Continuous Damage and Fracture*, 23-27 October 2000, Cachan, France, *Continuous Damage and Fracture,* edited by Benallal, A., at Elsevier France, 341-352.

With Sylvie Castagne, the damage elasto-plastic model from Zhu Yongyi was also applied to these experiments. It appeared that some improvement was necessary to get correlation between model predictions and reality. The following paper has been accepted for publication:

- Application of a damage model to an aluminum alloy, Castagne, S., Habraken, A.M., Cescotto, S., to appear in *Int. Journal of Damage.*

In his Ph.D. thesis, Zhu Yongyi had also developed an anisotropic elastoplastic damage model, but his work did not include an experimental approach to identify model parameters and validation step. Michaël Wauters, a Ph.D. student of mine, has applied this model on two steel sheets, and a set of accurate sheet tests was developed in order to check Young's modulus decrease in anisotropic steel sheets. His experiments rapidly demonstrated that the simple linear hardening proposed by Yongyi Zhu leads to the prediction of a non-realistic behavior. Consequently Michaël Wauters has improved the model and performed different experiments to identify its parameters, validate its basic assumptions and validate its prediction. A first summary of this work can be found in:

- A fully coupled elasto-plastic damage model applied to anisotropic materials, materials, Wauters, M., Habraken, A.M., Duchêne, L., *14th Engineering Mechanics Conference,* May 21-24, Austin, Texas, USA, CD Rom Compiled by D. R. Maniar, edited by J.L. Tassoulas, The University of Texas at Austin (6 pages).
- Calibration of an anisotropic elastoplastic damage model for sheet metal forming, Wauters, Michaël, Diplôme d'études approfondies en Sciences Appliquées, Université de Liège, (June 2000).

Michaël Wauters's Ph.D. thesis should be completed later on.

2.7. Forging models

A strong cooperation with FORCAST, a forging industry producing cylinders for rolling mills, induced both experimental and numerical progresses. On the numerical front, in 1996, we developed a strategy to model their forging process as a generalized plane state. A comparison of the stress and strain states produced by a few strokes of different hammer and anvil geometries have helped to make some progress in the

understanding of physical events occurring during the process. An account of this work is given in:

- Procédés Intelligents de Mise en Œuvre par Forgeage Dynamique, Programme Mobilisateur Multimatériaux de la Région Wallonne, Rapport Final, Habraken A.M., Wang, X.C., (1996).

After further investigations and discussions, it appeared that three-dimensional simulations were necessary to represent the industrial reality. Again a set of simulations compared results of different tool shapes, helping engineers in decision-making. The efficient thermal-elasto-visco-plastic law of the Norton type, developed with Jean-François Charles and Frédéric Pascon, enabled investigation of the cooling effect during forging. A lot of computations were done; the following publication summarizes some of these:

- Numerical modeling of the forging process of rolls for rolling mills, Charles, J.F., Castagne, S., Zhang, L.H., Habraken, A.M., Cescotto, S., 8^{th} *int. Conf. on Metal Forming 3-7 September 2000, Metal Forming 2000* edited by Pietrzyk, M., Kusiak, J., Majta, J., Hartley, P., Pillinger, I. at Balkema, (2000), 625-631.

Jean-François Charles also developed experimental hot compression tests with the help of Philippe Boeraeve and technicians of the department laboratory. The goal was to identify the parameters of Norton's law. These tests are performed at "constant" temperature and "constant" strain rate. In fact, for rapid tests, the radiant furnace cannot compensate the adiabatic heat and the test does not take place at constant temperature. A subsequent development by Christophe Martin allows measuring this temperature variation during the test. The press, in the strain rate range of 10^{-4} to 10 sec^{-1}, correctly follows the constraint of constant strain rate. An Excel post processor provides the stress-strain curves from the measured force and displacement. This use of tests to reach stress-strain curves does not completely neglect the barreling effect that prevents homogeneous stress and strain states, but simply applies Orowan's formula. From these data, another Excel treatment computes Norton's parameters:

- Modelling of Elasto-Visco-Plastic Behaviour of Steels at High Temperatures, Charles, J.F., Habraken, A.M., Lecomte, J., NUMIFORM, *Simulation of Materials Processing : Theory, Methods and Applications*, 22-25 June 1998,edited by Huetink, Baaijens, at Balkema., Enschede, The Netherlands, 277-282.

Jean-François Charles also developed a first inverse approach, neglecting the variation temperature during the tests. A initial set of Norton's parameters is used in a set of FEM simulations modeling the different experiments. Then comparisons between predicted and measured force-displacement curves and an optimization approach provide a new set of Norton's parameters and a new iteration is computed. When the difference between predicted and measured force-displacement curves reaches a minimum, it is

assumed that the Norton's parameter set is the good one. Of course, local minimums can appear. This point as well as the effect of temperature must still be investigated.

2.8. Recrystallization model

Thanks to an industrial project for Union Minière devoted to zinc rolling simulation, Jean-François Charles and I have implemented a dynamic recrystallization model in the LAGAMINE code. This model uses the strain rate, temperature and strain level computed by the FEM code to follow the recrystallization phenomena. It is a post-processor activated inside the constitutive law, so the FEM simulation results give the recrystallized fraction of the final state product. The research is described in the following article:

- Dynamic Recrystallization during Zinc Rolling, Habraken, A.M., Charles, J.F., Wégria, J. Cescotto, S. , *Int. J. of Forming Processes,* **1**, (1998), 53-73.

A second model, where recrystallization affects mechanical behavior, has been proposed. Applying Sellars's approach, each material point is subdivided into substructures defined by their volume fraction. Their hardening degree is directly linked to the recrystallization process and the macroscopic strain.

The problem with such models is not really their numerical implementation, even if this is not so simple for the coupled one. The difficult point is the parameters identification. Coupling the hot compression tests described above with microscopic observations performed by the Service de Métallurgie Sidérurgie of ULG, we have tried to follow the dynamic recrystallisation process. However, a delay still exists between the hot deformation and the quench process that freezes the microscopic state. So some doubts remain about the information. It could cover meta-dynamic or even fast static recrystallization. Nevertheless, first results have been published in:

- Numerical modeling of the forging process of rolls for rolling mills, Charles, J.F., Castagne, S., Zhang, L.H., Habraken, A.M., Cescotto, S., *8th int. Conf. on Metal Forming 3-7 September 2000, Metal Forming 2000* edited by Pietrzyk, M., Kusiak, J., Majta, J., Hartley, P., Pillinger, I. at Balkema, (2000), 625-631.

This research is currently in progress. Parameters identification should also be improved by the use of inverse modeling.

3. ACTIVITIES AS RESEARCH ASSOCIATE

The above description of my technical activity gives an idea of my work which includes applying for projects with the industry, the University, the Région Wallonne and the

European Research organization. Then I hire, instructs and guide engineers to do the research or, in very rare cases, I handle the project alone.

I also attend conferences, where I present the research of my group and try to follow the scientific progress in the metal forming field. As member of twelve Ph.D. thesis juries, I have had opportunity to follow the research of other European teams in a very accurate and timely way. As a member of the Board of Directors of ESAFORM (European Scientific Association for material FORMING), I have organized its 2001 international conference, which has attracted more than 250 participants.

I actively participate in the educational process at the University by advising Ph.D. students and engineering students writing their final papers. As an elected member of the scientific staff of the Engineering Faculty, I participate to its daily life : this means belonging to various committees. For the last four years, I have been a member of the University Research Council. This decision-making group, composed of the University authorities, one professor and one scientist from each faculty, selects the research projects to be financed by the University or submitted to other institutions (Région Wallonne, French Community, etc.).

PART B

MODELING THE PLASTIC ANISOTROPY OF METALS BY FINITE ELEMENT METHOD

GraSMech Course
February 2000

Thèse présentée en vue de l'obtention du grade d'Agrégé de l'Enseignement Supérieur
par Anne-Marie HABRAKEN

Année académique 2000-2001

Part B - Introduction

This section consists of a postgraduate course that I taught in February 2000 within the frame of the Graduate School in Computational and Experimental Mechanics (GraSMech). My GraSMech students were supposed to attend an introduction to micromechanics by Professor Paul van Houtte during the first semester. His course contents are referenced as van Houtte, 1995. This is why this reference often appears in my own course.

I propose an important state-of-the-art review in the field of polycrystal micro-macro models implemented in Finite Element Method (FEM) as well as a summary of my personal research on this topic. My goal in doing such an important literature survey is to optimize further guidance of my research group.

Since 1994, my co-workers and I have been working on the development of a FEM approach, which couples plasticity and texture models. In fact, this research has been developed within the frame of 2 projects:

- a European COST 512 project, entitled "Integration of Micromechanical Models for the Plastic Deformation of Polycrystalline Materials with FE modeling of Forming Process"
- a Région Wallonne project entitled "Integration of Micro-Macro Interactions in Finite Element Modeling of Metal Forming".

An intensive collaboration with the team of Paul van Houtte, professor at the Katholieke Universitijt of Leuven, has helped us to tackle this field. Paul van Houtte is a very well-known scientist in the field of texture research (van Houtte 1988, van Houtte 1992, van Houtte 1995, van Bael *et al.* 1994, van Bael *et al.* 1996, Winters *et al.* 1996). Besides Professor van Houtte, I am particularly grateful to Jan Winters, Bert van Bael and Eric Hoferlin, who kindly and patiently transmitted the practical knowledge needed for using the numerical tools exchanged between our teams.

Numerous colleagues from the MSM Department such as Serge Munhoven, Jean-Pol Radu, André Godinas, Naji El Masri and Laurent Duchêne, have participated in this research. In the text, their specific work will be identified in the referenced list of authors or by explicit mention of their name. The research is currently in progress with the Ph.D. thesis of Laurent Duchêne, which should be completed on next academic year (2001-2002).

References

Van Bael, A., Winters, J. , Van Houtte, P. (1994) The effect of strain hardening on R-value measurements. In *Numerical Predictions of Deformation Processes and the Behaviour of Real Materials (Proc. 15th Riso International Symposium*

on Materials Science), Andersen S.I., Bilde-Sørensen J.B., Lorentzen T., Pedersen O.B. & Sørensen N.J. Eds, Roskilde, Denmark, Risø Laboratory, 225-230.

Van Bael, A., Winters, J., Van Houtte, P. (1996) A semi-analytical approach for incorporating crystallographic data into elasto-plastic finite element formulations, *Textures of Materials,* Proceedings of the 11th Int. Conf. on Textures of Materials, vol. 1, ICOTOM-11, Sept. 16-20, Liang Z., Zuo L., Chu Y. Eds.

Van Houtte, P. (1988) A comprehensive mathematical formulation of an extended Taylor-Bishop-Hill model featuring relaxed constraints, the Renouard-Wintenberger theory and a strain rate sensitivity model, *Textures and Microstructures*, **8-9**, 313-350.

Van Houtte, P. (1992) Anisotropic Plasticity, *Numerical Modelling of Material Deformation Processes, Research, Development and Applicaitons,* Hartley, P., Pillinger, I., editors, Springer-Verglag.

Van Houtte, P. (1995) Micromechanics of polycrystalline materials, Chaire Francqui, Université de Liège.

Winters, J. (1996) Implementation of a texture-based yield locus into an elastoplastic finite element code. Application to sheet forming. Katholieke Universiteit Leuven, MTM department, Ph. D thesis.

CONTENTS

Notations B-1
Symbols
Abbreviations B-3
Latin letters B-3
Greek letters B-11

1. Introduction 1.1
References 1.3

2. Anisotropic phenomenological yield loci 2.1
2.1 Initial shape of yield loci 2.1
2.1.1 Hill's approach 2.2
2.1.2 Barlat's and Karafillis's approach 2.6
2.1.3 A polar-coordinate representation of an orthotropic yield locus 2.14
2.1.4 Vegter'approach 2.17
2.1.5 Summary 2.20
2.2. Updated yield loci 2.21
References 2.23

3. Hardening models 3.1
3.1 Basic knowledge on crystal events 3.1
3.2 Crystallographic texture 3.3
3.3 Introduction to hardening models 3.5
3.4 Simple macroscopic isotropic hardening approaches 3.9
3.5 Macroscopic approaches with microscopic roots 3.10
3.5.1 Bergström-van Liempt-Vegter's model 3.10
3.5.2 Follansbee & Kocks's model 3.15
3.5.3 Schmitz's model 3.18
3.5.4 Miller –Mc Dowell's model 3.18
3.5.5 Teodosiu's model 3.24
3.6 Conclusion 3.30
References 3.31

4. Microscopic models and micro-macro approaches 4.1
4.1 Taylor's single crystal plasticity model 4.1
4.1.1 Description 4.1
4.1.2 Taylor's factor 4.4
4.2 Strain rate sensitivity approach for single crystal plasticity model 4.4
4.3 Evolution rule for CRSS value 4.5
4.4 Mechanical frame for single crystal plasticity 4.6
4.5 Polycrystal plasticity models 4.9
4.5.1 Description 4.9
4.5.2 Average Taylor's factor 4.11

4.6 Link between the evolution of the reference CRSS and macroscopic strain hardening 4.13
4.7 Summary 4.14
References 4.14

5. FEM Micro-Macro models without yield locus 5.1
5.1 Introduction 5.1
5.2 Microscopic FEM computations to model macroscopic behavior 5.1
5.2.1 Teodosiu et al. 1992 5.1
5.2.2 Acharya & Beaudoin's model 5.5
5.3 Macroscopic FEM simulations relying on discrete set of crystals 5.9
5.3.1 Taylor's model + Polycrystal models 5.10
5.3.2 Self-consistent approach + Polycrystal models 5.19
5.3.3 Homogenization approach + Polycrystal models 5.20
5.4 Macroscopic FEM simulations with microscopic models 5.24
5.5 FEM analysis applied on both ODF evolution and macroscopic process 5.26
5.5.1 Crystal orientation representation 5.27
5.5.2 Micro-Macro Links 5.28
5.5.3 Evolution rule of Orientation Distribution Function 5.29
5.5.4 Computation of the reorientation velocity field 5.30
5.5.5 Texture prediction under monotonic deformations 5.31
5.5.6 Application to aluminum rolling 5.32
5.5.7 Conclusion 5.33
5.6 Conclusion 5.35
References 5.35

6. FEM Micro-Macro models with yield locus 6.1
6.1 Introduction 6.1
6.2 Macroscopic models imbued from single crystal plasticity 6.2
6.2.1 3G model 6.2
6.2.2 Khan & Cheng's model 6.9
6.2.3 Aifantis' models 6.10
6.2.4 Conclusion 6.17
6.3 Analytical yield loci computed from texture data 6.17
6.3.1 Polycrystal yield locus obtained by Taylor's approach 6.17
6.3.2 Proposals applying concepts from Montheillet 6.19
6.3.3 Arminjon, Bacroix, Imbault...'s potential formulation 6.24
6.3.4 Van Houtte's potential formulation 6.29
6.3.5 Conclusion 6.38
6.4 Models developed by MSM 6.39
6.4.1 First steps in coupling FEM with texture codes 6.39
6.4.2 Texture updating coupled with FEM simulations 6.48
6.4.3 Hyperplane model 6.51
6.4.4 Interpolation approach 6.60

6.4.5 Conclusion 6.70
6.5 Validations of our models 6.70
6.5.1 Discrete sets of crystallographic orientations 6.70
6.5.2 π-sections of the yield locus computed by local and non local methods 6.72
6.5.3 Lankford coefficient prediction 6.74
6.5.4 Academic rolling validation with texture updating 6.76
6.5.5 Conclusions of validation step 6.79
6.5.6 Conclusion 6.80
References 6.80

7. Conclusions 7.1

Notations

Second order tensors are underlined once or noted with their 2 subscripts and fourth order tensor are identified by four subscripts or underlined twice. Capital Latin letters or Greek letters are used for these tensors. Einstein's summation on identical indices is always assumed unless otherwise specified.

The simple contracted tensor product is identified by ".".

$$\underline{C} = \underline{A}.\underline{B} \Leftrightarrow C_{ij} = A_{ik} B_{kj}$$

The tensorial product is :

$$\underline{\underline{C}} = \underline{A} \otimes \underline{B} \Leftrightarrow C_{ijkl} = A_{ij} B_{kl}$$

The double contracted tensor product is noted by ":"

$$s = \underline{A} : \underline{B} \Leftrightarrow s = A_{ij} B_{ij} \quad \underline{C} = \underline{\underline{S}} : \underline{B} \Leftrightarrow C_{ij} = S_{ijkl} B_{kl}$$
$$s = \underline{A} : \underline{\underline{S}} : \underline{B} \Leftrightarrow s = A_{ij} S_{ijkl} B_{kl}$$

The tensorial norm is defined by :

$$|\underline{A}| = \sqrt{\underline{A} : \underline{A}}$$
$$|\underline{\underline{S}}| = \sqrt{S_{ijkl} S_{ijkl}}$$

The inverse operator is defined by the superscript -1 :

$$\underline{A}^{-1} \underline{A} = \underline{I} \Leftrightarrow A^{-1}_{ik} A_{kj} = \delta_{ij}$$

with $\underline{I}$ the unit second order tensor, δ_{ik} Kronecker symbol.

The transverse operator is defined by the subscript T :

$$(A^T)_{ij} = A_{ji}$$

Vectors are also underlined once, but small Latin letters are used. They can also be noted with one subscript. The vector operations are :

$$\underline{s} = \underline{v}.\underline{u} \Leftrightarrow s = v_i u_i$$

$$\underline{C} = \underline{v} \otimes \underline{u} \Leftrightarrow C_{ij} = v_i u_j$$

$$|\underline{v}| = \sqrt{\underline{v}.\underline{v}} = \sqrt{v_i v_i}$$

If $\underline{v}$ is a vector and $\underline{A}$ a second order tensor :

$$\underline{u} = \underline{A}.\underline{v} \Leftrightarrow u_i = A_{ij} v_j$$

Scalars are not underlined.

The superscript * characterises unit vector :

$$\underline{u}^* \Rightarrow |\underline{u}^*| = 1$$

Abbreviations

CRSS	Critical Resolved Shear Stress characterizing one slip system
FEM	Finite Element Method
FLD	Forming Limit Diagram
MK	Marciniak Kuczynski
MSM	department of Mechanics of Structures and Materials
ODF	Orientation Distribution Function
RVE	Representative Volume Element

Latin letters

a	exponent in the yield surfaces proposed by Hill, Hosford, Barlat, Karafillis
a, b	material constants in Tourki's model
a,A,B,C,D,E	material constants in 3G model
a_m	annihilation of mobile dislocations
a_i	annihilation of immobile dislocations
$a_{1b}, a_{2b}, a_{3b}, a_{1n}, a_{2n}, a_{3n}$	functions of dislocation density in constitutive relations of Aifantis's model
a^{su}	matrix taking into account various types of dislocation interactions in Teodosiu's micro model
$\underline{a}$	unit vector oriented in the crystal direction in Aifantis'model
$\underline{a}$	vector (1 1 1 1 1) in the 5 dimensional space (interpolation approach)
$\underline{a},\underline{b}$	intermediate vectors in interpolation approach
A	constant representing the rate of annihilation of mobile dislocations in Bergström's model
A	constant in Miller & Mac Dowell's model
A	surface region in Acharya & Beaudoin's model
$A\ A_1 A_2 A_3$	material constants in Follansbee & Kocks' model
A, B, C	material constants in the yield surfaces proposed by Hill, Hosford, Barlat, Karafillis, Tourki
$\underline{A}$	macroscopic tensor in Aifantis' model equivalent to $\underline{A}^s$ tensor at microscopic level
$A^s_{ij}\ \underline{A}^s$	symmetric part of Schmid's tensor K^s_{ij}
$\underline{A}^s_i$	symmetric part of Schmid's tensor associated to texture component i

b_α b_R	shape-control parameter in Khan & Cheng's model
$\underline{b}$	Bürgers' vector in crystalline plasticity, b is its magnitude
$\underline{b}^c$	cumulative Burgers vector of all dislocations threading the region A in Acharya & Beaudoin's model
$\underline{b}^s$	unit vector in the slip direction for the slip system s
c	creation of dislocations in Bergström's model
$\hat{c}$	variation of dislocation density in Aifantis's model
C	constant in the expression of dislocation density for constant strain rate tensile tests
C	constant in the first Miller & Mac Dowell's model and function in their second model
C	curve bounding a surface region A in Acharya & Beaudoin's model
C^*	constant in second Miller & Mac Dowell's model
C_α	saturation rate of back stress (Teodosiu's macro model)
C_p	polarization rate of the persistent dislocation structures (Teodosiu's macro model)
C_s	saturation rate of S_D "direct" directional strength (Teodosiu's macro model)
C_l^{uv}	Fourier's coefficients in the series expansion representing the ODF
$\underline{\underline{C}}^e$	elastic tangent matrix
$\underline{\underline{C}}^{tan}$	non linear tangent matrix
dt, dG_{ij}, ...	increment of time, increment of shear strain, ...
dV	elementary volume
D	grain size
$\underline{\underline{D}}^{micro}$	stiffness 4th order tensor relating stress and strain rate in visco-plastic approach in Kumar & Dawson's model
e_i e_j e_k	basis of a rectangular Cartesian coordinate system
$\underline{\dot{e}}$ or $\dot{e}_p$ $p=1,5$	vector representation of plastic strain rate tensor in van Houtte's model
E	visco-plastic potential in strain rate space of Arminjon's model
E	earing percentage in cup drawing
E_c	complementary visco-plastic potential in stress space of Arminjon's model
f	statistical crystallite orientation distribution function, its variables are g, the set of Euler angles in Bunge's approach, $\underline{r}$ in Kumar & Dawson's approach or $\underline{a}$ in Aifantis' approach.

f_i	volume fraction of crystals belonging to texture component i
$\hat{f}$	source term in momentum exchange between dislocations and lattice in Aifantis's model
F	function in strain rate space which after scaling, gives the plastic multiplier $\dot{\lambda}$ in Arminjon's model
F_p	function describing the yield surface
$F_{p_1 p_2 \cdots p_N}$	coefficients of the series expansion in strain rate space of the yield locus in van Houtte's model
F,G,H,N,L,M	material anisotropic constants of Hill's 1948 yield locus
$\underline{F}$	deformation gradient tensor
$\underline{\tilde{F}}$	fluctuation field in deformation gradient tensor of the RVE in Miehe's approach
$\underline{F}^*$	elastic deformation gradient tensor
$\underline{F}^*$	elastic distortion + rigid rotation of the lattice , applied on the isoclinic configuration to recover the real configuration
$\underline{F}^p$	plastic deformation gradient tensor
g	function in Tourki's model, Follansbee & Kock's model or Teodosiu's macro model
g	orientation of one crystal, expressed by Euler angles
$g^j \quad j=R,\alpha$	function in Miller & Mac Dowell's model for isotropic hardening R and kinematic hardening α
G	shear modulus
$G_{12}\ G_{23}\ G_{31}$ *or* G_{ij}	shear strain in maximal shear planes (3G model)
$G_{p_1 p_2 \cdots p_N}$	coefficients of the series expansion in stress space of the yield locus in van Houtte's model
h	cup height used to determine the earing percentage
h	material parameter in Barlat's 1989 model
h_0	material parameter in hardening function in Anand's micro model
$h_1 h_2 h_3$	parameters related to grain size D in Nakamachi's model
h^{su}	hardening matrix in CRSS evolution rule
h^u	function in the CRSS evolution rule
H_0	material parameter in Voce type law in Dawson's micro model
H_{ij}	Hessian matrix, second derivative of the yield surface
$\underline{I}$	second order unit tensor

$j_b\ j_n$	size of the dislocation flux in glide or climb directions in Aifantis' model
$\underline{j}$	dislocation flux in Aifantis' model
$J(\underline{r}_0, t)$	determinant of the mapping corresponding to the trajectories of crystals through orientation space due to plastic deformation
J_1	first stress invariant = $\frac{1}{3} tr(\hat{\underline{\sigma}} - \underline{\alpha})$
J_2	second stress invariant = $\frac{1}{2}(\hat{\underline{\sigma}} - \underline{\alpha}) : (\hat{\underline{\sigma}} - \underline{\alpha})$
k	Boltzman's constant
k	scalar factor often used in interpolation approach to keep unit vector property
k, m, n, p, q	material constant in Tourki's model
$k_0\ k_1$	material constants in Acharya & Beaudoin's model
k_2	recovery function in Acharya & Beaudoin's model
K	material constant in the flow rule of the 3G model
K_{ij}^s	geometrical matrix describing the slip system s, generally called Schmid's tensor
$\underline{\underline{K}}$	fourth order texture tensor in Aifantis' average procedure
L_{ij}^s	plastic velocity gradient generated by a particular slip system s
$\underline{L}^{micro}$	velocity gradient applied to a crystal, its decomposition neglects elasticity
$\underline{\underline{L}}$	fourth order tensor describing material anisotropy in yield locus approach or in self-consistent scheme
$\underline{\underline{L}}^*$	4th rank interaction tensor in elastic self-consistent approach
$\underline{\underline{L}}^H$	4th rank Hill's constraint tensor in elasto-vico-plastic self-consistent approach
m	material constant defining the fraction of isotropic hardening in Teodosiu's macro model
$m^j \quad j=R, \alpha$	material parameter in g function of Miller & Mac Dowell's model
M	Taylor's factor for one crystal having an orientation g and submitted to a strain mode
$M_i^*(\underline{\dot{\varepsilon}}^p)$	function integral of Taylor's factor and harmonic functions describing the ODF in Arminjon's approach

M_i^{**}	approximated value of $M_i^*(\underline{\dot{\varepsilon}}^p)$ to identify β_k^i coefficients
$\overline{M^c}$	average Taylor's factor for a polycrystal
n	material rate-sensitivity exponent in a viscoplastic model
n'	strain hardening exponent in elastoplastic model
n_L	exponent in the rate function of latent strength of the persistent dislocation structures (Teodosiu's macro model)
$\underline{n}$ and $\underline{\hat{N}}$	unit normal vector and its associated skew symmetric tensor in Acharya & Beaudoin's model
$\underline{n}$	axis of rotation in Rodrigues's representation of crystal orientation
$\underline{n}^Y$	outward normal of the deformed configuration of the RVE
$\underline{n}^T$	outward normal of the initial configuration of the RVE with sometimes + or – superscript to localize its direction
$\underline{n}^s$	unit vector normal to the slip plane for the slip system s
N	dimension of the space
N_v	number of inclusions per unit of volume
$\underline{N}_{\dot{\varepsilon}^p}$	direction of the plastic strain rate tensor in Teodosiu's macro model
p	material parameter in Barlat's 1989 model
p^{su}	parameter of dynamic recovery due to cross slip in Nakamachi's micro model of CRSS evolution
$\underline{P}$	tensor associated to the polarity of the dislocation structures (Teodosiu's macro model)
q	material parameter weighting direct and latent part of directional strength S_D, S_L (Teodosiu's macro model)
q	parameter of non-uniformity of any scalar field
$q^j \quad j = R, \alpha$	material parameter in g function of Miller & Mac Dowell's model
q^{su}	interaction matrix of self and latent hardening in Nakamachi's micro model of CRSS evolution
$Q(u_p)$	approximate polynomial function of average Taylor's factor in van Houttes's model
$Q(\underline{s}^*)$	polynomial function describing stress yield locus in van Houtte's model

r	effective distance between the adjacent slip systems in Nakamachi's micro model
r	re-mobilization of immobile dislocations
r	Lankford coefficient, ratio of the transverse to the thickness strain during an uniaxial tensile test
$\underline{r}$	orientation vector of a crystal in Rodrigues' parametrization adopted by Kumar & Dawson's model
r_α	Lankford coefficient measured by a tensile test which longitudinal axis does an angle of α with the Rolling Direction
$\bar{r} = r_0 + r_{90} + 2\,r_{45}$	average Lankford coefficient for an anisotropic sheet
$\underline{r}_0$	Rodrigues' vector to define crystal orientation in initial reference texture
R	isotropic hardening variable, increase of plastic stress in Miller & Mac Dowell's model
$R_0\,R_2$	saturated values of isotropic hardening in Khan & Cheng's model
$R_{sat}^{(0)}$	(initial) saturation value of R variable
$\underline{R}$	rotation matrix
$\underline{R}_i^{\Phi}$	rotation matrix about the i-axis by the angle Φ
$\underline{R}^{elastic}$	crystal elastic rotation tensor in Acharya & Beaudoin's model
s	size of a deviatoric stress on the yield locus, also called stress radius
s	mean free path or average distance covered by mobile dislocations
s	slip system
$s_1\,s_2\,s_3$	parameters related to grain size D in Nakamachi's micro model
s_0	parameters related to dislocation density decrease due to glide work and thermomechanical effect in Nakamachi's micro model of CRSS evolution
s^s	mean free path or average distance covered by mobile dislocations in slip system s
s^{su}	softening matrix in Nakamachi's micro model of CRSS evolution
$\underline{s}$ or s_p $\quad p=1,5$	vector representation of deviatoric stress tensor in van Houtte's or hyperplane or interpolation approach
$\underline{s}^{(k)}$ or $s_p^{(k)}$	nodal stress point k of the yield locus used to build an hyperplane facet

$\underline{s}^{(i)}$	non unit stress vector associated to a unit direction in strain rate space $\underline{u}^{*(i)}$
$\underline{s} = s\underline{s}^*$	vector description of a deviatoric stress point on the yield locus in van Houtte's model
$\underline{s}^*$	unit vector defining a deviatoric stress direction
$\underline{s}^{*0}$	unit vector defining a deviatoric stress direction, center of a local description of the yield locus
$\underline{s}^{*(i)}$	unit vector representing a perturbed direction i around $\underline{s}^{*0}$, called domain limit vector (interpolation approach)
$\underline{s}'^{*0}$	unit vector in the direction of vector (1 1 1 1 1) in stress space
$\underline{s}'^{*(i)}$	unit vector representing a perturbed direction i around $\underline{s}'^{*0}$
$\underline{ss}^i$	contravariant vector associated to vector $\underline{s}^{*(i)}$
$\underline{ss}'^{(i)}$	contravariant vector associated to vector $\underline{s}^{(i)}$
$\underline{s}_A$	stress vector at the step beginning
$\underline{s}_B$	stress vector at the step end
$\underline{s}_{B\,trial}$	elastic stress predictor vector at the step end
S_D	scalar related to the strength of the dislocation structures associated with currently active slip systems, "direct" directional strength (Teodosiu's macro model)
S_{sat}	saturation value of S_D
S_L	norm of latent strength of the persistent dislocation structures
$\underline{\underline{S}}_L$	latent strength of the persistent dislocation structures
$\underline{\underline{S}}$	directional strength of dislocation structures (Teodosiu's macro model)
t	time
t_A, t_b, t_n	functions of dislocation density, interaction forces between dislocations in constitutive relations of Aifantis's model
$\underline{t}$	traction at the boundary in Miehe's proposal
T	absolute temperature in Kelvin degree
$\dot{\dot{T}}_l^{uv}$	harmonic function of Euler angle in the series expansion representing the ODF
$\underline{u}$ or u_p	strain rate mode $\underline{U}_{\dot{\varepsilon}^p}$ in its vector notation

$\underline{u}'$	all possible strain rate modes $\underline{U}_{\dot{\varepsilon}^P}$ in minimization process
$\underline{u}^*$	unit vector, direction of a strain rate vector
$\underline{u}^{*(i)}$	unit vector in strain rate space representing a perturbed direction i around a central direction $\underline{u}^{*0}$
U	rate of immobilization or annihilation of mobile dislocations
$\underline{U}_{\dot{\varepsilon}^P}$	strain rate mode tensor
$\underline{U}'_{\dot{\varepsilon}^P}$	unit strain rate mode tensor
$\underline{U}^X_{\dot{\varepsilon}^P}$	strain rate mode in principal strain rate axes
$\underline{v}$	unit vector in the 5 dimensional space, direction of the vector identified by coordinates (1 1 1 1 1)
$\underline{v}$	reorientation velocity vector in ODF conservation relation.
V	volume
V^*	volume fraction of crystals in a subset of orientation space Ω^* in Kumar & Dawson's model
$\underline{\tilde{w}}$	fluctuation field applied on the RVE in Miehe's model
W	viscosity constant in 3G model
W^P	plastic work
$\dot{W}^P$	plastic work rate
$x_1\ x_2$	transformation of principal stress axes in Tourki's work
$\underline{x}$	coordinates in the final configuration
$\underline{x}^*$	coordinates in the isoclinic configuration
$X_0\ X_1\ X_2$	saturated values of hardening in Kan & Cheng's model
X_k	4rth order strain rate term in Arminjon's description
$X_P Y_P Z_P$	cartesian coordinates of P point
$\underline{X}$	coordinates in the initial configuration
y_c	characteristic length associated to the annihilation process of dislocation dipoles
$Z^s_{ij}\ \underline{Z}^s$	anti-symmetric part of Schmid's tensor K^s_{ij}

Greek Letters

α	orientation angle between rolling direction and tensile direction in experimental test
α	material constant in relationship between uniaxial flow stress and dislocation density (Bergström's model) or CRSS and dislocation density
α	ratio between the CRSS associated to a particular slip system and a common reference CRSS
α_k	material coefficient in polynomial formulation of the plastic multiplier in Arminjon's approach
α_1 α_2	angles measuring the deviation of G_{12} gliding planes from the directions at 45° to principal stresses in 3G model
$\alpha_{sat}^{(0)}$	(initial) saturation value of the back stress norm (Miller & Mac Dowell's model, Teodosiu's macro model)
$\underline{\alpha}$	back-stress in kinematic hardening (Teodosiu's macro model, Miller & Mc Dowell's model...) also called dislocation stress in Aifantis's model
α β	material coefficients in Montheillet's yield function
β	variable in Bezier formula in Vegter's criterion
β	orientation of the principal stress directions with the Rolling Direction (Hill's model, Tourki's model, 3G model)
β	parameter defining the size of one hyperplane facet or of the interpolation domain
$\beta_1\beta_2\beta_3\beta_4$	set of 4 angles to represent a strain mode tensor
$\beta_1\beta_2\beta_3$	Euler angles defining the orientation of principal strain rate mode directions
β_4	deviation of the current strain rate mode with respect to an axisymmetric compression along the 3rd principal axis
β_k^i	linear coefficient between parameter α_k of Arminjon's approach and texture coefficients C_i
$\gamma^{macro\ or\ micro}$	deformed configuration in Miehe's model
$\dot{\gamma}^s$	slip rate associated to a slip system s
$\dot{\gamma}_0$	reference slip rate in microscopic viscoplastic flow rule
$\dot{\gamma}_{scaled}^s$	slip rate per unit equivalent strain rate
Γ	total slip in one crystal
$\Gamma^{macro\ or\ micro}$	initial configuration in Miehe's model

$\overline{\dot{\Gamma}}$	total average polycrystal slip rate
δ_{ij}	Kroneker symbol
Δ	angle step used to discretize Euler's space (Darrieulat & Piot)
ΔG	activation enthalpy
$\underline{\Lambda}$	measure of lattice incompatibility in Acharya & Beaudoin 1999
$\underline{\underline{\Lambda}}$	Eshelby's 4th order tensor
$\varepsilon_1\ \varepsilon_2\ \varepsilon_3$	principal strains
ε_{ps}	prestrain applied in one direction before a second loading
$\varepsilon_{eq}(\varepsilon^p_{eq})$	equivalent von Mises (plastic) strain $\sqrt{\frac{2}{3}\varepsilon_{ij}\varepsilon_{ij}}$
ε^p_e	integrated equivalent plastic strain (hardening internal variable computed from the integral of $d\varepsilon^P_{eq}$)
ε_m	mean strain
$\dot{\varepsilon}_0$	limit strain rate for thermally activated motion
$\dot{\varepsilon}^{(p)}_{eq}$	(plastic) von Mises equivalent plastic strain rate
$\dot{\varepsilon}^p_{eqa}$	anisotropic equivalent plastic strain rate associated to anisotropic equivalent stress to recover plastic dissipation
$\underline{\varepsilon}\ or\ \varepsilon_{ij}$	strain tensor
$\underline{\varepsilon}^{p\ micro}$	strain tensor at microscopic level (in one crystal)
$\underline{\dot{\varepsilon}}^{p\ micro}_i$	plastic strain rate tensor associated to the texture component i in Darrieulat's model
$\underline{\varepsilon}^{macro}\ or\ \underline{\overline{\varepsilon}}$	strain tensor at macroscopic level
$\underline{\varepsilon}^e$	elastic strain tensor
$\underline{\varepsilon}^p$	plastic strain tensor
$\underline{\hat{\varepsilon}}$	deviatoric strain tensor
ζ	material parameter in plastic spin function (Miller & Mac Dowell's model)
η	isoparametric coordinate in a reference plane in FEM formulation
η_i	one of the 5 η-coordinates used in stress space or in strain rate space in the interpolation approach
θ	polar angle associated with the polar-coordinate description used by Tourki, Ferron
θ	angle between central direction and domain limit vectors in interpolation approach

θ	scalar defining the implicit character of an integration scheme $0 \le \theta \le 1$
θ_{0*}	hardening rate due to dislocation accumulation in Voce's law (Follansbee-Kocks, Acharya-Beaudoin)
λ	plastic multiplier
λ^k	slip lattice incompatibility corresponding to system k in Acharya & Beaudoin's model
ξ	isoparametric coordinate in a reference plane in FEM formulation
$\rho_{(0)}$	(initial) total dislocation density
ρ_i	density of immobile dislocations
ρ_m	density of mobile dislocations
ρ^s	dislocation density related to slip system s
$\hat{\sigma}$	internal variable in Follansbee & Kocks' model, flow stress at 0°K associated to a defined dislocation substructure
$\sigma_1\ \sigma_2\ \sigma_3$	principal stresses
$\sigma_0\ \sigma_{45}\ \sigma_{90}\ \sigma_\alpha$	yield stress under uniaxial tension in one direction doing an angle 0, 45, 90, α with the Rolling Direction
σ_0	initial elastic limit (Bergström's model, Miller & Mac Dowell's model, Teodosiu's macro model…)
$\sigma_{0\,sta}$	static yield stress of a dislocation free material (Vegter's model)
$\sigma_{0\,dyn}$	dynamic part of the flow stress (Vegter's model)
σ_a	athermal stress component associated with interaction of dislocations with long range obstacles in Follansbee & Kocks' model
σ_b	yield value under equibiaxial plane solicitation
σ_{eq}	von Mises equivalent stress $\sqrt{\frac{3}{2}\hat{\sigma}_{ij}\hat{\sigma}_{ij}}$
σ_{eqa}	anisotropic equivalent stress
σ_F	yield stress under uniaxial tension in a reference direction
σ_m	hydrostatic (mean) stress $(1/3)\sigma_{ii}$
σ_{sat}	stress at zero strain hardening rate, called saturation stress (Follansbee & Kocks' model, Schmitz's model)
$\sigma_{sat\,0}$	saturation stress at 0°K (Follansbee & Kocks' model)
$\sigma_x\ \sigma_y\ \sigma_z\ \tau_{xy}\ \tau_{zx}\ \tau_{yz}$	stress components in the material orthotropic axes
$\underline{\sigma}$	Cauchy stress tensor

$\underline{\sigma}^{effective} = \underline{\sigma} - \underline{\alpha}$	macroscopic effective stress in Aifantis' model
$\underline{\hat{\sigma}}$	deviatoric Cauchy stress tensor
$\overset{\nabla}{\underline{\hat{\sigma}}}$	Jaumann deviatoric stress rate
$\underline{\sigma}^{micro}$	microscopic stress tensor, no *micro* superscript means macroscopic stress, sometimes superscript *macro* is effectively recalled
$\underline{\sigma}_i^{micro}$	microscopic stress tensor of texture component i in Darrieulat's approach
τ	yield stress in a pure shear test parallel to material orthotropic axes (Hill's yield locus),
τ	stress limit in Tresca's criterion, ($2\tau=\sigma_F$ yield stress in uniaxial tensile test)
τ^s	resolved shear stress acting on the slip system s
$\tau_{effective}$	resolved shear stress in Aifantis' model where 1 slip system is assumed and a cinematic hardening approach is applied at the microscopic level
τ_n	resolved climb component in Aifantis' model
$\tau^s_{c(0)}$	(initial) critical resolved shear stress acting on the slip system s often called CRSS
$\tau_{c(0)}$	(initial) common reference value assumed for CRSS in one crystal
τ_{sat}	saturation value of common reference CRSS
$\tau_{12}\ \tau_{23}\ \tau_{13}$	shear stress associated to shear strains $G_{12}\ G_{23}\ G_{13}$ (model 3G)
$\bar{\tau}_c$	average common reference CRSS in a polycrystal
$\underline{\tau}^{micro\ or\ macro}$	first Piola Kirschoff stress used in Miehe's model
Φ	amplitude of rotation in Rodrigues' description of crystal orientation
$\Phi_i(\xi,\eta)$	interpolation function in classical geometric space in isoparametric finite element
$\Phi_i(\xi_1,\xi_1,\xi_1,\xi_1)$	interpolation function in a reference stress space in the hyperplane discretization of the yield locus
$\Phi\ \Phi_1\ \Phi_2$	functions in Karafillis' model used to define the yield function
$\varphi_1\ \phi\ \varphi_2$	set of Euler's angle
Ψ_k	strain rate function used in polynomial description of plastic multiplier in Arminjon's approach
ω_0	scattering width angle with an ideal texture component

Ω	probability for re-mobilization or annihilation of immobile dislocations in Bergström's model
Ω^*	subset domain in crystal orientation space in Rodrigues space
Ω^t	whole domain in crystal orientation space of in Rodrigues space (Kumar & Dawson's model)
$\underline{\Omega}$	antisymmetric part of the velocity gradient tensor or total spin
$\underline{\Omega}^{micro}$	microscopic spin decomposed into the plastic spin and the rate of crystal lattice rotation
$\underline{\Omega}^{p}$	plastic spin
$\underline{\Omega}^{L}$	rate of crystal lattice rotation used to update texture
$\underline{\Omega}^{t}$	texture spin due to grain boundary effects in Aifantis' model

1. INTRODUCTION

If we look at the anisotropic plastic models proposed in the literature, 2 types of models exist: the phenomenological ones (chapter 2) and the micro-macro ones (chapters 5 and 6) based on polycrystalline and texture approach. The first ones do not need additional knowledge to be understood by a classical mechanical scientist; it is not the case for the models issued from texture approach. Therefore some basic information will be recalled for the non-specialist reader (chapter 4); however for shortness sake, this will be limited. For a deeper understanding, I recommend the lecture of Van Houtte 1995, Teodosiu 1997, Bunge & Esling 1997.

Roughly speaking, chapter 2 is dedicated to the initial shape of the yield locus. Then chapter 3 describes the hardening models. First, simple macroscopic hardening approaches are recalled; then, more complex formulations with microscopic roots are presented. Chapter 5 summarizes micro-macro approaches without yield locus which use homogenization techniques based on crystal computations (Beaudoin *et al.* 1995, Kumar & Dawson 1996, Anand & Kothari 1996, Nakamachi *et al.* 1999). Chapter 6 presents the other trends of yield locus computations, based on texture and crystal plasticity (Lequeu *et al.* 1987, Imbault 1993, van Houtte 1994, Duchêne *et al* .1999). The advantages and drawbacks of the different proposals will be defined as well as the model identification procedure since this is a key factor for practical applications.

The reason of the strong interest in the initial and up-dated shape of the yield locus or in the micro-macro approaches is related to the accuracy of the model predictions. The reliability of Finite Element Method simulations in deep drawing computations (Figure 1-1, Figure 1-2, Figure 1-3) as well as of Marciniak Kuczynski's (MK) predictions of Forming Limit Diagrams (FLD) (Figure 1-4, Figure 1-5) easily explain the reasons to improve the description of the yield locus or to use polycrystal models.

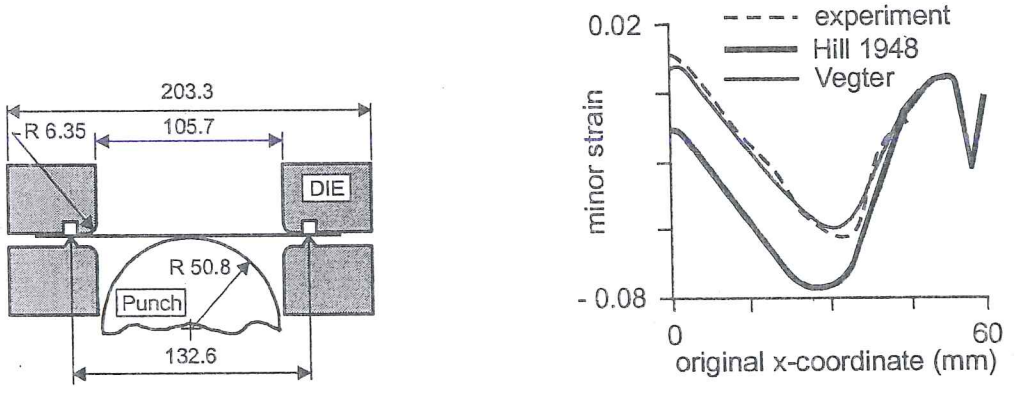

Figure 1-1 Simulated and measured minor strains along a symmetry axis of a Limiting Dome Height test, benchmark of the Numisheet 96 conference with draw quality mild IF steel (models with phenomenological description of yield locus, Pijlman *et al.* 1998).

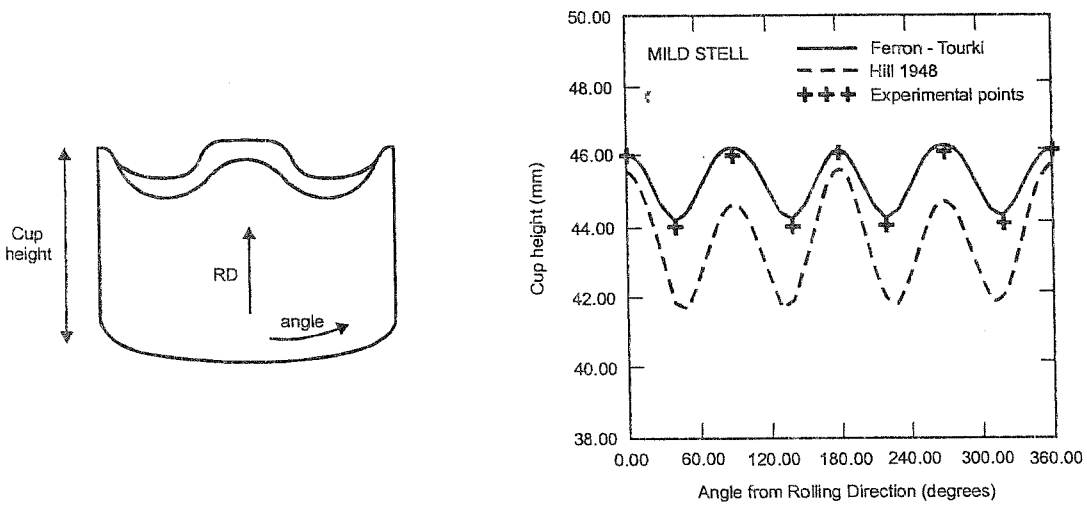

Figure 1-2 Deep drawing of a cylindrical cup : comparison between experimental and calculated earing profiles, mild steel supplied by SOLLAC (models with phenomenological description of yield locus, Tourki *et al.* 1996).

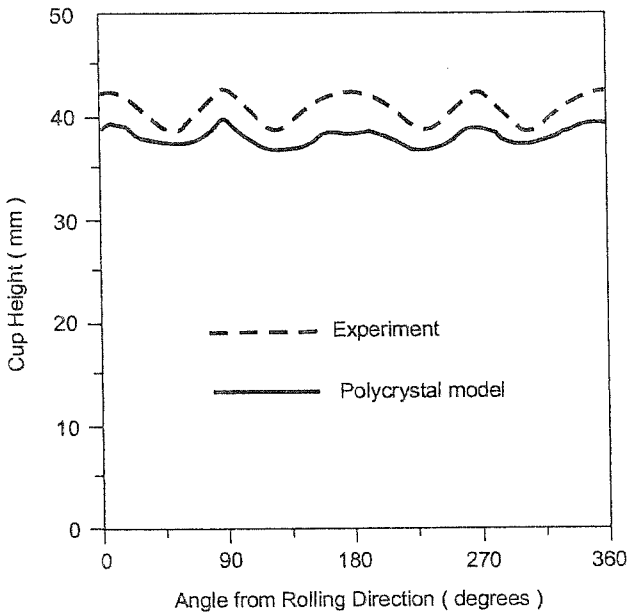

Figure 1-3 Deep drawing of a cylindrical cup: comparison between experimental and computed earing profiles for Al2008-T4 sheet (polycrystal model, Anand *et al.* 1997).

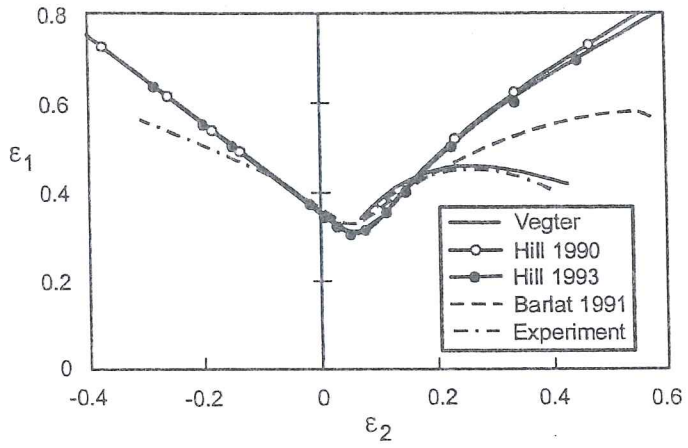

Figure 1-4 FLD predictions applied on bi-axial pre-strained specimens of an IF steel, using different yield loci and comparison with experiments (models with phenomenological description of yield locus, Vegter *et al.* 1999).

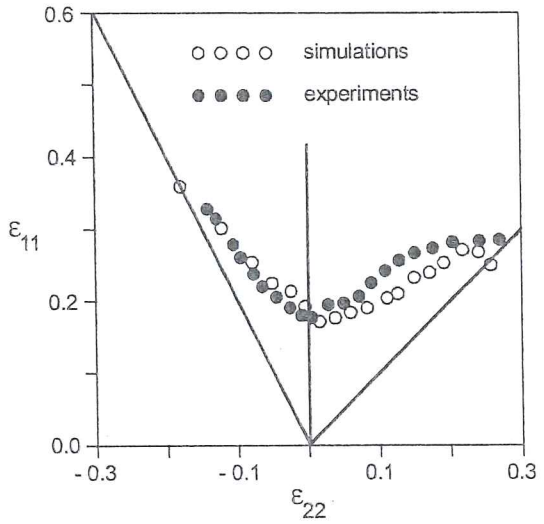

Figure 1-5 Polycrystal model predicted and measured FLD for as received AA6111-T4-C (polycrystal model, Wu *et al.* 1998).

Barlat 1987 has shown that the theoretical sheet forming limit strain at necking for balanced biaxial stretching is roughly 5 times larger for a material the yield surface of which is described by the von Mises criterion than for a material which follows the Tresca criterion, when all other properties are identical. This theoretical result, as well as the above figures and Marciniak Kuczynski's predictions, underline the importance of the yield locus shape.

References

Anand, L., Kothari, M. (1996) A Computational Procedure for Rate-Independent crystal plasticity, *J. Mech. Phys. Solids*, **44/4**, 525-558.

Anand, L., Balasubramanian S., Kothari, M. (1997) Constitutive Modeling of

Polycrystalline Metals at Large Strains : Application to Deformation Processing, *Large plastic deformation of crystalline aggregates*, International Centre for Mechanical Sciences, Courses and Lectures n° **376**, Springer Ed, 109-172.

Barlat, F., Becker, R.C., Hayashida, Y., Maeda, Y., Yanagawa, M., Chung, K., Brem, J.C., Lege, D.J., Matsui, K., Murtha, S.J., Hattori, S. (1997) Yielding description for solution strengthened aluminium alloys, *Int. J. of Plasticity*, **13-4**, 385-401.

Beaudoin, A.J., Dawson, P.R., Mathur, K.K., Kocks, U.F. (1995) A hybrid finite element formulation for polycrystal plasticity with consideration of macrostructural and microstructural linking, *Int. J. Plasticity*, **11/5**, 501-521.

Bunge, H.J., Esling, C. (1997) Texture et anisotropie des materiaux, *Techniques de l'ingénieur*, M 605/9, 1-39.

Duchêne L., Godinas A., Habraken, A.M.(1999) Metal Plastic Behaviour linked to Texture Analysis and FEM Method, NUMISHEET '99, 4th Int. Conf. and Workshop on Numerical Simulation of 3D Sheet Forming Processes, Besançon, France, 13-17 September 1999, Edité par J.C. Gélin, P. Picart, Université de Franche-Comté et ENSMM, 97-102.

Imbault, D. (1993) Un modèle micro-macro analytique pour la plasticitié des polycristaux anisotropes, thèse de docteur de l'Institut National Polytechnique de Grenoble.

Kumar, A., Dawson, P.R. (1996) The simulation of texture evolution with finite elements over orientation space, I. Development, *Comp. Methods Appl. Mech. Eng.*, **130**, 227-246.

Lequeu, Ph., Gilormini, P., Montheillet, F., Bacroix, B., Jonas, J.J. (1987) Yield surfaces for textured polycrystals, I. Crystallographic Approach, *Acta Metall.*, **35/2**, 439-451.

Nakamachi, E., Xie C.L., Hiraiwa, K., Harimoto, M. (1999) Development of elastic/crystalline viscoplastic finite element analysis code based on the meso-phenomenological material modeling, Numisheet'99, 13-17 September 1999, vol. 1, Besançon, France, 79-84.

Pijlman, H.H., Huetink, J., Carleer, B.D., Vegter, H. (1998) Application of the Vegter yield criterion and a physically based hardening rule on simulation of sheet forming, *Simulation of Materials Processing : Theory, Methods and Applications*, Balkema, Huetink & Baaijens Eds.

Teodosiu, C. (1997) Dislocation modelling of crystal plasticity, *Large plastic deformation of crystalline aggregates*, International Centre for Mechanical Sciences, Courses and Lectures n° **376**, Springer Ed, 21-80

Tourki, Z., Zeghloul, A., Ferron, G. (1996) Sheet metal forming simulations using a new model for orthotropic plasticity, *Computational Materials Science*, **5**, 255-262.

Van Houtte, P. (1994) Application of plastic potentials to strain rate sensitive and insensitive anisotropic materials, *Int. J. Plasticity*, **10**, 719-748.

Van Houtte, P. (1995) Micromechanics of polycrystalline materials, Chaire Francqui, Université de Liège.

Vegter, H., An Y., Pijlman H.H., Huetink J. (1999), Different approaches to describe

the plastic material behaviour of steel and aluminium-alloys in sheet forming, 2nd *ESAFORM Conference on Material Forming*, Guimaraes, Portugal, Covas J.A. Ed.

Wu, P.D., Neale, K.W., Van Der Giessen, E. (1998) Effects of strain paths on sheet metal limit strains, *Material Instabilities in Solids*, John Wiley&Sons Ltd, de Borst R.&Van der Giessen E., Eds.

2. ANISOTROPIC PHENOMENOLOGICAL YIELD LOCI

2.1. Initial shape of yield loci

The yield locus is the boundary between the elastic and plastic domains. It is a continuous surface in stress space, $F_p(\sigma_{ij}) = 0$, corresponding to all stress states that cause yielding. During plastic deformation, the updated yield locus will expand or contract, translate and distort. In this section, the initial shape of the yield locus associated with the first yielding is analyzed. Experimental evidence and theoretical considerations concerning the plastic behavior of materials have led to some restrictions on the mathematical representation of a yield surface. Following Bridgman's experimental observations (Bridgman 1923, 1952), hydrostatic pressure (25000 bars) does not induce plasticity in metals. More recently, Barlat *et al.* 1991 have measured a relative density change due to plastic deformation of the order of 10^{-3}. Extrapolating an approximate limit analysis of a porous medium, Gurson's model 1977 proposes a plastic behavior law affected by pressure. His goal is fracture prediction and far from rupture, the pressure effect is limited. In a hot sintering process, the initial porosity can be very high and the pressure effect is important. However, in general cases of sound classical metals characterized by low porosity, yield surfaces are taken to be pressure independent. Drucker (1951) showed that, based on a stability postulate, the yield surface must be convex. If the yield function is smooth with no vertex, convexity ensures the uniqueness of the plastic strain rate for a given stress state.

Mathematically, the yield surface F_p is convex if, for given stresses σ_{ij} and plastic strain rates $\dot{\varepsilon}_{ij}^p$, any stress state σ_{ij}^* inside or on the yield surface obeys the following relationship:

$$(\sigma_{ij} - \sigma_{ij}^*)\dot{\varepsilon}_{ij}^p \geq 0 \tag{2-1}$$

If the function F_p is twice differentiable, its Hessian matrix H is defined by :

$$H_{ij} = \frac{\partial^2 F_p}{\partial \sigma_i \partial \sigma_j} \tag{2-2}$$

F_p is convex if the H matrix is semi-definite, that is, if its eigenvalues are positive or zero. Another consequence of Drucker's 1951 postulate is that the flow rule for stable materials is associated. The yield surface is the same as the plastic potential, so the strain rate vector is orthogonal to the yield surface. The associated flow rule is:

$$\dot{\varepsilon}_{ij}^p = \dot{\lambda}\frac{\partial F_p}{\partial \sigma_{ij}} \tag{2-3}$$

Hecker 1976 or Phillips 1986, who reviewed numerous critical experiments to assess the yield surface shape, found that the normality rule was never violated. This is also confirmed by the work of Hayakawa & Murakami 1998 in damage mechanics. Indeed, all the yield surfaces listed hereafter respect these 3 characteristics. Table 1 summarizes the evolution of the well-known Hill's 1948 equation. Then Table 2 introduces Barlat's and Karafillis' models. Ferron-Tourki's model is presented next. Finally, Vegter's models are presented since they seem to be well validated and adapted to FEM computations. In addition to these tables, some comments help to understand the origin of the presented models, their parameters identification method as well as their experimental validation. Let us note that except for Karafillis'model and Vegter's model, all the others are restricted to anisotropic materials exhibiting orthotropic symmetry, i.e. to materials which possess 3 mutually orthogonal planes of symmetry at every point. Actually, most scientists agree that this restriction is not a very significant constraint because most mechanically processed materials are orthotropic in their initial state. Typical examples are rolled sheets or plates.
Hereafter, when an angle α defines a direction, the reference is always the Rolling Direction (RD). For instance, the notation σ_α means the current yield stress in uniaxial tension along a direction at an angle α with the Rolling Direction. An anisotropic plastic model defined by $F(\sigma_{ij})=0$ can be used only if the reference axes are defined. They are often chosen as the material orthotropic directions : x =Rolling Direction = RD, y =Tranverse Direction = TD, z = Thickness or Normal Direction = ND.
Other reviews of phenomenological anisotropic models can be found in Vial *et al.* 1983, Kobayashi *et al.* 1985, Barlat 1987, Arminjon *et al.* 1994, Mahmudi 1995, Kuwabara & van Bael 1999, Banabic 2000. Note that the present work and Banabic's 2000 review were conducted separately but at the same moment. Both reviews have selected nearly identical models as the most appropriate to simulate metal sheet behavior.

2.1.1. Hill's approach

Table 1 is dedicated to Hill's research. The classical quadratic yield criterion, **Hill 1948** (Table 1), is well suited to specific metals and textures, but lacks flexibility. As mentioned in Vial *et al.* 1983, Hill's old criterion gives a better correlation with metals having an average Lankford's coefficient $\bar{r}$ greater than 1 but is less acceptable when $\bar{r}$ is less than 1. This average value is computed by:

$$\bar{r}=\frac{1}{4}(r_0+2r_{45}+r_{90}) \qquad (2\text{-}4)$$

This proposal has advantages that explain its intensive use:
-it improves the simple assumption of neglecting anisotropy,
-it is simple to implement in a FEM code and available in numerous commercial codes,
-only 3 tensile tests at 0°, 45°, 90° are required to determine the material parameters.

Law Name	Description	Characteristics	References
Hill 1948	$F(\sigma_y-\sigma_z)^2+G(\sigma_z-\sigma_x)^2+H(\sigma_x-\sigma_y)^2$ $+2L\tau_{yz}^2+2M\tau_{zx}^2+2N\tau_{xy}^2=2\sigma_F^2$	General quadratic equation with 6 parameters, crude approximation of the yield surface shape computed from polycrystal models.	Hill 1948,Vial 1997, Barlat *et al.* 1991, Vial & Hosford 1983,...
Hill 1979	$F\lvert\sigma_y-\sigma_z\rvert^a+G\lvert\sigma_z-\sigma_x\rvert^a+H\lvert\sigma_x-\sigma_y\rvert^a$ $+A\lvert2\sigma_x-\sigma_y-\sigma_z\rvert^a+B\lvert2\sigma_y-\sigma_z-\sigma_x\rvert^a$ $+C\lvert2\sigma_z-\sigma_x-\sigma_y\rvert^a=\sigma_F^a$	Hill with variable exponent (non integer) and no shear stress term so that orthotropic material axes and principal stress axes must be superimposed.	Vial 1997, Barlat *et al.* 1991, Suh *et al.* 1996, Vial & Hosford 1983.
Hill 1990	$\lvert\sigma_1+\sigma_2\rvert^a+\frac{\sigma_b^a}{\tau^a}\lvert\sigma_1-\sigma_2\rvert^a+\left\lvert\sigma_1^2+\sigma_2^2\right\rvert^{\frac{a}{2}-1}$ $\left\{2A(\sigma_1^2-\sigma_2^2)+B(\sigma_1-\sigma_2)^2\cos 2\beta\right\}=(2\sigma_b)^2$	Extension of Hill 79 that suppresses its limitation in loading directions but is only defined for plane stress case.	Hill 1990 Barlat *et al.* 1991, Vegter *et al.*1999, Kuwabare & van Bael 1999.
Hill 1993	$\frac{\sigma_x^2}{\sigma_0^2}-C\frac{\sigma_x\sigma_y}{\sigma_0\sigma_{90}}+\frac{\sigma_y^2}{\sigma_{90}^2}+$ $\left\{(A+B)-\frac{(A\sigma_x+B\sigma_y}{\sigma_b}\right\}\frac{\sigma_x\sigma_y}{\sigma_0\sigma_{90}}=1$	Expression enabling to model different r_0 and r_{90} values, when uniaxial stresses in rolling σ_0 and tranversal σ_{90} direction are almost equal. Only defined for plane stress case and loads applied along orthotropic axes (no shear component).	Hill 1993, Banabic 1996, Banabic,*et al.* 1999, Vegter *et al.* 1999.

Notations :

$A,B,C,F,G,H,L,M,N,\ a$ = material parameters

$\sigma_x,\sigma_y,\sigma_z,\tau_{xy},\tau_{zx},\tau_{yz}$ = stress components in the material orthotropic axes

σ_1,σ_2 = principal stress components oriented by an anticlockwise angle β with the RD axis

σ_b = yield value under plane equibiaxial stress state

τ = yield stress in pure shear test parallel to orthotropic axes (plane stress case)

σ_F= yield stress under uniaxial tension in a reference direction

Table 1 Hill's models.

Hill's 1979 equation (Table 1) is a proposal that adds linear combinations of the deviatoric stresses affected by a *non integer exponent a.* As checked by various authors (see Table 1), this law offers sufficient flexibility when orthotropy and loading are co-axial. This is however a strong limitation.

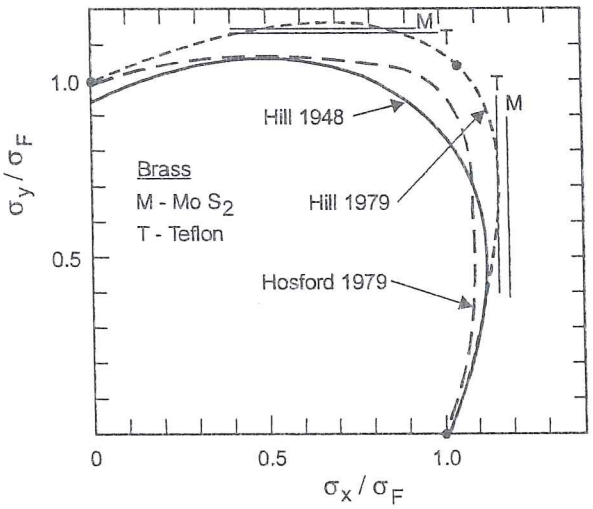

Figure 2-1 Comparison of experimental data with predicted yield loci normalized by uniaxial tension at a strain of 0.1. Experimental data are indicated by solid points and by horizontal and vertical tangents obtained from plane-strain tests (from Vial *et al.* 1983).

When applied to plane stress state and in-plane isotropy, Hill's 1979 proposal reduces to :

$$|\sigma_1+\sigma_2|^a+(1+2\bar{r})\ |\sigma_1-\sigma_2|^a=2(1+\bar{r})\sigma_F^a \qquad (2\text{-}5)$$

So, 3 tensile tests at 0°, 45°, 90° are necessary to reach $\bar{r}$ and Wagoner 1980 proposes a method for calculating a by comparing plane-strain and uniaxial stress-strain curves. Suh *et al.* 1996 have checked that using a variable value of a for 2008-T4 aluminum enables to improve Hill's 1979 predictions.

In Suh's study, the exponent used to simulate the behavior of 70/30 brass with Hill's 1979 model has shown minor change, so that a constant value gives quite accurate results. In fact, a variable a exponent is one way to relax the isotropic hardening assumption.

In 1990, Hill proposes a new yield criterion (**Hill 1990** Table 1) adapted to in-plane anisotropy and to any loading orientation. It reduces to Hill 1948 when a=2 and recovers Hill 1979 when both A and B vanish. It can be checked that the relation defined in Table 1 is equivalent to a homogeneous function of degree a if the stress components are expressed in the orthotropic axes. If the exponent a is known, the material parameters A and B are computed from the results σ_0, σ_{45}, σ_{90} of uniaxial

tests in directions 0°, 45° and 90° and from the yield stress σ_b under equibiaxial tension:

$$A=\frac{1}{4}\left[\left(\frac{2\sigma_b}{\sigma_{90}}\right)^a-\left(\frac{2\sigma_b}{\sigma_0}\right)^a\right] \qquad B=\frac{1}{2}\left[\left(\frac{2\sigma_b}{\sigma_0}\right)^a+\left(\frac{2\sigma_b}{\sigma_{90}}\right)^a\right]-\left(\frac{2\sigma_b}{\sigma_{45}}\right)^a \tag{2-6}$$

The following relation can be used to replace the ratio σ_b^a / τ^a :

$$1+2r_{45}=-\frac{\sigma_b^a}{\tau^a} \tag{2-7}$$

Hill does not explicitly define a calibration method. However, the 3 preceding equations, coupled with the predicted yield stress σ_α for uniaxial tensions performed in directions doing an angle α with the rolling direction:

$$\left(\frac{2\sigma_b}{\sigma_\alpha}\right)^a=1+\frac{\sigma_b^a}{\tau^a}-2A\cos 2\alpha+B\cos^2 2\alpha \tag{2-8}$$

allow to reach the 5 parameters : σ_b, τ, A, B, a.

Hill's 1993 proposal aims to model materials characterized by extreme properties such as $\sigma_0=\sigma_{90}$ together with $r_0 \neq r_{90}$, or by $r_0=r_{90}$ together with $\sigma_0 \neq \sigma_{90}$. The equation is defined in Table 1 and the 3 constants A,B,C can be reached thanks to the following relations (Hill 1993), which require results from uniaxial tests in directions 0° and 90° and from equibiaxial tension:

$$\frac{C}{\sigma_0\sigma_{90}}=\frac{1}{\sigma_0^2}+\frac{1}{\sigma_{90}^2}+\frac{1}{\sigma_b^2} \tag{2-9}$$

$$\left(\frac{1}{\sigma_0}+\frac{1}{\sigma_{90}}-\frac{1}{\sigma_b}\right)A=\frac{2r_0(\sigma_b-\sigma_{90})}{(1+r_0)\sigma_0^2}-\frac{2r_{90}\sigma_b}{(1+r_{90})\sigma_{90}^2}+\frac{C}{\sigma_0} \tag{2-10}$$

$$\left(\frac{1}{\sigma_0}+\frac{1}{\sigma_{90}}-\frac{1}{\sigma_b}\right)B=\frac{2r_{90}(\sigma_b-\sigma_0)}{(1+r_{90})\sigma_{90}^2}-\frac{2r_0\sigma_b}{(1+r_0)\sigma_0^2}+\frac{C}{\sigma_{90}} \tag{2-11}$$

The parameters are very easy to reach and, as checked by Banabic *et al. 99*, Hill 93 provides a quite good correlation with experimental results (Figure 2-2).

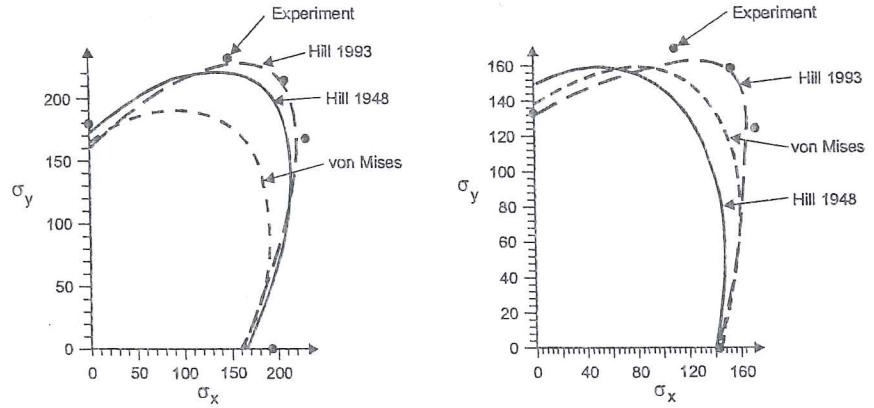

Figure 2-2 Yield loci obtained from biaxial tensile tests and compared with computed yield functions; stresses in MPa (from Banabic *et al.* 1999).

Vegter *et al.*1999 show an application of Hill 1990 and Hill 1993 criteria (Figure 2-3).

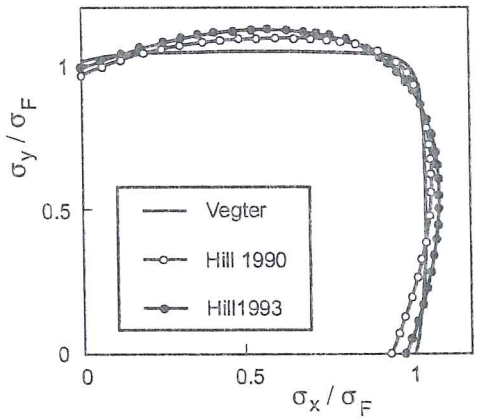

Figure 2-3 Comparison of yield loci : Vegter's line passes through the experimental points for Al-6000 (from Vegter *et al.* 1999).

2.1.2. Barlat's and Karafillis' approach

The presentation of Karafillis *et al.* 1993 is reproduced here as it provides a nice general frame to explain his proposal as well as Barlat's 1989 and 1991. First looking at isotropic yield surfaces, Karafillis recalls that Mendelson 1968 has shown the existence of bounds in an isotropic yield surface of a material with a fixed yield stress in uniaxial tension. These bounds are derived from symmetry and convexity considerations. The lower bound coincides with the limiting maximum shear stress yield surface as described by Tresca's 1864 criterion, whereas the upper bound was proposed by Hosford 1972. In the deviatoric plane section of the yield surface, the lower bound is inscribed in the von Mises' yield circle which, in turn, is inscribed in the upper bound hexagon (Figure 2-4). This deviatoric plane, also called Π plane, is perpendicular to the line representing hydrostatic pressure states and contains the

stress origin point. The relations to compute the projection of a stress state onto the Π plane can be found in van Bael 1994 or Khan & Huang 1995.

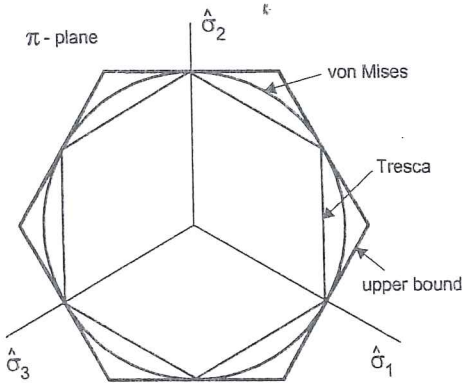

Figure 2-4 The upper bound, the lower bound and the von Mises' yield surface in the Π-plane (from Karafillis *et al.* 1993).

Isotropic yield surfaces lying between the bounds defined by von Mises' yield surface and Tresca's yield surface can be mathematically described by **Hosford's 1972 criterion**. His proposal is a modification of the von Mises' mathematical description of a yield surface, where an exponent other than 2 is used:

$$(\hat{\sigma}_1 - \hat{\sigma}_2)^{2a} + (\hat{\sigma}_2 - \hat{\sigma}_3)^{2a} + (\hat{\sigma}_3 - \hat{\sigma}_1)^{2a} = 2\sigma_F^{2a} \qquad (2\text{-}12)$$

with a integer >1, $\hat{\sigma}_1\ \hat{\sigma}_2\ \hat{\sigma}_3$ the principal values of the deviatoric stress tensor $\underline{\hat{\sigma}}$ and σ_F the yield stress under uniaxial tension. This relation is equivalent to von Mises' equation when a=1 and to Tresca's equation when a=∞. Intermediate values of a describe all the yield surfaces lying between the two proposals (Figure 2-5). Equation (2-12) is identical to relation "Karafillis 1993 (a)" in Table 2 if $\underline{\hat{\sigma}}$ is substituted by $\underline{s}$.

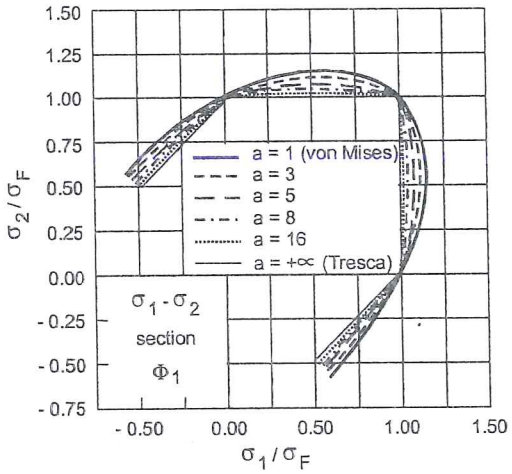

Figure 2-5 Different isotropic yield surfaces between the von Mises' yield surface and the lower bound (Tresca), sections in principal stress plane (from Karafillis *et al.* 1993).

Law Name	Description	Characteristics	References
Barlat 1989	$A\lvert K_1+K_2\rvert^a + A\lvert K_1-K_2\rvert^a + (2-A)\lvert 2K_2\rvert^a = 2\sigma_F^a$ (a) $K_1 = (\sigma_x + h\sigma_y)/2$ (b) $K_2 = \sqrt{\left[(\sigma_x - h\sigma_y)/2\right]^2 + (p\sigma_{xy})^2}$ (c)	Generalization of isotropic Hosford's (1972) equation with a shear term, defined by 4 parameters, *a, h, p, A* plane stress case.	Vial 1997, Barlat &Lian 1989, Berg *et al.* 1998, Moshfegh *et al.* 1998, Andersson *et al.* 1999.
Barlat 1991	$\lvert s_1-s_2\rvert^a + \lvert s_2-s_3\rvert^a + \lvert s_3-s_1\rvert^a = 2\sigma_F^2$ (a) with $\underline{s} = \underline{\underline{L}}\ \underline{\sigma}$ (b) $\underline{\underline{L}} = \begin{bmatrix} (c_2+c_3)/3 & -c_3/3 & -c_2/3 & 0 & 0 & 0 \\ -c_3/3 & (c_3+c_1)/3 & -c_1/3 & 0 & 0 & 0 \\ -c_2/3 & -c_1/3 & (c_1+c_3)/3 & 0 & 0 & 0 \\ 0 & 0 & 0 & c_4 & 0 & 0 \\ 0 & 0 & 0 & 0 & c_5 & 0 \\ 0 & 0 & 0 & 0 & 0 & c_6 \end{bmatrix}$ (c)	Generalization of isotropic Hosford's (1972) equation with a shear term, defined by 6 anisotropy coefficients c_1 to c_6 + exponent *m* adapted for general stress state and orthotropic symmetric material. The 4th order tensor can be represented by a 6x6 matrix in the axis of orthotropic symmetry (RD, TD, ND).	Barlat *et al.* 1991, Hayashida *et al.*1995, Suh *et al.* 1996, Vegter *et al.* 1999.
Karafillis 1993	$\Phi_1 = \lvert s_1-s_2\rvert^{2a} + \lvert s_2-s_3\rvert^{2a} + \lvert s_3-s_1\rvert^{2a} = 2\sigma_F^{2a}$ (a) $\Phi_2 = s_1^{2a} + s_2^{2a} + s_3^{2a} = \frac{2^{2a}+2}{3^{2a}}\sigma_F^{2a}$ (b) $\Phi = (1-C)\Phi_1 + C\frac{3^{2a}}{2^{2a-1}+1}\Phi_2 = 2\sigma_F^{2a}$ (c) $\underline{s} = \underline{\underline{L}}\ \underline{\sigma}$ with $\underline{\underline{L}}$ tensor 4th order (d)	Generalization of Barlat's 91 work to non orthotropic material.	Karafillis & Boyce 1993, Andersson *et al.* 1999 Barlat *et al.* 1997.
Barlat 1997	$\Phi = A\lvert s_1-s_2\rvert^a + B\lvert s_2-s_3\rvert^a + C\lvert s_3-s_1\rvert^a = 2\sigma_F^a$ with $\underline{s}$ and $\underline{\underline{L}}$ defined as in Barlat 1991	Extension of Barlat 1991 to model high pure shear yield stress and to better fit r_0 and r_{90} (plane stress case).	Barlat *et al.* 1997 Vegter *et al.* 1999.

s_1, s_2, s_3 = eigenvalues of tensor $\underline{s}$

$\underline{\sigma}$ = stress tensor in orthotropic axes

$\underline{\underline{L}}$ = linear operator

$\sigma_x, \sigma_y, \sigma_{xy}$ = stress components on the orthotropic axes

σ_F = uniaxial plastic stress in a reference direction

Table 2 Barlat's and Karafillis' models.

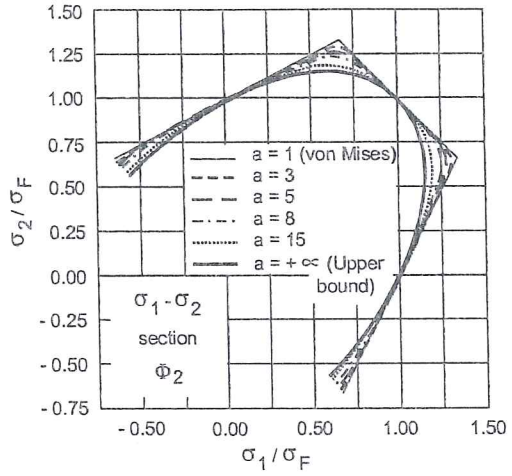

Figure 2-6 Different isotropic yield surfaces between the von Mises' yield surface and the upper bound : sections in principal stress plane (from Karafillis *et al.* 1993).

In fact, the surfaces lying between von Mises' yield surface and the upper bound (Figure 2-6) are described by "Karafillis 1993 (b)" in Table 2 if $\underline{s}$ is substituted by $\hat{\underline{\sigma}}$. When $a=1$ the yield surface corresponds to von Mises' yield surface whereas when $a=\infty$ the upper bound yield surface is recovered. So to describe a generic isotropic yield surface lying between the lower bound and the upper bound, a generalized mathematical relation mixing Karafillis 1993 relations (a) and (b) in Table 2 is needed. It is the goal of relation (c) where the constant C belong to [0,1]. If $a=15$ is chosen, Φ_1 and Φ_2 describe yield surfaces very close to the lower and the upper bound respectively. By varying the value of the mixing factor C, a family of yield surfaces is created which spans the space between the 2 bounds, set by the selection of a (Figure 2-7).

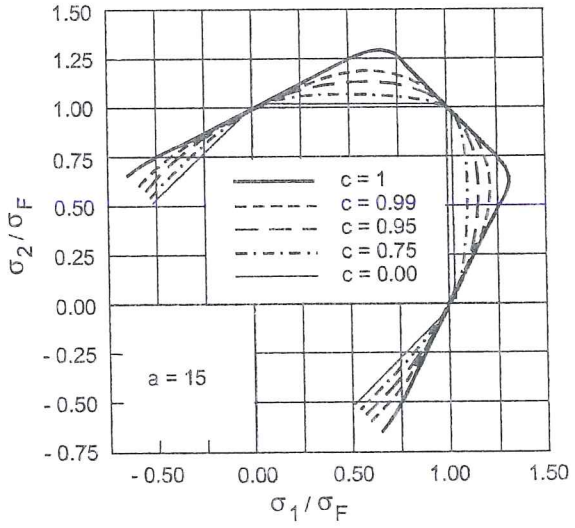

Figure 2-7 Different isotropic yield surfaces between the lower bound (Tresca) and the upper bound : sections in principal stress plane (from Karafillis *et al.* 1993).

Barlat *et al.* **1991** use a linear transformation of the 6 components of a stress state (Barlat 1991b, Table 2). The obtained transformed stress state is then used in Hosford's 1972 yield criterion (2-12). The 6 parameters describing anisotropy can be deduced from uniaxial yield stresses measured at 0°,45°,90° from the rolling direction. The exponent a can take any real value larger than 1 but practically, a should be larger than 6, depending on the anisotropy induced by texture and on the crystal type. In fact, a can be tuned to optimize the predictions of the yield locus shape.

Barlat's 1989 work already contains the same type of approach but is limited to plane stress state (see Table 2). This formulation has the advantage of clearly showing the effect of the shear component which modifies the sections of the yield locus (Figure 2-8, Figure 2-9, Figure 2-10). The 4 parameters A,h,p,a of Barlat's 1989 model are determined as explained by Barlat & Lian 1989 or Berg *et al.* 1998: a= 6 for b.c.c. metals; a= 8 for f.c.c. metals (from numerous polycrystal model comparisons)

$$A = 2 - 2\sqrt{\frac{r_0}{1+r_0}\frac{r_{90}}{1+r_{90}}} \qquad h = \sqrt{\frac{r_0}{1+r_0}\frac{r_{90}}{1+r_{90}}} \tag{2-13}$$

$$p = \frac{\sigma_F}{\tau}\left(\frac{2}{2A + 2^a(2-A)}\right)^{1/a} \tag{2-14}$$

where σ_F is the yield stress in uniaxial tension, τ is the yield stress for pure shear. In practice, p varies since the ratio $\frac{\sigma_F}{\tau}$ is not a constant function of the equivalent strain. This affects the shape of the yield surface as demonstrated by Berg *et al.* 1998. It is worth mentioning that Barlat 1991 does not reduce to Barlat 1989 in the plane stress case because the linear transformations of stresses are different in these two cases.

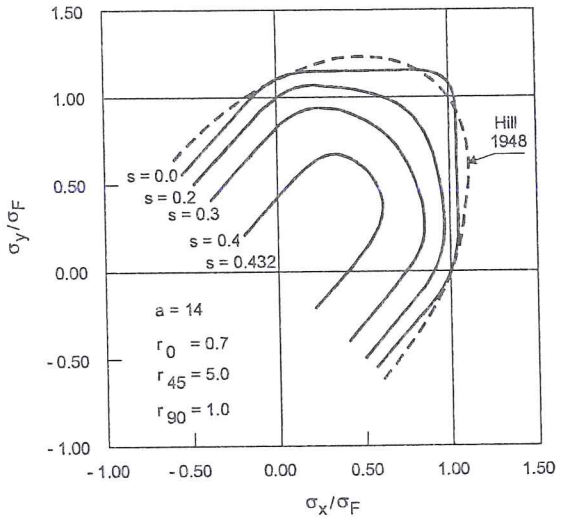

Figure 2-8 Plane stress yield surface proposed by Barlat & Lian 1989 where a=14, A, h, p are calculated with r_0=0.7, r_{90}=1, r_{45}=5 and $S = \sigma_{xy}/\sigma_F$; (material containing 50% brass texture and 50% of randomly distributed grains), adapted from Barlat & Lian 1989.

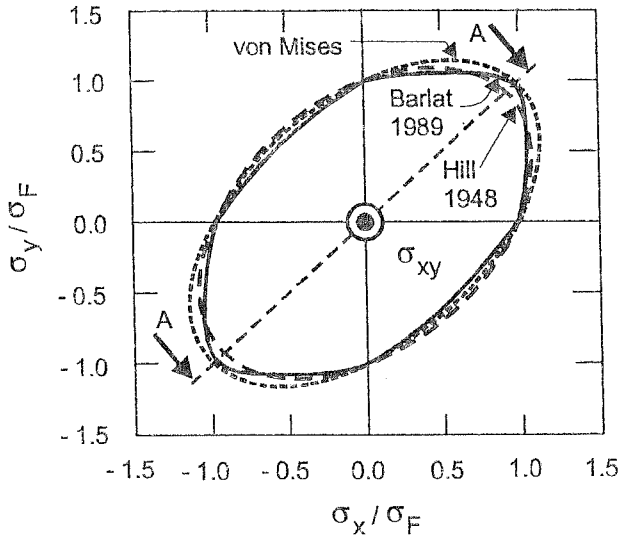

Figure 2-9 Comparison of yield surfaces of Al 2024 aluminium alloy for $\sigma_{xy} = 0$ (from Berg *et al.* 1998).

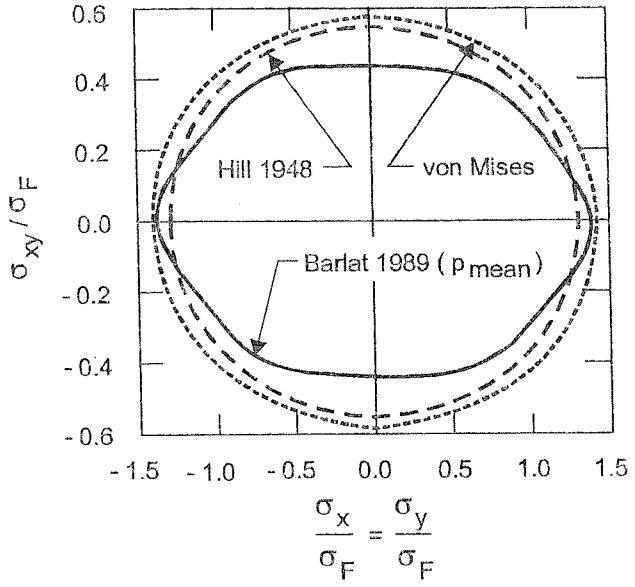

Figure 2-10 Cross section A_A of the yield surfaces of Figure 2-9, (from Berg *et al.* 1998).

For anisotropic material, Barlat 1991 as well as **Karafillis** *et al.*, **1993** consider a tensor $\underline{s}$, resulting of a linear transformation $\underline{\underline{L}}$ of the actual stress tensor $\underline{\sigma}$. In the case of isotropic material, this linear transformation simply yields the deviatoric stress tensor of the actual material stress state. This explains why, in the general anisotropic case, Karafillis calls the transformed tensor $\underline{s}$ "*isotropic plasticity equivalent deviatoric stress tensor*". Then, as in Barlat's 1991 proposal, Karafillis introduces his transformed tensor $\underline{s}$ in an isotropic yield criterion. Of course he chooses the general one described above. The fourth order tensor $\underline{\underline{L}}$ used by

Karafillis to transform the stress is more flexible than the simple choice made by Barlat and can be associated with material symmetries which range from the lowest level of triclinic symmetry to the highest level of full symmetry (Table 3).

Material symmetry	Rotations which leave $\underline{\underline{L}}$ invariant	Number of independent elements of $\underline{\underline{L}}$
Triclinic	No rotation	15
Monoclinic	$\underline{R}_2^{\pi}$	8
Orthotropic	$\underline{R}_1^{\pi}, \underline{R}_2^{\pi}$	6
Trigonal	$\underline{R}_3^{2\pi/3}, \underline{R}_1^{\pi}$	4
Tetragonal	$\underline{R}_3^{\pi/2}, \underline{R}_1^{\pi}$	4
Transversely isotropic	all $\underline{R}_3^{\phi}, \underline{R}_1^{\pi}$	3
Cubic	$\underline{R}_1^{\pi/2}, \underline{R}_2^{\pi/2}, \underline{R}_3^{\pi/2}$	2
Isotropic	All rotations	1

R_i^{ϕ} denotes a rotation about the i-axis by the angle ϕ.

Table 3 Characteristics of $\underline{\underline{L}}$ tensor according to material symmetry from Karafillis *et al.* 1993.

This provides a potential for the representation of any anisotropic state of the material. More details on symmetry properties and constraints applied to $\underline{\underline{L}}$ can be found in Karafillis *et al.* 1993. Finally, for orthotropic materials, 3 uniaxial tensile tests of specimens cut at 0°, 45°, 90° with respect to rolling direction allow to completely determine C and $\underline{\underline{L}}$. Remark that, in this orthotropic case, Karafillis' transformation tensor $\underline{\underline{L}}$ reduces to Barlat's 1991 (Table 2). Figure 2-11 and Figure 2-12 show Karafillis'results compared with other models and experiments.

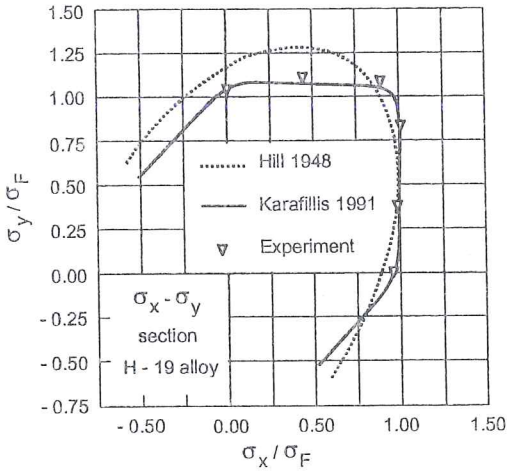

Figure 2-11 The yield surface of the H-19 can stock aluminum alloy in the orthotropic stress axes (from Karafillis *et al.* 1993).

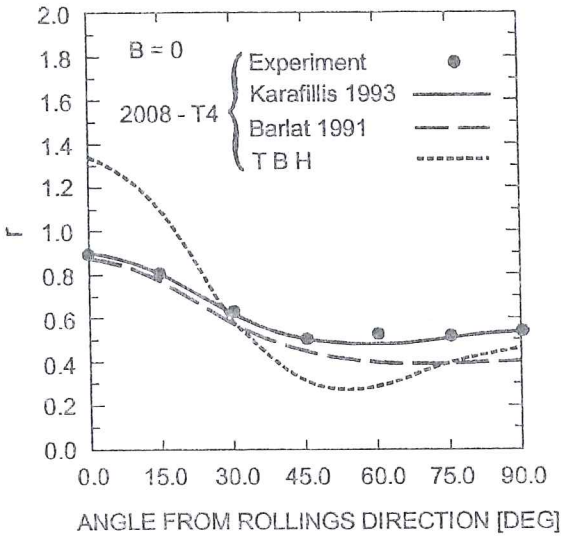

Figure 2-12 Lankford coefficient as a function of the angle with the rolling direction for 2008-T4 aluminum alloy , TBR =Taylor 1938-Bishop & Hill 1951 polycrystal model, (from Karafillis *et al.* 1993).

Hill 1948 (Table 1), Barlat 1989 and Karafillis 1993 (Table 2) were implemented in the commercial code LS-DYNA3D. Andersson *et al.* 1999 use it to simulate deep drawing tests of aluminum sheets and compare their FEM results to experiments. Their results show that Karafillis'model yields the best agreement with the experimental results and that CPU times are in the same range: Hill 1948 =1, Barlat 1989 =1.5 and Karafillis 1993 =1.1. Andersson *et al.* 1999 describe also the optimization code, they have developed, to identify Karafillis 1993 parameters from tensile tests in 3 different directions.

Barlat's 1997 proposal (Table 2) generalizes his 1991 model, as Barlat has checked that the additional coefficient C proposed by Karafillis is an isotropic constant which does not help to reproduce the behavior of an Al-Mg sheet with 80% cold reduction. For the plane stress case, only 6 independent coefficients characterize anisotropy. They can be deduced from 4 tests: uniaxial tension at 0°, 45°, 90° to the rolling direction and equal biaxial bulge test. The proposed yield surface appears to fit nicely to experiments (Figure 2-13). However, if it is used to predict r ratios, it agrees with r_0 and r_{90}, but r_{45} is significantly under-estimated. This observation suggests that an additional parameter could be introduced in the formulation to accommodate r_{45}.

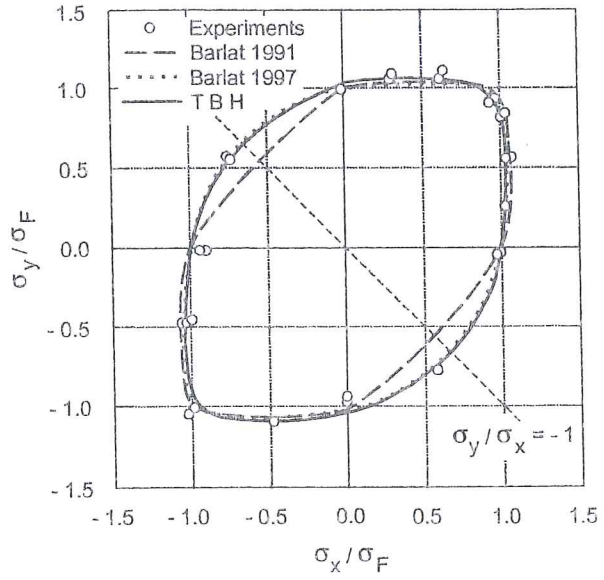

Figure 2-13 Yield surface for material : Al-2.5%Mg, 150 µm grain size, 80% cold reduction before annealing; experiments and yield function predictions from 3 models: Taylor-Bishop-Hill polycrystal, Barlat 1991 and Barlat 1997 (from Barlat *et al.* 1997).

2.1.3. A polar-coordinate representation of an orthotropic yield locus

Ferron *et al. 1994*, Tourki *et al. 1994*, Tourki *et al. 1996* investigate the form taken by the constitutive equations when orthotropic plasticity under plane stress is analyzed by using a polar coordinate representation of the yield surface in the principal stress space. They assume a parametric representation :

$$x_1 = \frac{\sigma_1 + \sigma_2}{2\sigma_b} = g(\theta,\beta)\cos\theta \qquad x_2 = \frac{\sigma_1 - \sigma_2}{2\sigma_b} = g(\theta,\beta)\sin\theta \tag{2-15}$$

where σ_b is the equibiaxial yield stress, β is an angle defining the orientation of the principal axes of the stress tensor with respect to the in-plane material anisotropy axes, $g(\theta,\beta)$ represents the length of the radius for a point on the yield locus in (x_1,x_2) axes, θ is the polar angle associated with the above polar coordinate description. This formulation is an extension of the one proposed by Budiansky 1984 in case of planar isotropy where the angle β is immaterial.

Looking at orthotropic symmetry, convexity and consistency of the yield function, Ferron *et al. 1994* propose a form of the $g(\theta,\beta)$ function. Then, they build a new criterion as an extension of Drucker's 1949 isotropic yield criterion expressed under plane stress in polar coordinate form. Their yield criterion for planar isotropy is :

$$(1-k)g(\theta)^{-6} = F(\theta) = (\cos^2\theta + A\sin^2\theta)^3 - k\cos^2\theta(\cos^2\theta - B\sin^2\theta)^2 \tag{2-16}$$

where A and B are dimensionless and positive constants. In case of planar anisotropy, it becomes :

$$(1-k)^{m/6} g(\theta,\beta)^{-m} = F(\theta)^{m/6} + 2a \sin\theta \cos^{2n-1}\theta \cos 2\beta + b \sin^{2p}\theta \cos^{2q} 2\beta \quad (2\text{-}17)$$

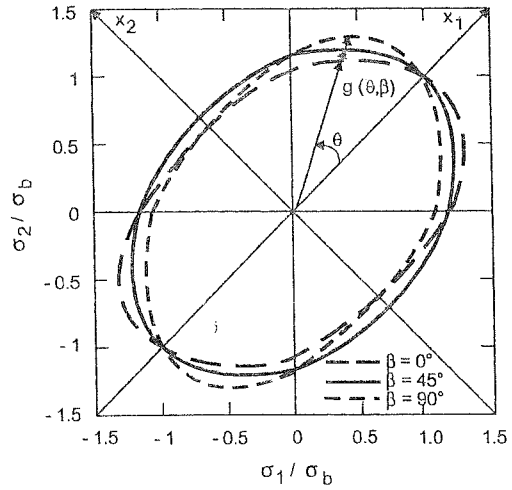

Figure 2-14 Polar coordinate representation of the yield surface in principal stress space (σ_1,σ_2), the yield loci are parameterized by angle β, (from Ferron *et al.* 1994).

This yield function involves 9 parameters: the 3 parameters k, A, B introduced to account for planar isotropy and the 6 parameters m, n, p, q, a, b depicting the orientation dependence of yielding. Remark that Hill 1948 is retrieved with k=0, m=2 and n=p=q=1. The effect of increasing k from 0 to some positive value, defining the limit for convexity, is to produce a flattening of the yield locus near pure shear and plane strain tension/compression. One property of the yield function (2-17) is to be able to accommodate a ratio of equibiaxial yield stress to uniaxial yield stress independently of the measured r-value in uniaxial tension. Increasing the exponents n and p leads to a decrease of the width of the annulus generated by the yield locus in (σ_1,σ_2) space when β varies (see Figure 2-14).

In practice, according to Ferron *et al.* 1994, a good fit of experimental or theoretical crystallographic data is generally obtained with m=n=p=2 and q=1, which leaves 5 parameters to identify. The appendix of this article accurately describes the way to determine these 5 material parameters. The 3 parameters k, A, B of the isotropic yield criterion can be deduced from 3 measurements : pure shear yield stress, equi-biaxial yield stress and Lankford coefficient. However a simplified approach using only uniaxial tension tests is available. For the anisotropic case, it is proposed first to determine k, A, B from a test performed for $\beta = \pi/4$, then to compute a and b from the experimental values of r_0 and r_{90} and of the parameters m,n,p,q.

Experimental validation for a mild steel is shown on Figure 1-2. Comparisons with Taylor-Bishop-Hill computations for a 2008-T4 aluminum alloy are presented on Figure 2-15, Figure 2-16, Figure 2-17. For this material, the parameters were identified as : k=0.55, A=2.2, B=3.71, m=n=p=2, q=1, a=0.24, b=0.47.

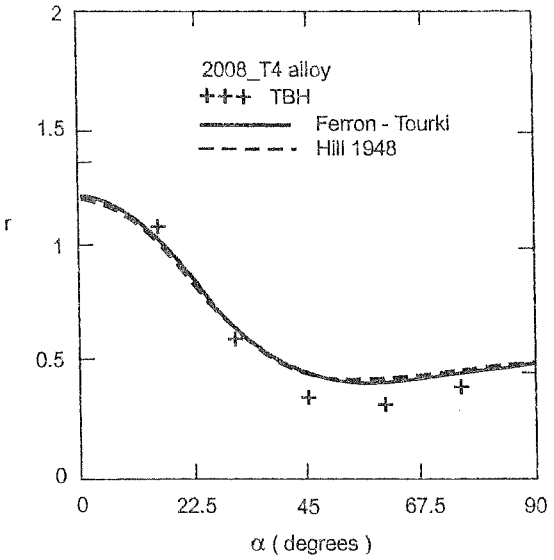

Figure 2-15 Orientation dependence of the Lankford coefficient for a 2008-T4 aluminum alloy according to Taylor-Bishop-Hill's approach, Hill's 1948 yield criterion or Ferron & Tourki's yield criterion (from Ferron *et al. 1994*).

These results confirm that shear or normal strains as well as stresses are well described by this model. Angle α characterizes the angle between the uniaxial tensile direction and the rolling direction.

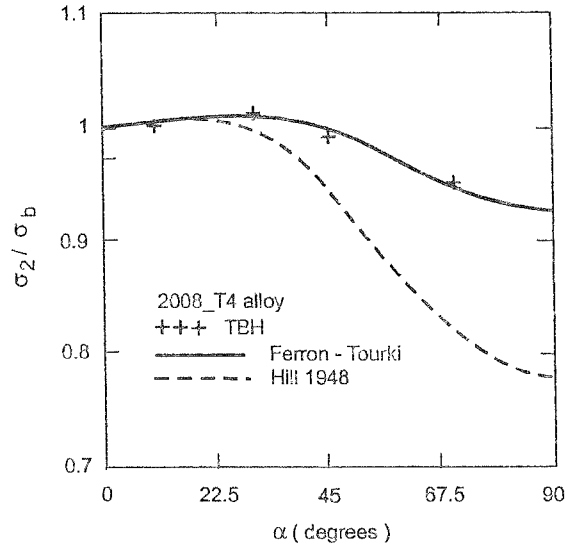

Figure 2-16 Orientation dependence of the normalized uniaxial yield stress for a 2008-T4 aluminum alloy according to Taylor-Bishop-Hill's approach, Hill's 1948 yield criterion or Ferron & Tourki's yield criterion (from Ferron *et al. 1994*).

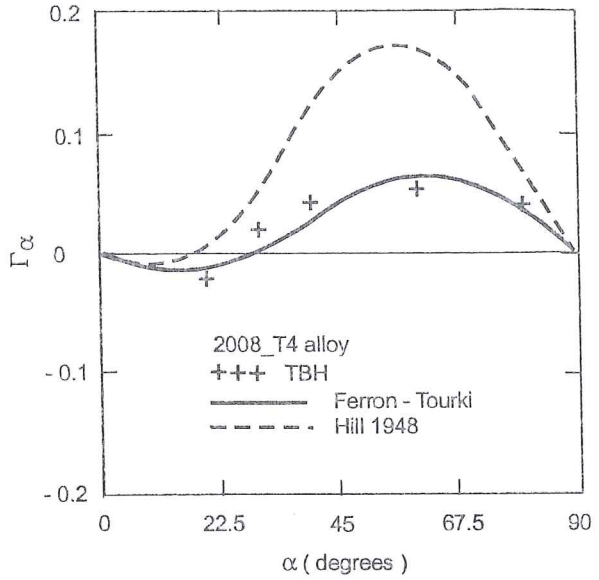

Figure 2-17 Orientation dependence of the shear parameters $\Gamma_\alpha = \dot{\varepsilon}_{12} / \dot{\varepsilon}_{11}$ in uniaxial tension for a 2008-T4 aluminum alloy according Taylor-Bishop-Hill's approach, Hill's 1948 yield criterion or Ferron & Tourki's yield criterion (from Ferron *et al. 1994*).

2.1.4. Vegter's approach

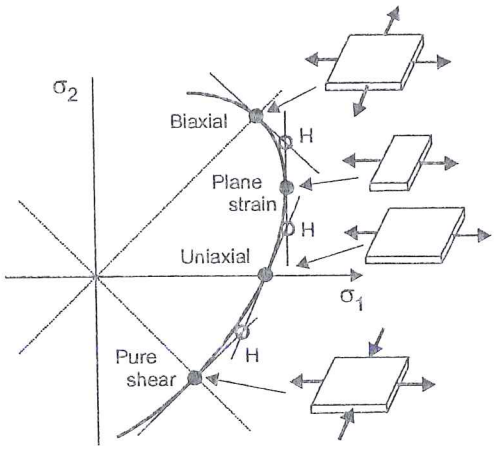

Figure 2-18 Vegter's yield locus in the principal stress space, reference points (black circles) defined by experiments and hinge points (white circle), adapted from Carleer *et al.*1997

Vegter's approach (Carleer *et al.*1997, Vegter 1998, Vegter *et al.* 1999a,b, Pijlam *et al.* 1998) proposes a yield criterion directly based on data of the pure shear test, the uniaxial test, the plane strain test and the biaxial test. Figure 2-18 clearly summarizes this criterion for a planar isotropic material behavior. A complete yield surface is described by 12 Bezier interpolation functions. When σ_1 and σ_2 are defined in such a way that $\sigma_1 \geq \sigma_2$, only the part of the surface beneath the line $\sigma_1 = \sigma_2$ is needed. As

the material is assumed to behave identically in tension and compression, the part of the surface beneath the line $\sigma_1 = -\sigma_2$ can be derived from the part above that line. As a result, the complete yielding of the material can be described using the measurements for a quarter of the yield surface. Vegter's yield function is restricted to plane stress state. It is defined as :

$$\sigma_{veg}(\sigma_x, \sigma_y, \sigma_{xy}) - \sigma_{yield} = 0 \tag{2-18}$$

where σ_{veg} is a kind of equivalent stress depending on the stress components in orthotropic axes $\sigma_x, \sigma_y, \sigma_{xy}$ and σ_{yield} is the yield stress.

In case of planar isotropic material behavior, σ_{yield} is the uniaxial yield stress σ_F. The second order Bezier interpolations allow to describe the normalized yield surface.

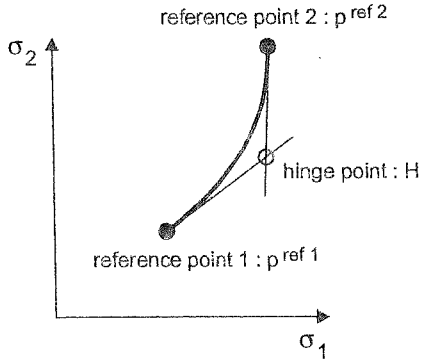

Figure 2-19 Bezier curve in Vegter's yield locus, adapted from Carleer *et al.*1997.

For a part going from reference point 1 to reference point 2 with hinge point H (Figure 2-19), one has :

$$\frac{\sigma_1}{\sigma_{veg}} = (1-\beta)^2 p_1^{ref1} + 2\beta(1-\beta) p_1^{hinge} + \beta^2 p_1^{ref2} \tag{2-19a}$$

$$\frac{\sigma_2}{\sigma_{veg}} = (1-\beta)^2 p_2^{ref1} + 2\beta(1-\beta) p_2^{hinge} + \beta^2 p_2^{ref2} \tag{2-19b}$$

where σ_1, σ_2 are principal stresses, β is a curvilinear coordinate increasing from 0 to 1 and representing the location on the curve between the reference points, $p_i^{ref\,j}$ and p_i^{hinge} are respectively the components i of the reference point j and the hinge point. Both equations (2-19a) and (2-19b) give an expression for σ_{veg}. Equating these expressions allows to find β as a solution of a second order equation. This solution is chosen to satisfy the condition $0 \leq \beta \leq 1$. The expression of σ_{veg} is then found by substituting β into (2-19a) or (2-19b).

For planar anisotropy, the 4 tests (pure shear, uniaxial, plane strain and biaxial tests) are performed for directions of 0°, 45°, 90° from the Rolling Direction and an

interpolation function $\underline{p}^{ref}(\alpha)$ is used to find interpolated reference points from the measured points $\underline{p}_{\alpha}^{ref}$:

$$\underline{p}^{ref}(\alpha) = \frac{\underline{p}_0^{ref} + 2\underline{p}_{45}^{ref} + \underline{p}_{90}^{ref}}{4} + \frac{\underline{p}_0^{ref} - \underline{p}_{90}^{ref}}{2}\cos 2\alpha + \frac{\underline{p}_0^{ref} - 2\underline{p}_{45}^{ref} + \underline{p}_{90}^{ref}}{4}\cos 4\alpha \quad (2\text{-}20)$$

Here α is the angle of the principal stresses to the Rolling Direction. The function $\underline{p}^{ref}(\alpha)$ can be regarded as a Fourier series with only 3 terms; it can be extended if orthotropic properties are not respected. So, with the new interpolated reference points, Vegter's yield criterion can be constructed.

This description of the yield locus shape is coupled with a strain hardening model based on the development of the dislocation cell structure with strain (Bergström 1969, see section 3.5.1.).

Figure 1-1 and Figure 1-4 show the quality of this model. However its experimental identification is quite expensive: pure shear, uniaxial, plane strain and biaxial tests in one direction in case of planar isotropy or in 3 directions for planar anisotropy. As pointed by Vegter *et al.* 1999b, it is important to reach high experimental accuracy and to correct experimental results if non homogeneity or non isothermal conditions happen. Piljman *et al.* 1999 use FEM to study a multiaxial test equipment and demonstrate that the deformation state cannot be directly related to the displacements of the clamps.

An important characteristic of Vegter's model is its flexibility. For instance, Figure 2-20 shows a variant called Vegter-flat, in which the reference point corresponding to plane strain is very close to the hinge point located between plane strain and biaxial states. The agreement with the measured Forming Limit Diagram shown on Figure 2-21 is significantly improved. This last effect shows the extreme sensitivity of the FLD prediction to the shape of the yield locus.

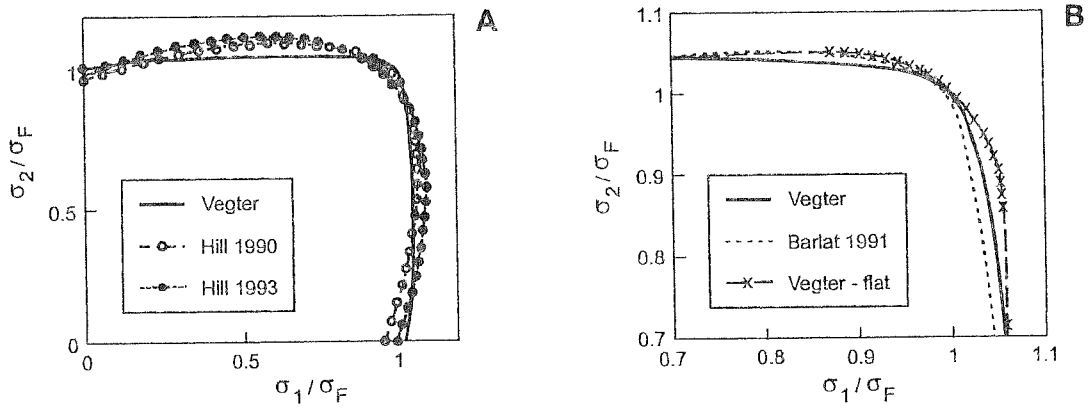

Figure 2-20 Comparison of different yield loci descriptions for Al-6000 (from Vegter *et al.* 1999).

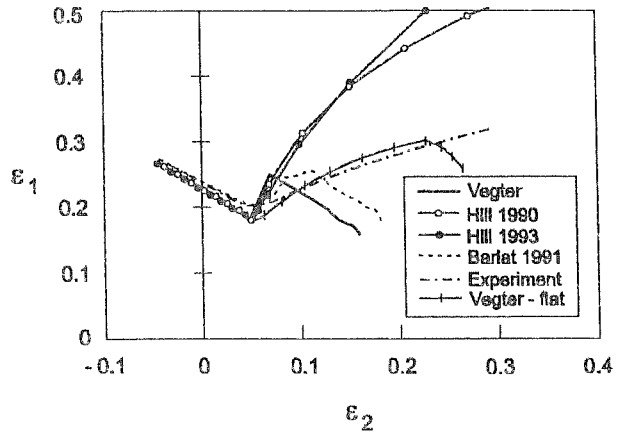

Figure 2-21 FLD predictions for the Al-6000 (90° to RD) using different yield criteria and comparison with experiments (from Vegter *et al.* 1999).

2.1.5. Summary

To conclude this section devoted to the initial shape of yield loci, it can be said that scientists have found new formulations of anisotropic yield loci that seem closer to experimental evidence. However the number of parameters used to determine these new criteria increases with their flexibility. So, according to the requested accuracy, the available experimental equipment and the criteria implemented in the used FEM code, one has to make his own choice to describe anisotropic material behavior.

The Table 4 summarizes the parameter number and the experimental tests necessary to identify the yield loci listed above, in their initial shape, without hardening description. Note that some tests give different information like yield stress and Lankford coefficient for a uniaxial tensile test. According to the parameters identification process and to the model purpose and flexibility, both results are required or just one is used. Choosing stress value or Lankford coefficient to identify the model parameters is not equivalent. Without surprise, one can provide two sets of parameters for one model starting from identical tests. One set of parameters recovers stress information and the other strain information. This apparent difficulty comes from the approximations of these phenomenological models, unable to reproduce physics with perfect accuracy.

Yield loci	Parameter number	Experiments	Described state
Hill 1948	6 parameters	3 uniaxial tests 0; 45; 90°	3D State
Hill 1979	7 parameters	3 uniaxial tests + plane strain test	3D State
Hill 1990	5 parameters	3 uniaxial tests + equibiaxial tensile test	Plane Stress State
Hill 1993	5 parameters	2 uniaxial tests 0;90° + equibiaxial tensile test	Plane Stress State
Karafillis 93	6 + 2 parameters	3 uniaxial tests	3D State
Barlat 1989	4 parameters	2 uniaxial tests + pure shear test	Plane Stress State
Barlat 1991	6 + 1 parameters	3 uniaxial tests	3D State
Barlat 1997	6 + 1 parameters	3 uniaxial tests + equibiaxial bulge	Plane Stress State
Vegter 1998	12 parameters	12 tests: pure shear test, uniaxial test, plane strain test, equibiaxial test repeated in 0; 45; 90°	Plane Stress State

Table 4 - Phenomenological yield loci for orthotropic case; initial shape description.

2.2. Updated yield loci

It is a fundamental issue of the physics of metal plasticity that any particular yield surface is the product of microstructural and textural evolutions imposed by the specific strain path or loading history undergone by the material element of interest. Starting with a given material piece, the initial shape of the yield locus is easily identified by stress states that initiate plastic strains, as the changes in texture during such tests will be imperceptible. It is quite harder to find a general agreement on how to measure an updated yield locus. One possibility used by a lot of authors (Vial *et al.* 1983, Tourki *et al.*1996, Kuwabara & van Bael 1999) is to determine work contours instead of updated yield loci. They generate a new locus by joining stress states - for example (σ_1, σ_2) points - for which an equal amount of (plastic) work has been spent per unit volume. Usually, radial stress paths (i.e. constant σ_1 / σ_2 ratio) are chosen. As stated by Hill 1993, it cannot be a yield locus when it connects states with different textures. In fact, these different stress states cannot possibly lie on a neutral loading path.

In practice, the initial phenomenological yield criteria described in the preceding section must be associated with a hardening rule to model plastic deformation beyond plasticity initiation. As described in next section, these hardening models

depend on internal variables and allow to compute the new size, shape and position of the yield locus. So, the updated yield locus must connect points representing stress states characterized by identical values of internal variables. For simple macroscopic hardening models, the *plastic work* is often taken as the only internal state variable, which validates the use of the work contours mentioned above, even though this surface connects stress points related to different material textures. This plastic work is easily computed by:

$$W^P = \int \underline{\sigma} : d\underline{\varepsilon}^P \tag{2-21}$$

Another simple approach is to use an *integrated equivalent plastic strain* as the only internal variable. So, the updated yield locus is related to stress states with identical integrated plastic strain. Let us note that this *integrated equivalent plastic strain* is computed by :

$$\varepsilon_e^p = \int d\varepsilon_{eq}^P \text{ with } \quad d\varepsilon_{eq}^p = \frac{2}{\sqrt{3}}\left(\frac{1}{2} d\underline{\varepsilon}^P : d\underline{\varepsilon}^P\right)^{1/2} \tag{2-22}$$

This value should not be confused with the equivalent plastic strain:

$$\varepsilon_{eq}^P = \frac{2}{\sqrt{3}} \quad \left(\frac{1}{2}\underline{\varepsilon}^P : \underline{\varepsilon}^P\right)^{1/2} \tag{2-23}$$

As pointed out by Khan & Huang 1995, for von Mises' yield locus, the *strain hardening hypothesis* (ε_e^P = internal variable) and the *work hardening hypothesis* (W^P = internal variable) are equivalent. For anisotropic yield loci, if the above definition of integrated equivalent plastic strain is used, the *strain hardening hypothesis* and the *work hardening hypothesis* are of course not equivalent. However, in general, the equivalence is retained because the definition of the integrated equivalent plastic strain is adapted : it is now computed by the integration of $\dot{\varepsilon}_{eqa}^p$, the *anisotropic equivalent plastic strain rate*, directly deduced from the plastic dissipation:

$$\sigma_{eqa}\, \dot{\varepsilon}_{eqa}^p = \sigma_{ij} \dot{\varepsilon}_{ij}^p \text{ with } \sigma_{eqa} = \sqrt{\sigma_{ij} L_{ijkl} \sigma_{kl}} \tag{2-24}$$

where tensor $\underline{\underline{L}}$ represents the material anisotropy when assuming that the yield locus can be expressed by a function

$$F_p = \sqrt{\sigma_{ij} L_{ijkl} \sigma_{kl}} - \sigma_F = 0 \tag{2-25}$$

This 4th order tensor $\underline{\underline{L}}$ can be directly deduced in Hill's approach or in some texture based yield locus (see chapter 6).

The $\underline{\underline{L}}$ tensor used in Barlat's or Karafillis' approaches (see Table 2) describes also the material anisotropy but does not fit with relation (2-25). The same notations were chosen however, because both tensors translate material anisotropy.

So, hereafter, $\dot{\varepsilon}^{P}_{eq}$ represents the rate of the equivalent plastic strain given by (2-23) while $\dot{\varepsilon}^{P}_{eqa}$ and σ_{eqa} are defined by (2-24) and L_{ijkl} by (2-25) since no more discussion on Barlat's or Karafillis' model appears. Note that, in presence of kinematic hardening, the stress is replaced by the overstress in σ_{eqa}.

For hardening approaches with strong microscopic roots, the equality of internal hardening state variables effectively implies that all the points connected by the yield locus are related to the same material state. This is closer to the microscopic concept of hardening and constitutes an incitement to measure actual updated yield loci rather than work contours.

Beyond the elastic-plastic transient zone (Aernoudt et al., 1987), the yield loci directly deduced from the measured updated material texture should be good approximations of the actual shape of updated yield loci. However their size often depends on isotropic hardening variables, which are a too crude representation of the reality.

In conclusion, this paragraph shows the prominent role of the hardening approach to determine updated yield locus.

References

Aernoudt, E., Gil-Sevillano J. & Van Houtte, P. (1987) Constitutive Relations and Their Physical Basis, S.I. Andersen et al. Eds, RisØ National Laboratory, Roskilde, Denmark, 1-38.

Andersson, A., Ohlsson C-A, Mattiasson, K. and Persson B. (1999) Implementation and Evaluation of the Karafillis-Boyce Material Model for Anisotropic Metal Sheets, Numisheet'99, 13-17 September 1999, **1**, Besançon, France, 115-121.

Arminjon, M., Bacroix, B., Imbault, D. and Raphanel, J.K. (1994) A fourth-order plastic potential for anisotropic metals and its analytical calculation from texture function, *Acta Mechanica*, **107**, 33.

Banabic, D. (1996) Forming limit diagrams predicted by using the new Hill's yield criterion, *Proceedings of the 3rd Int. Conf. Numisheet'96* Numerical Simulation of 3-D Sheet Metal Forming Processes – Verification of Simulations with Experiments, Lee, Kinzel, Wagoner Eds., the Ohio State University.

Banabic, D. (1997) Sheet metal formability predicted by using the new Hill's yield criterion, *Advanced Methods in Materials Processing Defects*, Predeleanu M. & Gilormini P., 257-264.

Barlat, F. (1987) Crystallographic texture, anisotropic yield surfaces and forming limits of sheet metal. *Materials Science and Engineering*, **91**, 55.

Barlat, F. and Lian, J. (1989) Plastic behaviour and stretchability of sheet metals. Part 1 : a yield function for orthotropic sheets under plane stress conditions, *Int. J. of Plasticity*, **5**, 51.

Barlat, F., Lege, D.J., Brem, J.C. (1991) A six-component yield function for

anisotropic materials. *Int. J. of Plasticity*, 7, 693.

Barlat, F., Becker, R.C., Hayashida, Y., Maeda, Y., Yanagawa, M., Chung, K., Brem, J.C., Lege, D.J., Matsui, K., Murtha, S.J., Hattori, S. (1997) Yielding description for solution strengthened aluminium alloys, *Int. J. of Plasticity*, **13/4**, 385-401.

Berg, H., Hora, P., Reissner, J. (1998) Simulation of sheet metal forming processes using different anisotropic constitutive models, *Simulation of materials processing : theory, methods and applications*, Huetink & Baaijens Eds, Balkema.

Bergstrom, Y. (1969/70) A dislocation model for the stress strain behaviour of polycrystalline α-Fe with special emphasis on the variation of the densities of mobile and immobile dislocations, *Mat. Sci. Eng.*, 5, 179-192.

Bishop, J.W.F., Hill, R. (1951) A theory of the plastic distortion of a polycrystalline aggregate under combined stresses and a theoretical derivation of the plastic properties of polycrystalline face-centered metals, *Philos. Mag.*, 42, 414-427, 1298-1307.

Bridgman, P.W. (1923) The compressibility of thirty metal as a function of pressure and temperature, *Proc. Am. Acad. Arts Sci*, **58**, 165.

Bridgman, P.W. (1952) Studies in large plastic flow and fracture. *Metallurgy and Metallurgical Engineering Series*, New-York, McGraw-Hill.

Budianski, B. (1984) Anisotropic plasticity of plane-isotropic sheets, *Mechanics of Material Behaviour*, Dvorak G.J. and Shield R.T. Eds, Elsevier, 15.

Carleer, B.D., Meinders, T., Pijlman, H.H., Huetink, J., Vegter, H. (1997) A planar anisotropic yield function based on multi axial stress states in finite elements, *Computational plasticity – fundamentals and applications*, Owen, Onate and Hinton Eds.

Drucker, D.C. (1951) A more fundamental approach to plastic stress-strain relations, in *Proc. First US Nat. Congr. Applied Mechanics*, ASME, New-York, 487-491.

Ferron, G., Makkouk, R., Morreale J. (1994) A parametric description of orthotropic plasticity in metal sheets. *Int. J. of Plasticity*, **10/5**, 431-449.

Gurson, A.L. (1977) Continuum theory of ductile rupture by void nucleation and growth. *J. Engng. Materials Technology* **99**, 2-15.

Hayakawa, K., Murakami, S., (1998) Space of damage conjugate force and damage potential of elastic-plastic-damage materials, *Damage Mechanics in Engineering Materials*, Voyiadjis, G.Z., Ju, J.W., Chaboche J.L. Eds, 27-44.

Hayashida, Y., Maeda, Y., Matsui, K., Hashimoto, N., Hattori S., Yanagawa M., Chung, K., Barlat F., Brem J.C., Lege D.J., Murtha, S.J. (1995) FEM analysis of punch stretching and cup drawing tests for aluminium alloys using a planar anisotropic yield function, *Simulation of Materials Processing : Theory, Methods and Applications*, Shen&Dawson Eds, Balkema, 717.

Hecker, S.S. (1976) Experimental studies of yield phenomena in biaxially loaded metals, in Strick-Lin, J.A., Saczalski, K.J. Eds, Constitutive equations in viscoplasticity : computational and engineering aspects, ASME, New-York, 1-33.

Hill, R. (1948) A theory of the yielding and plastic flow of anisotropic materials.

Proc. Royal Soc. London, A193, 281-297.
Hill, R. (1990) Constitutive Modelling of Orthotropic Plasticity in Sheet Metals, *J. Mech. Phys. Solids*, **38/3**, 405-417.
Hill, R. (1993) A user-friendly theory of orthotropic plasticity in sheet metals, *Int. J. Mech. Sci.*, **35/1**, 19-25.
Holt, D.L. (1970) Dislocation cell formation in metals, *J. Appl. Phys.*, **41**, 3197-3201.
Hosford W.F. (1972) A generalized isotropic yield criterion, *J. Appl. Mech. Trans. ASME*, **39**, 607-609.
Karafillis, A.P., Boyce, M.C. (1993) A general anisotropic yield criterion using bounds and a transformation weighting tensor, *J. Mech. Phys. Solids*, **41/12**, 1859-1886.
Khan A.S., Huang S. (1995) Continuum theory of plasticity, Wiley & Sons Eds.
Kobayashi, S., Caddell, R.M. and Hosford, W.F. (1985) Examination of Hill's latest yield criterion using experimental data for various anisotropic sheet metals. *Int. J. of Mech. Sci.*, **27**, 509.
Kuwabara, T., Van Bael, A. (1999) Measurement and Analysis of Yield Locus of Sheet al.uminium Alloy 6XXX, Numisheet'99, 13-17 September 1999, **1**, Besançon, France, 85-90.
Mahmudi (1995) Yield loci of anisotropic aluminium sheets, *Int. J. of Mech. Sci.*, **37**, 919.
Mendelson A. (1968) Plasticity : Theory and Application, MacMillan, New-York, 87.
Moshfegh, R., Nilsson, L., Jensen M.R., Danckert J. (1998) Finite Element Simulation of the Hydromechanical Deep Drawing Process, *1st ESAFORM Conference on Material Forming*, Sophia-Antipolis (France), 17-20 March 1998, J.L. Chenot, J.F. Agassant, P. Montmittonet, B. Vergnes, N. Billon Eds.
Phillips, A. (1986) A review of quasi-static experimental plasticity and viscoplasticity, *Int. J. of Plasticity*, **2**, 315.
Pijlman, H.H., Brinkman J., Huetink, J., Vegter, H. The Vegter Yield Criterion Based on Multi-Axial Measurements, Numisheet'99, 13-17 September 1999, vol. 1, Besançon, France, 109-114.
Suh, Y.S., Saunders, F.I., Wagoner, R.H. (1996) Anisotropic yield functions with plastic-strain induced anisotropy, *Int. J. of Plasticity*, **12/3**, 417-438.
Taylor, G.I. (1938) Plastic strains in metals, *J. Inst. Metals*, **62**, 307-324.
Tourki, Z., Makkouk R., Zeghloul A., Ferron G. (1994) Orthotropic plasticity in metal sheets : a theoretical framework, *J. Mater. Process. Technol.*, **45**, 453-458.
Tourki, Z., Zeghloul, A., Ferron, G. (1996) Sheet metal forming simulations using a new model for orthotropic plasticity, *Computational Materials Science*, **5**, 255-262.
Van Bael, A. (1994) Anisotropic yield loci derived from crystallographic data and their application in finite element simulations of plastic forming processes, proefschrift voorgedragen tot het behalen van het doctoraat in de toegepaste wetenschappen, Katholieke Universiteit Leuven.
Vegter, H., An Y., Pijlman J.J., Carlee B.D., Huetink J. (1998), Advanced Material

Models in Simulation of Sheet Forming Processes and Prediction of Forming Limits, *1st ESAFORM Conference on Material Forming*, Sophia Antipolis, Chenot, Agassant, Montmitonnet, Vergnes, Billon Eds.

Vegter, H., An Y., Pijlman H.H., Huetink J. (1999a), Different approaches to describe the plastic material behaviour of steel and aluminium-alloys in sheet forming, *2nd ESAFORM Conference on Material Forming*, Guimaraes, Portugal, Covas J.A. Ed.

Vegter, H., An Y., Pijlman H.H., Huetink J. (1999b), Advanced Mechanical Testing on Aluminium Alloys and Low Carbon Steels for Sheet Forming, Numisheet'99, 13-17 September 1999, **1**, Besançon, France, 3-8.

Vial, C., Caddell, R.M. and Hosford, W.F. (1983) Yield loci of anisotropic sheet metals, *Int. J. of Mech. Sci.*, **25**, 899.

Vial-Edwards, C. (1997) Yield loci of FCC and BCC sheet metals, *Int. J. of Plasticity*, **13/5**, 521-531.

Wagoner, R.H. (1980) Measurement and analysis of plane strain work hardening, *Metall. Trans. A*, **11A**, 165.

3. HARDENING MODELS

3.1. Basic knowledge on crystal events

Ewing & Rosenhain 1900 have established that the plastic deformation of a crystal occurs by slipping on some crystallographic planes (*slip* or *glide planes*), by slipping in some crystallographic directions (*slip* or *glide direction*) or by twinning, another crystallographic phenomenon.
However, the elementary theoretical estimation of the shear strength of a perfect crystal given by Frenckel 1926 yields values of the order of 10^{-1} G (G=shear modulus of the crystal). Knowing that the observed shear strength is of the order of $10^{-6} \approx 10^{-4}$ G, scientists have proposed the concept of crystal defects, called dislocations, that reduce the strength of the crystal. Figure 3-1 and Figure 3-2 present two basic types of dislocations, the edge and screw dislocations, and show the *dislocation line* AB. The motion of dislocations results in crystal shearing.

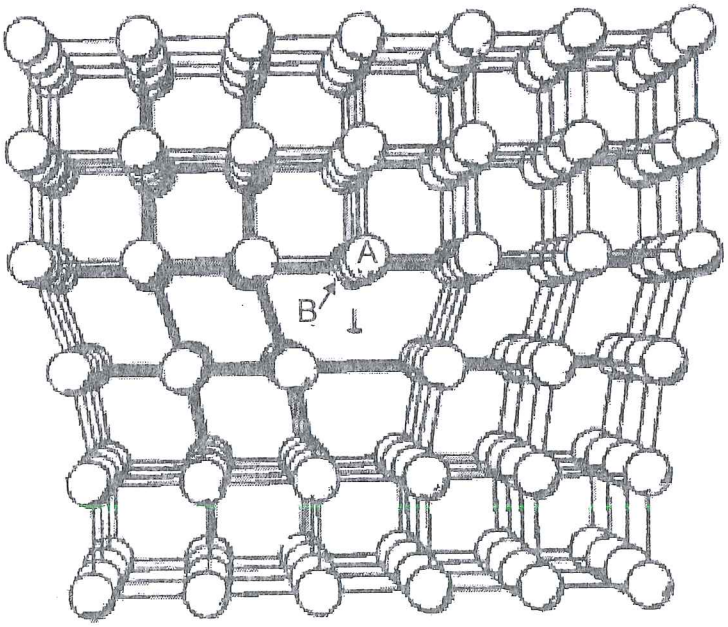

Figure 3-1 Edge dislocation (from Magnée, 1994).

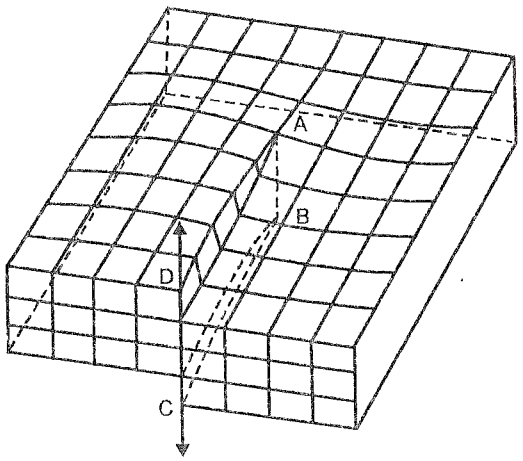

Figure 3-2 Screw dislocation (from Khan & Huang, 1995).

Burgers' vector $\underline{b}$ is introduced to describe the slip direction of a dislocation. It is determined by Burgers' circuit, a closed path involving two lattice directions and surrounding the dislocation line (Figure 3-3).

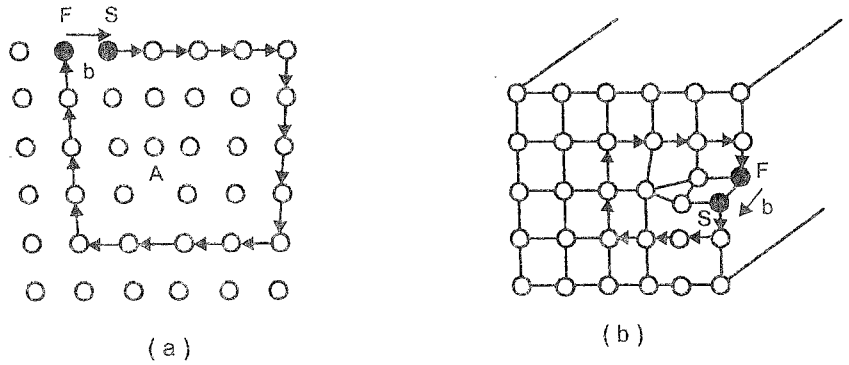

Figure 3-3 Burgers' circuit for edge (a) and screw (b) dislocation defining Burgers' vector $\underline{b}$ (from Khan & Huang, 1995).

It should be pointed out that, for screw dislocation, Burgers' vector is parallel to its dislocation line, while for edge dislocation, Burgers' vector is perpendicular to the dislocation line.

A slip or glide system is characterized by the combination of a slip plane and a slip direction. Experimental observations show that, in most metals, the slip planes are usually those planes with the closest atomic packing, while the slip directions are always the closest packed directions on the slip planes. Once reference axes are defined, a slip system is described by its geometrical matrix K_{ij}^s also called *Schmid's tensor* :

$$K_{ij}^s = b_i^s \, n_j^s \tag{3-1}$$

n_j^s unit vector normal to the slip plane for the slip system s;

b_j^s unit vector in the slip direction for the slip system s.

A_{ij}^s *and* Z_{ij}^s are respectively the symmetric and the anti-symmetric parts of K_{ij}^s.
Another approach to characterize one slip system is to use Miller's indices to represent the slip planes and directions. For instance, for b.c.c metals, 24 {1 1 0} <1 1 1> and {112}<111> slip systems are available and, for f.c.c metals, 12 {111}<110> are generally assumed (van Houtte 1995).

The critical resolved shear stress CRSS τ_c^s is the shear stress to apply in order to sustain the long range propagation of a dislocation according to a slip system *s*, under the superposed effects of all coexisting structural features which represent obstacles of different strengths. In practice, the *resolved shear stress* τ^s acting on a slip system *s* can be derived by projecting the microscopic stress $\underline{\sigma}^{micro}$ on the slip plane with the help of the corresponding A_{ij}^s matrix. This determination can be checked, if one computes the energy dissipated by the strain rate tensor $\underline{\dot{\varepsilon}}^p$ associated to a single shear of one active slip system:

$$\dot{\gamma}^s \tau^s = \dot{\varepsilon}_{ij}^p \dot{\sigma}_{ij}^{micro} = A_{ij}^s \dot{\gamma}^s \sigma_{ij}^{micro}$$

$$\tau^s = A_{ij}^s \sigma_{ij}^{micro} \qquad \text{(3-2):}$$

The slip *s* occurs according to Schmid's law if the shear stress τ^s reaches the CRSS τ_c^s. This defines the yield locus of a single crystal:

$$-\tau_c^s \le \tau^s \le \tau_c^s \qquad \text{(3-3)}$$

Equals signs hold for plastic deformation, while inequalities apply to the elastic domain. In this elastoplastic formulation, the detection of active slip systems can be done either by Bishop-Hill's approach or by Taylor's approach. These methods are dual ones and are well summarized in van Houtte 1988. Taylor's approach will be summarized in Chapter 4.

3.2. Crystallographic texture

In a polycrystalline sample, each crystal is characterized by its volume fraction *dV* and by its orientation, symbolically designated by *g*. More specifically, the set of Euler's angles (φ_1, ϕ, φ_2), describing the orientation of the crystal reference system with respect to the sample (external) reference system, is most often used (Bunge, 1982).

Figure 3-4 shows the physical meaning of φ_1, ϕ, φ_2. With *dV(g)/V* as the volume fraction of crystals having their orientation within *dg* around *g*, the *statistical crystallite orientation distribution function* (ODF) *f(g)* is then defined as :

$$\frac{dV(g)}{V} = f(g)dg \quad \text{with} \quad dg = \frac{1}{8\pi^2}\sin\phi \, d\varphi_1 \, d\phi \, d\varphi_2 \tag{3-4}$$

It provides a quantitative description of the crystallographic texture of the polycrystal; high values indicate preferred orientations, and $f(g) \equiv 1$ a completely random texture.

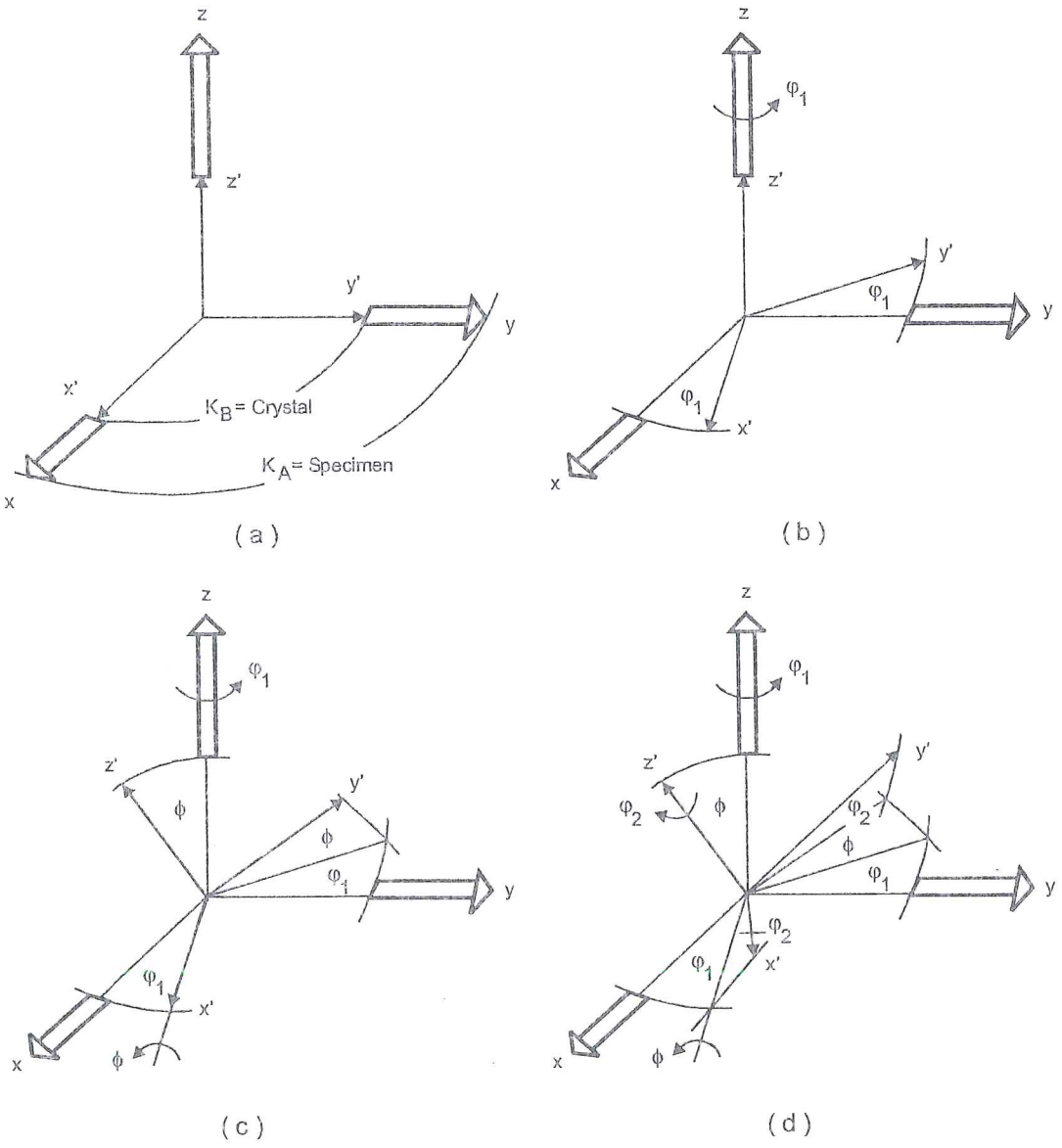

Figure 3-4 Definition of Euler's angles (from van Houtte 1995).

Because of the crystal symmetry, several symmetrically equivalent choices exist for a crystal reference system. The classical ranges for the three Euler's angles, $0 \le \varphi_1 \le 2\pi, 0 \le \phi \le \pi$ and $0 \le \varphi_2 \le 2\pi$, may therefore be reduced. Besides, symmetries in the forming process may lead to an initial texture with similar statistical symmetries. This so-called sample symmetry allows again for a reduction

of the part of Euler's space to be considered. For example, in the case of cubic crystals without sample symmetry, the ranges $[0,2\pi]x[0,\pi/2]x[O,\pi/2]$ are to be used; with additional orthorombic sample symmetry, $[O,\pi/2]x[0,\pi/2]x[O,\pi/2]$ will be sufficient (Van Bael 1994).
Using the harmonic method proposed by Bunge 1982, the ODF $f(g)$ can be represented by a series expansion :

$$f(g) \equiv \sum_{l=0}^{l_{max}} \sum_{\mu=1}^{\mu_{max}(l)} \sum_{\nu=1}^{\nu_{max}} C_l^{\mu\nu} \dot{T}_l^{\mu\nu}(g) \qquad (3\text{-}5)$$

with l_{max} the maximum degree of the series expansion, $\dot{T}_l^{\mu\nu}(g)$ harmonic functions of Euler's angles and $C_l^{\mu\nu}$ their Fourier's coefficients describing the texture. For instance, truncating at l_{max} = 22, a ODF for cubic crystals and orthorombic sample symmetry is represented by a set of 185 $C_l^{\mu\nu}$ - coefficients (355 in the absence of sample symmetry). These can for example be obtained, after appropriate mathematical processing, from a set of X-ray diffraction pole figures, measured on a sample with the help of a texture goniometer (Bunge, 1982).

3.3. Introduction to hardening models

From a microscopic point of view, hardening is often presented as **material** and **geometric** (Miller & McDowel 1996). The dislocations remaining inside a volume element modify its state through the elastic field they produce. They also constitute obstacles to the production and motion of further dislocation, a phenomenon which is perceived as the material (strain) hardening of the crystal. The geometric (textural) hardening is related to the effect of lattice rotation, which can either raise or lower the stress required for yielding. In tension and compression, texturing generally increases the yield stress while in torsion its value is reduced. In Chapter 4, presenting the microscopic models used in micro-macro analysis, these 2 components clearly appear in hardening models. However, in most hardening models linked to phenomenological yield loci, the geometric hardening is neglected. In the models presented hereafter, it is the case for Bergström-van Liempt-Vegter's model, Follansbee-Kocks' model, Schmitz's model and Teodosiu's model. However Miller's model tries to take both phenomena into account.

From a macroscopic point of view, **isotropic** and **kinematic** hardening models are usually considered. Let us recall that isotropic hardening assumes that the subsequent yield surface is obtained by a uniform expansion of the initial yield surface. So, the centers of the initial and updated yield loci are the same and the shape modification of the yield locus induced by plastic deformations is neglected. Kinematic hardening assumes that, during the process of plastic loading, the yield surface translates in stress space while its shape and size remain unchanged. This model is motivated by the Bauschinger effect in the uniaxial tension-compression experiments (Figure 3-5).

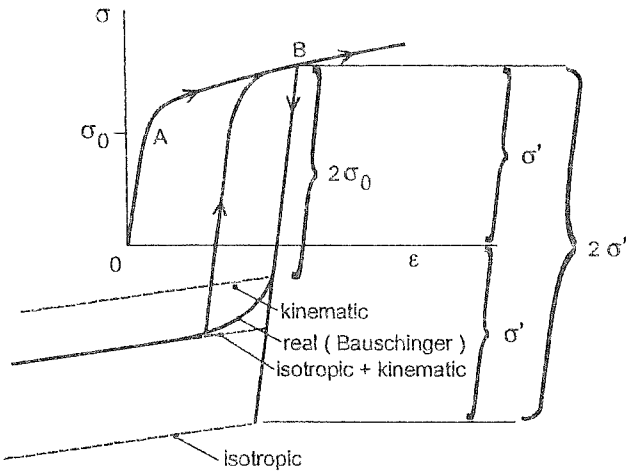

Figure 3-5 The Bauschinger effect, isotropic and kinematic hardening (adapted from Huétink *et al.* 1995)

Assuming an isotropic hardening rule, all the yield surfaces presented in section 2 can be written in the form :

$$F(\underline{\sigma},\alpha_k,\underline{\underline{L}}) = f(\underline{\sigma},\underline{\underline{L}}) - \sigma_F(\alpha_k) \tag{3-6}$$

with α_k : hardening scalar internal variables;

$\underline{\underline{L}}$: a material tensor characterizing material anisotropy;

σ_F : a threshold value, function of the internal variables.

The different approaches of isotropic hardening depend on the choice of the internal variables α_k and of the threshold function σ_F.

Due to kinematic hardening in the process of plastic deformation, the general formulation of the yield surface hereabove takes the form :

$$F(\underline{\sigma},\underline{\alpha},\alpha_k,\underline{\underline{L}}) = f(\underline{\sigma}-\underline{\alpha},\underline{\underline{L}}) - \sigma_F(\alpha_k) \tag{3-7}$$

where $\underline{\alpha}$ is a tensorial hardening parameter, usually called *back stress*, which represents the center of the yield surface in the stress space. The first proposal by Prager 1955 implies that the yield surface moves along the direction of the plastic strain rate:

$$d\underline{\alpha} = c\, d\underline{\varepsilon}^p \tag{3-8}$$

where c is a material constant. This formulation does not give consistent results for 3-dimensional and 2-dimensional stress states and predicts softening in transverse direction due to uniaxial tension. To overcome these shortcomings, Ziegler 1959 proposed the following modification of Prager's model :

$$d\underline{\alpha} = (\underline{\sigma}-\underline{\alpha})\, d\mu \tag{3-9}$$

where $d\mu$ is a proportionality scalar constant determined thanks to the consistency

condition (Khan & Huang 1995) :

$$d\mu = \frac{\partial f / \partial \underline{\sigma} : d\underline{\sigma}}{\partial f / \partial \underline{\sigma} : (\underline{\sigma} - \underline{\alpha})} \tag{3-10}$$

The schematic representations of Prager's and Ziegler's models are shown in Figure 3-6.

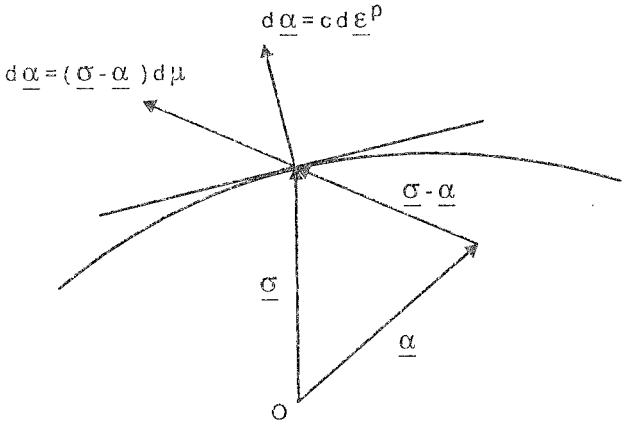

Figure 3-6 Prager's and Ziegler's kinematic hardening models (from Khan&Huang 1995).

The attempts to model the response of engineering materials under symmetric, unsymmetric or random cyclic loading, reversal or successive different directional deformations paths show the limits of the classical isotropic or kinematic hardening models. Two ways are possible to improve the macroscopic models:

- the use of multi-surfaces model shortly summarized hereafter;
- the use of internal variables closely linked to the underlying physics, described in section 3.5.

Multi-surface models have been introduced by Mroz 1967, Dafalias & Popov 1975. In Mroz' model, the nonlinearity of the stress-strain curve is introduced by defining a set of hardening moduli associated with several initially concentric surfaces which can translate rigidly and expand uniformly. In Dafalias & Popov's model, the nonlinearity is described by modeling the continuous variation of a hardening modulus based on the concept of 2 surfaces : the yield locus and the bounding locus. These two surfaces allow to define a distance *d* in the stress space, representing the difference between the current loading state and the bounding state. This variable distance has been found very important to define the variation of the hardening modulus. This approach has met a great success and other double yield surfaces models have been developed (Krieg 1975, Philips & Lee 1979).

This basic concept is explained with Huétink's *et al.* 1995 proposal. These authors use a classical Hill's yield surface translated by kinematic hardening, called "*kinematic yield surface*", and a fictitious yield surface, referred hereafter as the "*isotropic yield surface*" (Figure 3-7). The latter surface corresponds to the

application of isotropic hardening on the initial yield locus. It keeps the memory of the maximum stress reached during the deformation path.

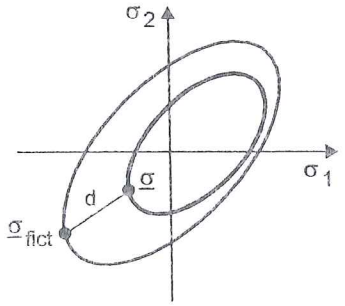

Figure 3-7 Kinematic and isotropic yield surfaces and definition of the distance d between the current stress point $\underline{\sigma}$ and a stress point $\underline{\sigma}_{fict}$ on the fictitious isotropic yield surface (from Huétink *et al.* 1995).

Their hypothesis is that the rate of hardening depends on distance d. The fictitious isotropic yield surface (re)starts growing when the kinematic surface touches the isotropic yield surface. Let us follow a cyclic loading experiment (A→B→C→D→E) as defined on Figure 3-8.

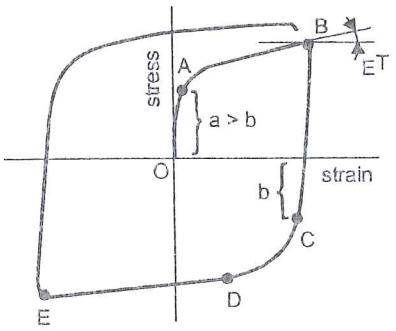

Figure 3-8 Stress-strain relation during an experiment of cyclic loading (from Huétink *et al.* 1995).

When starting with virgin material, the isotropic and kinematic yield surfaces coincide, as depicted in Figure 3-9[a]. During the deformation process, the fictitious isotropic yield surface grows due to the accumulated strain and the kinematic yield surface translates in such a way that $\underline{\sigma}$ remains on both the isotropic and the kinematic yield surfaces, as illustrated by Figure 3-9[b] (A→ B). In this case, the distance d is zero and the hardening rate is equal to the slope of the monotonic stress-strain curve E^T (Figure 3-8). When the deformation direction changes (B→), the stress $\underline{\sigma}$ lies inside the kinematic yield surface and the material is elastic.

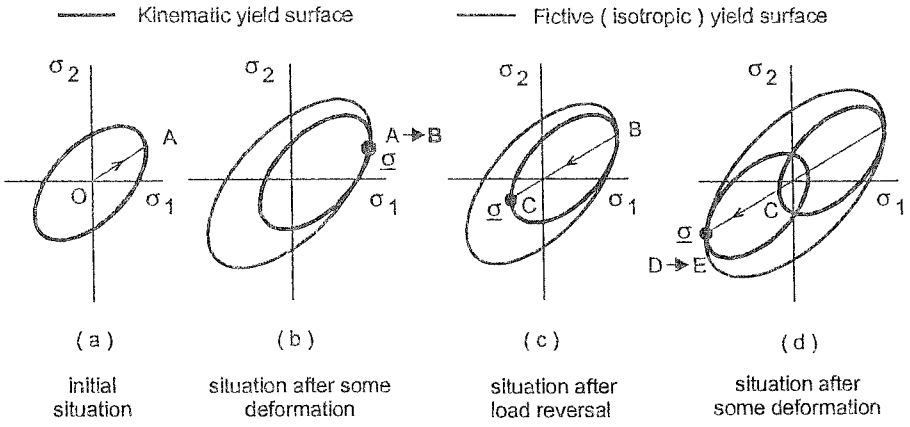

Figure 3-9 Yield surfaces, kinematic and isotropic hardening (from Huétink *et al.* 1995).

After a further increase of the load in the reversed direction, $\underline{\sigma}$ moves to the opposite side of the yield surface, see Figure 3-9^c, and plasticity starts to occur again. At this moment, the distance d is important and a relatively fast hardening occurs. The hardening rate decreases when the kinematic yield surface approaches the fictitious isotropic yield surface (point D in Figure 3-9^d). After $\underline{\sigma}$ touches the isotropic yield surface, hardening is controlled by the growth of the isotropic yield surface, see Figure 3-9^d. The mathematical description can be found in Huétink *et al.* 1995.

Some proposals of hardening rules associated with models using only one yield surface are now listed. Section 3.4 presents purely macroscopic models while section 3.5 proposes macroscopic models strongly linked to the microscopic events. As it will be seen, even with strong microscopic roots, such models can still be compatible with phenomenological descriptions of the yield locus and give a fair description of the experimental behavior.

3.4. Simple macroscopic isotropic hardening approaches

As used in Hill's or Barlat's relations (see Tables 1 and 2 of Chapter 2), the threshold value is defined by σ_F, the yield stress deduced from uniaxial tension. Different equations have been proposed for this tensile stress-strain curve $\sigma_F = f(\varepsilon)$:

$$\sigma_F = \sigma_0 + H\varepsilon^{n'} \qquad \text{Ludwick 1909}$$

$$\sigma_F = H\varepsilon^{n'} \qquad \text{Hollomon 1944}$$

$$\sigma_F = \sigma_0 + (\sigma_s - \sigma_0)\,[1 - exp(-n'\varepsilon)] \qquad \text{Voce 1948}$$

$$\sigma_F = H(\varepsilon_s + \varepsilon)^{n'} \qquad \text{Swift 1947}$$

$$\sigma_F = \sigma_0\, tanh(\frac{E\varepsilon}{\sigma_0}) \qquad \text{Prager 1938}$$

$$\varepsilon = \frac{\sigma_F}{E} + H\left(\frac{\sigma_F}{E}\right)^{n'} \qquad \text{Ramberg \& Osgood 1943}$$

(3-11)

where σ_F, ε refer to Cauchy's stress and the logarithmic strain respectively, $E, H, n', \sigma_0, \sigma_s, \varepsilon_s$ are material constants and must be determined experimentally. For this uniaxial test, the strain is additionally decomposed into an elastic part ε^e and a plastic one ε^P.

$$\varepsilon = \varepsilon^e + \varepsilon^P \tag{3-12}$$

The link between this uniaxial state and the actual three dimensional stress-strain state relies on the chosen internal variables α_k.

3.5. Macroscopic approaches with strong microscopic roots

3.5.1. Bergström - van Liempt - Vegter's model

Bergström 1969 proposes a model which intends to describe slow constant strain-rate tensile tests on polycrystalline α-Fe at room temperature. It considers only the homogeneous deformation, i.e. the deformation that occurs up to the point where necking begins. This model starts from the well known relationship between the uniaxial flow stress σ_F and the total dislocation density ρ (total length of dislocations per volume unit):

$$\sigma_F = \sigma_0 + \alpha G b \sqrt{\rho} \tag{3-13}$$

where σ_o is the elastic limit, G the shear modulus, b the magnitude of Burgers' vector and α a material constant.

Then, it establishes the relation between dislocation density ρ and strain ε. Only the average behavior of a large number of dislocations is considered and it is assumed that :

- ρ is composed of a mobile dislocation density ρ_m and an immobile dislocation density ρ_i,
- ρ_m is a constant, hence strain independent,
- The variation of ρ_i with ε is determined by 4 processes, namely creation, immobilization, re-mobilization and annihilation of dislocations (see Figure 3-10),
- The effects of changes in dislocation structure can be neglected.

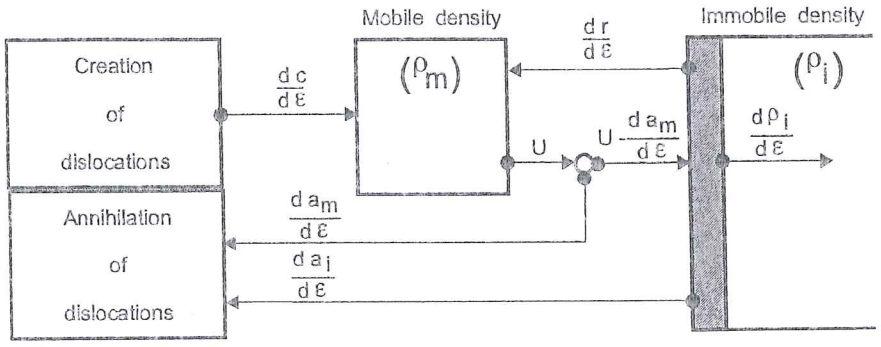

Figure 3-10 Illustration of the dislocation model (adapted from Bergström 1969)

As the density of mobile dislocations ρ_m is constant, the processes causing an increase of ρ_m, creation ($dc/d\varepsilon$) and re-mobilization($dr/d\varepsilon$), are balanced by the processes of annihilation ($da_m/d\varepsilon$) and immobilization ($U-(da_m/d\varepsilon)$), causing a decrease of ρ_m. The term $da_i/d\varepsilon$ covers the annihilation of immobile dislocations. The density of immobile dislocations ρ_i increases with strain ε.

Three main parameters are introduced :

- $U(\varepsilon)$: a function measuring the rate at which mobile dislocations are immobilized or annihilated.
- Ω : a constant measuring the probability for re-mobilization or annihilation of immobile dislocations at room temperature; it is assumed <<1.
- A : a constant measuring the rate at which mobile dislocations annihilate by reacting with other mobile dislocations, grain boundaries, specimen surface, etc.

According to Figure 3-10 and the parameters introduced hereabove, the variation of the total dislocation density with strain is obtained:

$$\frac{d\rho}{d\varepsilon}=\frac{d\rho_i}{d\varepsilon}=U(\varepsilon)-\frac{da_m}{d\varepsilon}-(\frac{dr}{d\varepsilon}+\frac{da_i}{d\varepsilon})=U(\varepsilon)-A-\Omega\rho \qquad (3\text{-}14)$$

Since U is proportional to v (average velocity of mobile dislocations) and to ρ_m, and inversely proportional to s (mean free path or average distance covered by mobile dislocations), following relation is obtained:

$$U(t)=\frac{v\rho_m}{s(t)} \qquad (3\text{-}15)$$

where the time t is the variable. Then, using the proportion:

$$\dot{\varepsilon} \div \overline{M}\, b\, \rho_m\, v \qquad (3\text{-}16)$$

where $\overline{M}$ is the average Taylor's factor depending on the orientation of crystals which will be defined in section 4.5.2, relation (3-15) becomes :

$$U(\varepsilon) \div \frac{1}{Mb\, s(\varepsilon)} \tag{3-17}$$

if strain ε is used as variable.

In constant strain rate tensile tests, it has been found that the total dislocation density ρ, for strains up to approximately 10%, varies with strain as:

$$\rho = C\varepsilon + \rho_0 \tag{3-18}$$

in which C and ρ_0 are experimental constants. The previous relations (3-14) and (3-18) imply $(U\text{-}A)=C$ if, as assumed above, $\Omega \ll 1$. So the assumption that A is strain independent implies that it is also the case for U in the strain range in which relation (3-18) is valid. Beyond this range, a dislocation cell structure develops in the α-Fe "which changes little on further deformation". This strong hypothesis is not valid at large strains and is a limit of Bergström's model. The experimental observation that the dislocation density within the cells is very low supports the assumption that when a dislocation moves, it does so from one cell wall to the other. This suggests that the mean free path s is proportional to the size of the cells. So, according to relation (3-17), U does not change as long as the cell diameter and the crystal orientations remain constant.

Assuming U to be independent of strain, relation (3-14) can be integrated with the limit condition $\rho = \rho_0$ at $\varepsilon = 0$ and the following expression is obtained:

$$\rho = \frac{U - A}{\Omega}(1 - e^{-\Omega\varepsilon}) + \rho_0 e^{-\Omega\varepsilon} \tag{3-19}$$

Finally, Bergström proposes the following stress-strain relationship deduced from equations (3-13) and (3-19):

$$\sigma_F = \sigma_0 + \alpha G b \left\{ \frac{U - A}{\Omega}(1 - e^{-\Omega\varepsilon}) + \rho_0 e^{-\Omega\varepsilon} \right\} \tag{3-20}$$

In this case, σ_0 is the flow stress of the undeformed polycrystal.

This model presents an horizontal asymptote in the stress-strain curve. If the relation (3-20) is fitted on experimental data, the work hardening rate vanishes at strains greater than the experimental strain range. It is however reported in the literature, that work hardening persists up to very high strains. One possibility to improve this model is to maintain relation (3-17) but with a mean free path of mobile dislocations s which varies with strain. This has been proposed by van Liempt 1994, who keeps the idea of a mean free path s proportional to the cell size and assumes an evolution rule for the cell size at large strains:

- cells shrink in size during plastic deformation as the average cell diameter is inversely proportional to $\sqrt{\rho}$;
- cells will be strained with the bulk of material;

- for cells deformed in plane strain, the cell thickness is proportional to $\frac{1}{\sqrt{\rho}} e^{-\beta\varepsilon}$

  where β is a material constant and ε is the macroscopic strain.

The experimental observation of the cell size (van Liempt 1994) allows to reach a constant value of $\beta = 0.18$. Finally, van Liempt's proposal for the differential equation of dislocation density is :

$$\frac{d\rho}{d\varepsilon} = B\sqrt{\rho}\, e^{\beta\varepsilon} - \Omega\rho \tag{3-21}$$

where B is assumed constant but takes into account the average Taylor's factor.

The introduction of relation (3-21) in relation (3-13) produces the following form of the stress strain relation:

$$\sigma_F = \sigma_0 + \alpha G b\left[\frac{B}{\Omega + 2\beta}\left(e^{(\frac{\Omega}{2}+\beta)\varepsilon} - 1\right) + \sqrt{\rho}\right] e^{-\Omega\varepsilon/2} \tag{3-22}$$

So, instead of reaching a saturation level, this equation behave exponentially at high strains. Rietman *et al.* 1997 present finite element simulations using this model.

Vegter 1991 uses Bergström's theory to describe the interaction processes between dislocations and cell structures as well as the influence of the change of shape of the dislocation cell with large strains proposed by van Liempt 1994. To these two concepts, Vegter 1991 adds a modification for the flow stress at high strains and temperature different from room temperature. He derives the following relation for the uniaxial reference flow stress (Pijlman *et al.* 1998) :

$$\sigma_F = \sigma_o + \Delta\sigma_m\left[\beta.(\varepsilon_o + \varepsilon) + \left\{1 - e^{-\Omega(\varepsilon_o+\varepsilon)}\right\}^{n'}\right] \tag{3-23}$$

with :

σ_o the initial yield stress, which depends on strain rate and temperature;

ε the uniaxial strain;

ε_o predeformation parameter;

$\Delta\sigma_m$ a constant representing the stress increase by strain hardening;

β a constant describing the change of shape of the dislocation cells, necessary for large strain behavior;

Ω a constant describing the annihilation of dislocations, necessary for low strain behavior;

n' the strain hardening exponent.

As parameter σ_0 depends on the effect of strain rate and temperature, according to Kabriell and Dahl 1982, it can be split into 2 terms :

$$\sigma_o = \sigma_{o\,sta} + \sigma_{o\,dyn} \tag{3-24}$$

with:

$\sigma_{o\,sta}$ the static yield stress of a dislocation free material;

$\sigma_{o\,dyn}$ the dynamic part of the flow stress.

Krabiell and Dahl 1982 derived the relation of the dynamic part of the flow stress $\sigma_{o\,dyn}$ with strain rate and temperature, based on the thermally activated motion of dislocations over obstacles. In case of steel, these obstacles are mainly the hills and valleys in the slip plane (Peierls' force). This leads to the following equation for the activation enthalpy:

$$\Delta G = -kT\,ln\left(\frac{\dot{\varepsilon}}{\dot{\varepsilon}_o}\right) \tag{3-25}$$

with:

k Boltzman's constant;

T absolute temperature in K°;

$\dot{\varepsilon}$ the strain rate;

$\dot{\varepsilon}_o$ the limit strain rate for thermally activated motion.

Using the latter relation (3-25), Vegter 1991 derives the contribution of the strain rate to the flow stress:

$$\sigma_{o\,dyn} = \sigma_o^* \left\{1 - \frac{\Delta G}{\Delta G_{max}}\right\}^{m'} \quad \text{with } 0 < \Delta G < \Delta G_{max}$$

$$\sigma_{o\,dyn} = \sigma_o^* \text{ with } \Delta G < 0$$

$$\sigma_{o\,dyn} = 0 \text{ with } \Delta G > \Delta G_{max} \tag{3-26}$$

with:

σ_o^* the limit dynamic flow stress;

m' the exponent for the dynamic stress;

ΔG the activation enthalpy;

ΔG_{max} the maximum activation enthalpy.

The final relation for the flow stress as a function of the strain and strain rate is obtained by combining (3-24), (3-25), (3-26) :

$$\sigma_F = \sigma_{o\,sta} + \Delta\sigma_m \left[\beta.(\varepsilon_o + \varepsilon + \left\{1 - e^{-\Omega(\varepsilon_o+\varepsilon)}\right\}^{n'}\right] + \sigma_o^* \left\{1 + \frac{kT}{\Delta G_{max}} ln\left(\frac{\dot{\varepsilon}}{\dot{\varepsilon}_o}\right)\right\}^{m'} \tag{3-27}$$

In this relation :

- ε_0 is 0.005 for steel and 0 for aluminum, which corresponds to the amount of pre-deformation during the skin pass.
- n' : strain hardening exponent is fixed at 0,75 (Vegter 1991). The fit on a stress

strain curve is not sufficiently discriminating for the determination of this exponent. The reason for this choice is based on the evaluation of the diameter of the dislocation cells. If they remain constant (in volume), the value of n' is 0,5; if they decrease according to Holt 1970, the value of n' is 1. The value 0.75 is just a pragmatic choice in between.

- $\Delta G_{max}, \dot{\varepsilon}_0, m', \sigma_0^*$: strain rate and temperature constants are deduced from tensile tests at strain rates ranging from 10^{-4} to 1 s^{-1}. Such tests are available in Vegter 1991; and some values are proposed in table 5 from Vegter *et al.* 1999.
- $\sigma_{0\,sta}, \Delta\sigma_m, \beta, \Omega$: strain hardening constants are derived from tensile tests which yield a planar isotropic flow stress.

Strain hardening constants							Strain rate constants			
material	$\sigma_{0\,sta}$ (MPa)	$\Delta\sigma_m$ (MPa)	β	Ω	ε_0	n'	σ_o^* (MPa)	ΔG_0 (eV)	m'	ε_o^* (s^{-1})
IF-steel	96.2	271.0	0.25	9.27	0.005	0.75	600.0	0.8	2.2	10^8
Al-6000	107.1	179.6	0.25	8.07	0.000	0.75	20.0	0.8	1.0	10^8

Table 5 Material parameters for the Vegter's final flow stress function (from Vegter *et al.* 1999).

3.5.2. Follansbee & Kocks's model

This model uses a single internal variable to describe the flow stress reference curve over a wide range of strain rates (for instance, 10^{-4} to 10^{+4} s^{-1}). It has been developed and validated for pure copper by Follansbee & Kocks 1988, but it has been used later for other metals like tantalum, tantalum - tungsten alloys (Maudlin *et al.* 1999). The foundation of the model is the separation of the phenomena related to the constant dislocation structure and the phenomena related to the structure evolution. The basic assumptions are:

- the plastic deformation occurs by accumulation and motion of dislocations,
- the mechanism controlling the rate of deformation is the interaction of dislocations with defects: grain boundaries, forest dislocations, (dislocations not parallel to the glide plane of the moving dislocation), solute atoms, ...
- for pure f.c.c metals, the dominant short range obstacles are the forest dislocations.

The internal variable is called the mechanical threshold stress $\hat{\sigma}$: it represents the flow stress at 0° K and depends on the dislocation structures present in the material. The flow stress proposal is defined by :

$$\sigma_F = \sigma_a + (\hat{\sigma} - \sigma_a)\left\{1 - \left[\frac{kT\,ln(\dot{\varepsilon}_0 / \dot{\varepsilon})}{g_0 G b^3}\right]^{1/q}\right\}^{1/p} \qquad (3\text{-}28)$$

where σ_a is the athermal component characterizing the (rate independent) interactions of dislocations with long range barriers such as grain boundaries; in practice, it is chosen as the yield stress of the undeformed material. The second component characterizes the rate dependent interactions of dislocations with short range obstacles such as forest dislocation, solute atoms... Thermal activation reduces this component. k is Boltzmann's constant, $\dot{\varepsilon}_0$ a reference constant strain rate, g_0 a normalized activation energy for dislocation/dislocation interactions, G the shear modulus, b the magnitude of Burgers' vector, p and q constants characterizing the statistically averaged shape of the obstacle profile ($0 \le p \le 1, 1 \le q \le 2$). In the method of parameter identification, p and q are chosen in such a way that realistic g_0 are obtained. The second term of (3-28) shows some similitude with the third term of Vergter's model (3-27), also related to thermal and strain rate effects. The evolution of the mechanical threshold stress $\hat{\sigma}$ attempts to model the evolution of the dislocation structure considered as the balance between dislocation accumulation and dynamic recovery :

$$\frac{d\hat{\sigma}}{d\varepsilon} = \theta_0 - \theta_0 \frac{\hat{\sigma} - \sigma_a}{\sigma_{sat} - \sigma_a} \tag{3-29}$$

where θ_0 represents the hardening rate due to the dislocation accumulation and the second term covers the dislocation annihilation processes. σ_{sat} is the stress at zero strain hardening rate, often called: the saturation stress. This linear variation of the strain hardening rate with stress is often termed as Voce behavior. Estrin & Ecking 1984 have given physical significance to this relation by considering the competition between dislocations. However another function, close to the previous one, produces better experimental fits for copper :

$$\frac{d\hat{\sigma}}{d\varepsilon} = \theta_0 (1 - g(\frac{\hat{\sigma} - \sigma_a}{\sigma_{sat} - \sigma_a})) \tag{3-30}$$

Relations for g, θ_0, σ_{sat} are specific for each material. For copper, Follansbee & Kocks 1988 use:

$$g = \frac{tanh(2X)}{tanh(2)} \text{ with } X = \frac{\hat{\sigma} - \sigma_a}{\sigma_{sat} - \sigma_a} \tag{3-31.a}$$

$$ln\frac{\dot{\varepsilon}}{\dot{\varepsilon}_0} = \frac{Gb^3 A}{kT} ln(\frac{\sigma_{sat}}{\sigma_{sat\,o}}) \tag{3-31.b}$$

$$\theta_0 = A_1 + A_2 \ln\dot{\varepsilon} + A_3\dot{\varepsilon} \tag{3-31.c}$$

where $\dot{\varepsilon}_o$, A, A_1, A_2, A_3 are material constants, $\sigma_{sat\,o}$ is the saturation stress for deformation at 0° K. The relation (3-31.c), deduced from experiments, is related to the « increased strain rate sensitivity » of the flow stress found in copper and other f.c.c. metals at high strain rates (> 10^3 s^{-1}). In fact, a constant initial strain hardening

$\theta_0 = A_1$ means that dislocations are immobilized after traveling a distance proportional to the average distance between dislocations. However, at very high strain rates, it might be speculated that the distance before dislocation immobilization is simply the distance that a dislocation can move during the imposed time duration of the deformation. This explains the second and third terms of relation (3-31.c).

As shown by Figure 3-11, with a single set of material parameters, this model is able to predict stress strain curves at various constant levels of strain rate.

Figure 3-12 shows that this model can predict effects of strain rate modifications if they happen at low strain but not at high strain.

Follansbee & Kocks 1988 provide a good description of their method to identify the material parameters : A, A_1, A_2, A_3, $\sigma_{sat\,o}$, σ_a, G, b, g_0, p, q, θ_0, $\dot{\varepsilon}_o$.

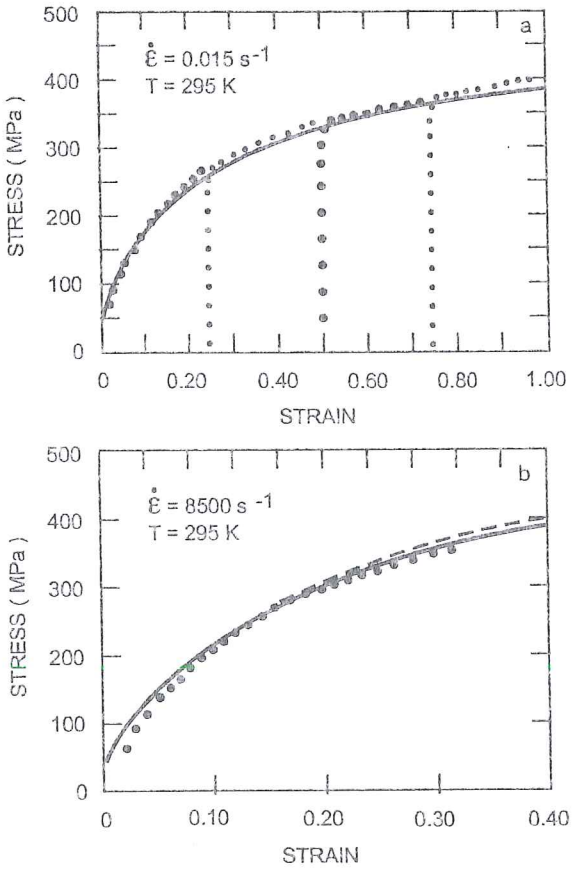

Figure 3-11 Follansbee & Kocks' model predictions for isothermal (_ _ _) or adiabatic (___) assumptions compared to experiments (...) on copper (from Follansbee & Kocks 1988).

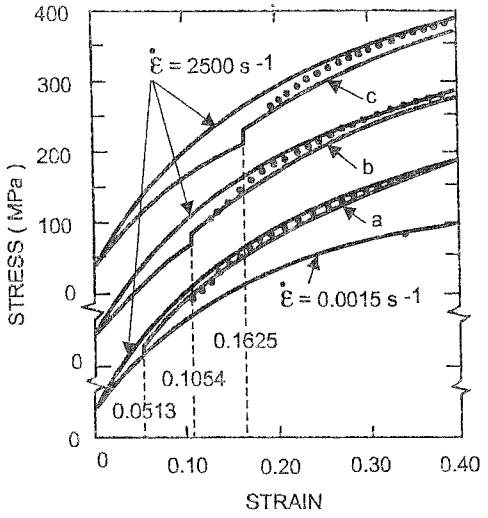

Figure 3-12 Follansbee & Kocks' model predictions compared to 3 experimental results for a strain rate change from $\dot{\varepsilon} = 0.0015\ s^{-1}$ to $\dot{\varepsilon} = 2500 s^{-1}$ at strain of $\varepsilon =$ 0.0513 ; 0.1054 and 0.1625 (from Follansbee & Kocks 1988).

3.5.3. Schmitz's model

Another example of macroscopic hardening law based on dislocation analysis combined with some phenomenological approach is proposed by Schmitz 1995. His goal is to simulate the behavior of a ferritic steel at high temperature for a model of the rolling process. He finally uses an isotropic von Mises' surface the size of which is defined by the following reference stress :

$$\frac{d\sigma_F}{d\varepsilon} = \frac{k}{\sigma_{sat}}\left(\frac{\sigma_{sat}^2}{\sigma_F} - \sigma_F\right) \tag{3-32}$$

$$Z = \dot{\varepsilon}\ exp\left(\frac{Q}{RT}\right) = B\,exp\left(\beta\sigma_{sat}\right) \tag{3-33}$$

with

σ_{sat}	saturation stress;
Z	Zener Hollomon temperature compensated strain rate;
Q	activation energy for deformation;
R	universal gas constant;
K, B, β	material constant.

3.5.4. Miller-Mc Dowell's model

Experimental observations and physical explanations

If von Mises' equivalent stress is plotted versus von Mises' equivalent strain for experimental data obtained from free-end torsion tests and compression tests, it is

typically observed (Figure 3-13) that the curve corresponding to torsion is lower.

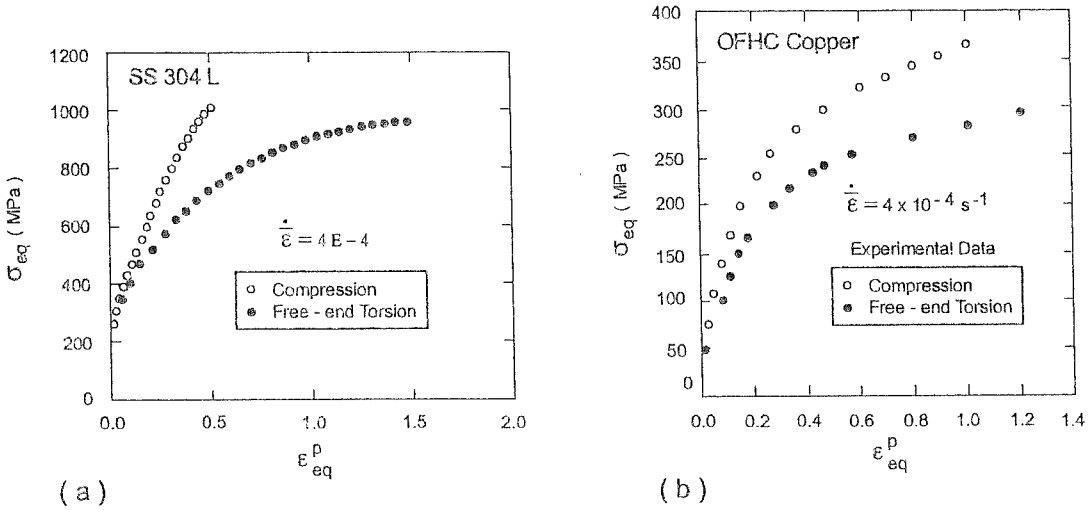

Figure 3-13 Experimental data deduced from compression and free-end torsion tests
(a) 304L stainless steel (from Miller & Mc Dowell 1996)
(b) OHFC copper (from Miller & Mc Dowell 1994).

For a f.c.c crystal structure and an initially isotropic material, on the basis of *average Taylor's factors* $\overline{M}$ for torsion and tension, the effective yield stress in torsion is expected to be 7 % lower than in tension (Miller & Mc Dowell 1996). The exact mathematical definition of this average Taylor's factor is given in Chapter 4. Physically, it represents an average of the slip rates on active slip systems for each crystal. This factor depends on the texture of the metal (i.e. the orientation of its crystals) and on the type of deformation. It has been argued that the stress level difference becomes more significant at larger strains, since the textures formed in compression and tension tend to increase the average Taylor's factor $\overline{M}$ above the isotropic value (textural hardening) while the textures formed in torsion tend to decrease the average Taylor's factor $\overline{M}$ (texture softening). However, a polycrystal model explicitly taking the texture effect into account and using a hardening rule linked only to microscopic equivalent plastic strain ($\varepsilon_{eq}^{p\,macro}$) is not able to reproduce experimental observations. So geometric (textural) hardening alone does not explain the reality. In practice, a larger average Taylor's factor $\overline{M}$ implies more crystallographic slip activity to accommodate the same macroscopic equivalent strain. This leads to an increased slip system hardening in compression as compared to torsion. In conclusion, in addition to textural hardening, slip-dependent strain-hardening must be invoked to explain the stress level difference observed on Figure 3-13.

So, a polycrystal model with a hardening rule taking into account both $\varepsilon_{eq}^{p\,macro}$ and $\overline{M}$ can reproduce the above reported difference between compression and torsion (Miller *et al.* 1995).

During torsion tests at large strains, second order effects are induced. Depending on the boundary conditions at the ends of the gage length, these effects produce either an induced axial stress (fixed-end) or an axial extension (free-end), the latter being called the Swift effect. Such phenomena cannot be explained with the assumption of an isotropic material submitted to a pure torsion state. The hypothesis of deformations induced by a material becoming anisotropic helps to understand these effects.

Figure 3-14 presents the effect of different modes of deformation as well as axial extension during free-end torsion tests.

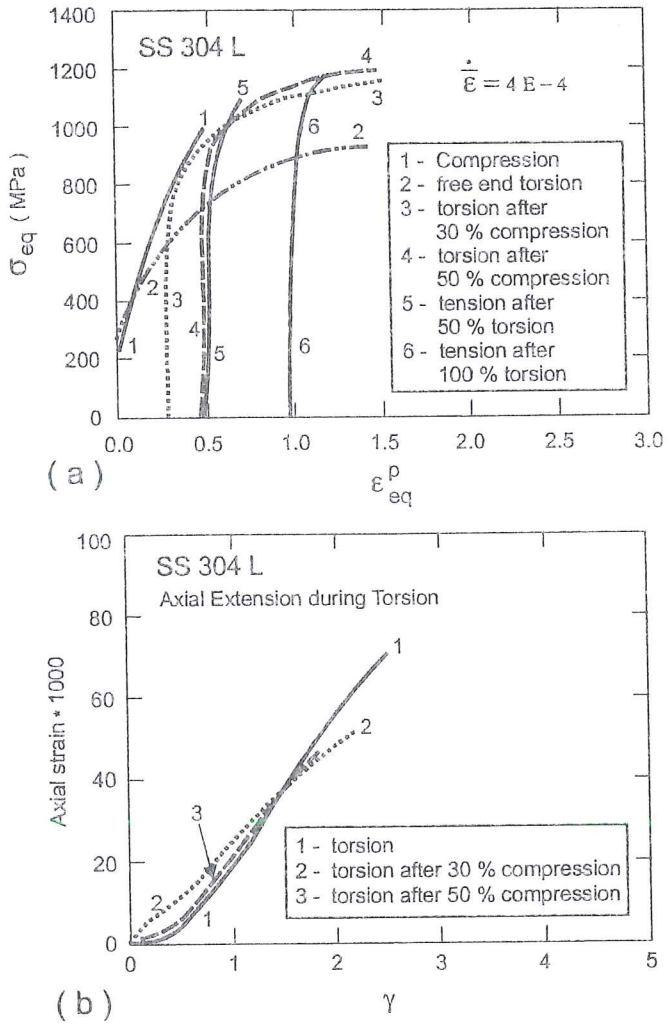

Figure 3-14 Experimental results from compression, free-end torsion and sequential tests conducted on SS 304L (a) equivalent stress-strain response, (b) axial strain response for torsional test (from Miller&Mc Dowell 1996).

First macroscopic model

A macroscopic model using a yield function F_p based only on the equivalent stress (here the von Mises' yield surface) and employing a purely isotropic hardening will predict the same $(\sigma_{eq}, \varepsilon^p_{eq})$ curves for torsion and compression.

$$F_p = \sigma_{eq} - \sigma_0 - R \tag{3-34}$$

$$\dot{R} = C\,(R_{sat} - R)\dot{\varepsilon}^p_{eq}$$

with

σ_o	initial plastic stress;	R_{sat}	saturation value of R;
R	increase of plastic stress;	C	material constant.
$\dot{\varepsilon}^p_{eq}$	plastic strain rate equivalent;		

One way to reproduce experimental observations is to introduce a kinematic hardening as well as a plastic spin $\underline{\Omega}^p$. More details on plastic spin concept can be found in Hoferlin 2001. For single crystal approach, the plastic spin is the difference that does exist between the rate of rotation of the crystal substructure and the rotational flow of the continuous medium $\underline{\Omega}$. For the case of polycrystals , Mandel 1971 suggested to use as constitutive spin the average of each single crystal lattice spin. However numerous phenomenological approaches have been proposed. Here is the choice of Miller and Mc Dowel:

$$\overset{\nabla}{\underline{\alpha}} = C(\alpha_{sat}\frac{\underline{\hat{\sigma}} - \underline{\alpha}}{|\underline{\hat{\sigma}} - \underline{\alpha}|} - \underline{\alpha})\,\dot{\varepsilon}^p_{eq} \tag{3-35}$$

$$\overset{\nabla}{\underline{\alpha}} = \dot{\underline{\alpha}} - (\underline{\Omega} - \underline{\Omega}^p).\underline{\alpha} + \underline{\alpha}.(\underline{\Omega} - \underline{\Omega}^p) \tag{3-36}$$

$$\underline{\Omega}^p = \zeta\, e^{C\,\varepsilon^p_{\ell}}(\underline{\alpha}.\underline{\dot{\varepsilon}}^p - \underline{\dot{\varepsilon}}^p.\underline{\alpha}) \tag{3-37}$$

where (3-36) is Jaumann's objective rate of the back stress, $\underline{\Omega}$ is the antisymmetric part of the total velocity gradient and $\underline{\alpha}$ is the back stress.

During uniaxial compression, $\underline{\dot{\varepsilon}}^p$ and $\underline{\alpha}$ are coaxial; hence the plastic spin is null. During torsion, plastic spin exists and the material parameter ζ is fitted from the axial extension data measured during a free-end torsion experiment.

The kinematic hardening and the plastic spin $\underline{\Omega}^p$ generally allow to reproduce the geometric hardening or texture effect. As explained above, this effect alone cannot reproduce all the physical phenomena and it is not surprising that this von Mises model coupled with kinematic and isotropic hardening fails to predict experimental results.

Improved macroscopic hardening model

The above macroscopic model is modified to include the third invariant of overstress J_3^* in the yield function and in the evolution equations of the hardening variables $\underline{\alpha}$ and R.

$$J_3^* = \frac{1}{3} tr(\underline{\hat{\sigma}} - \underline{\alpha})^3 \tag{3-38}$$

The value of J_3^* is 0 for a free-end torsion test, $\frac{2}{27}(\sigma_{11} - \alpha_{11})^3$ for a uniaxial tensile test and $-\frac{2}{27}(\sigma_{11} - \alpha_{11})^3$ for a uniaxial compression test. So, an even power of J_3^* can be used to delineate torsion from compression and tension, while an odd power of J_3^* delineates compression from tension. The exact form of the F_p proposal can be found in Miller & Mc Dowell 1996. A simplified version of this hardening model is presented. In fact, the saturation levels (see relations (3-34) and (3-35)) are functions of J_3^*:

$$R_{sat} = R_{sat}^0 g^R \tag{3-39}$$

$$\alpha_{sat} = \alpha_{sat}^0 g^\alpha \tag{3-40}$$

$$g^j = 1 + \frac{m^j}{(q^j + 1)} \frac{27}{4} \left[\frac{J_3^{*2}}{J_2^{*3}} + q^j \left(\frac{J_3^{*2}}{J_2^{*3}} \right)_{max} \right] \qquad j = R, \alpha \tag{3-41}$$

with $J_2^* = \frac{1}{2} tr(\underline{\sigma} - \underline{\alpha})^2$.

The parameter m^R is motivated by the differences in isotropic strain-hardening between torsion and compression as discussed earlier. The quantity $\left(\frac{J_3^{*2}}{J_2^{*3}} \right)_{max}$ and positive values of q^R are motivated by the high hardening level observed in Figure 3-14 during the torsion phase of the compression-followed-by-torsion test compared to the pure torsion test.

The scalar coefficient C_{in} relation (3-34) is now a function of the degree of coaxiality of the back stress and the inelastic strain rate:

$$C = \frac{C^*}{\left[A + \frac{\underline{\alpha}}{|\underline{\alpha}|} : \frac{\underline{\dot{\varepsilon}}^p}{|\underline{\dot{\varepsilon}}^p|} \right]} \tag{3-42}$$

where C^* and A are material constants. This expression is motivated by the nature of directional hardening sources (dislocation substructures, crystallographic texture,

etc). A sudden direction change in the loading path can produce a discontinuous rise of the strain hardening rate. Such an effect appears when evolving from a simple structure like that found in torsion to a more complicated diffuse structure found in uniaxial compression or tension. Remember that slips occur on planes oriented most closely to the plane of maximum shear. There are conceptually an infinite number of such planes during uniaxial compression or tension, but only two during a torsion test.

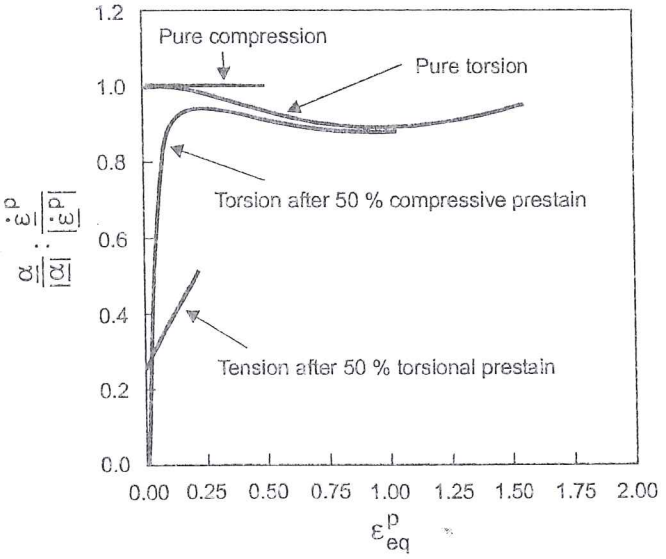

Figure 3-15 Inner product $\frac{\underline{\alpha}}{|\underline{\alpha}|} : \frac{\underline{\dot{\varepsilon}}^p}{|\underline{\dot{\varepsilon}}^p|}$ for different loading paths (from Miller&Mc Dowell 1996).

The inner product $\frac{\underline{\alpha}}{|\underline{\alpha}|} : \frac{\underline{\dot{\varepsilon}}^p}{|\underline{\dot{\varepsilon}}^p|}$ is shown on Figure 3-15 for compression (where coaxiality results in unity value), torsion, torsion after 50% compressive prestrain and tension after 50% torsional prestrain. After a compressive prestrain, the direction of $\underline{\alpha}$ quickly evolves to near that of pure torsion. The direction of $\underline{\alpha}$ during tension after torsional prestrain evolves more slowly towards coaxiality. This is consistent with the high initial strain-hardening rate observed on the torsion-followed-by-tension experimental data (Figure 3-14).

This "simplified version "of Miller's hardening model uses 9 parameters : C^*, A, α_{sat}, $R_{sat}, m^R, q^R, m^\alpha, q^\alpha, \zeta$. In fact the complete version requires 18 parameters as each hardening variable is doubled in order to have 2 hardening sets : the first one reflects the slip interaction phenomena and the second one the deformation induced anisotropy. Details can be found in Miller & Mc Dowell 1996.

These authors apply their model to predict the experimental results shown on Figure 3-14. Simulation and experiment results are very close. From this comparison, one

could believe that this model solves all the problems. However, as underlined in Miller *et al.* 1995, the first invariant J_3^* is 0 for a plane strain compression as for a torsion test while their equivalent stress-strain curves do not coincide (see Figure 3-16). In the same paper, a classical Taylor's polycrystal model has been modified to reproduce this experimental behavior. The average Taylor's factor has been added to the internal variables to modify the hardening functions and this improved model predicts the difference in stress-strain curves.

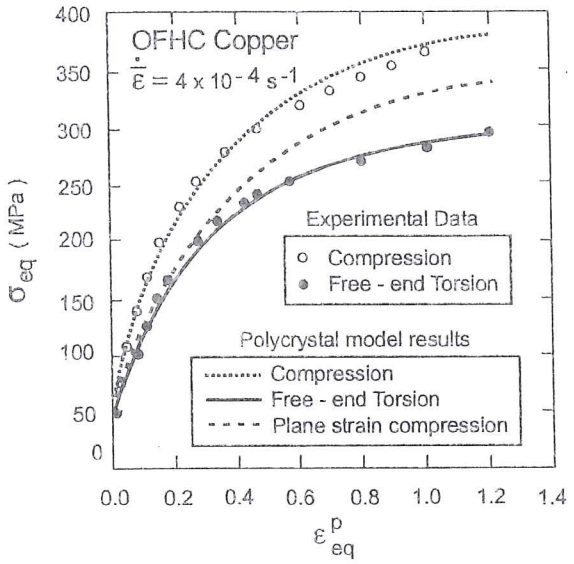

Figure 3-16 Comparison of experimental and simulated stress-strain curves for compression, torsion and plane strain compression (from Miller *et al.* 1995).

3.5.5. Teodosiu's model

Teodosiu & Hu 1998 propose a work-hardening model for cold deformation of metals, able to reproduce experimental observations such as the influence of a pre-deformation on the subsequent work-hardening behavior. For instance, this model can predict the observed work-hardening stagnation under reversed deformation at large strains and the work-softening during a subsequent orthogonal deformation. Dedicated to room temperature behavior, the model neglects viscous effects. Another assumption is that the evolution of the dislocation structure is the predominant effect at moderately large strains, with the influence of the initial texture. The effect of texture evolution is neglected.

This macroscopic model by Teodosiu is different from his microscopic one presented in Chapter 5. So, in the notations table, both Teodosiu's models appear with "micro" or "macro" identification.

Teodosiu and Hu assume that the plastic behavior of metals depends not only on the current state of deformation but also on the deformation history. This influence of the

deformation history can reasonably be represented by the current values of a sufficient number of microstructural parameters, called internal variables.

The complete set of internal state variables of this model is denoted by ($\underline{\underline{S}}$, $\underline{P}$, $\underline{\alpha}$). $\underline{\underline{S}}$ and $\underline{\alpha}$ have the dimension of stress, $\underline{P}$ has no dimension. $\underline{\underline{S}}$ is a fourth-order tensor, $\underline{P}$ and $\underline{\alpha}$ are second-order tensors. For a well-annealed material, all their initial values are zero.

The first tensor variable $\underline{\underline{S}}$ describes the directional strength of an intragranular structure. For instance, after a sufficient amount of monotonic deformation, persistent dislocation structures gradually form. In this stage of work-hardening, plastic slip is mainly carried out by one slip system and the dominant persistent dislocation structures are planar arrays, which are more or less parallel to the main slip plane and which will be called "*dislocation sheets*". The misorientation across a dislocation sheet is closely connected with its polarity. Here the term "*polarity*" means that, on each side of the sheet, there exists an excess of dislocations of the same sign, this sign being different on each side of the sheet.

In the present model, $\underline{\underline{S}}$ is the most important variable describing the evolution of the dislocation structures. The choice of its order is due to the necessity to describe the anisotropic contribution of persistent dislocation structures to the flow stress.

The second tensor variable $\underline{P}$ is associated with the polarity of the persistent dislocation structures, which is due to the excess of dislocations of the same sign on each side of a dislocation sheet. When a microstructure is not at all polarized, $\underline{P} = \underline{0}$. On the other hand, when a microstructure is completely polarized after a monotonic deformation, then $\underline{P} = \underline{N}_{\dot{\varepsilon}^p}$ where $\underline{N}_{\dot{\varepsilon}^p}$ is the direction of the plastic strain rate tensor defined by :

$$\underline{N}_{\dot{\varepsilon}^p} = \frac{\underline{\dot{\varepsilon}}^p}{\left|\underline{\dot{\varepsilon}}^p\right|} \tag{3-43}$$

therefore, it is assumed, without loss of generality, that $0 < \left|\underline{P}\right| < 1$.

The third variable $\underline{\alpha}$ describes the back stress due to microscopic heterogeneous deformation, for instance dislocation pile-ups. It corresponds to the traditional kinematic hardening in the macroscopic framework and allows to describe typical effects of large-amplitude cyclic deformations, including cyclic hardening or softening.

This model is now applied to a yield criterion described by a fourth order tensor $\underline{\underline{L}}$ representing the initial anisotropy.

Teodosiu assumes that texture is responsible of this anisotropy and neglects texture evolution. So, any phenomenological yield locus defined in Chapter 2 could be used.

$$F_p = \sigma_{eqa} - \sigma_O - m\left|\underline{\underline{S}}\right| = 0 \tag{3-44}$$

where σ_O is the initial yield stress, $m\left|\underline{\underline{S}}\right|$ represents the isotropic hardening related to the persistent dislocation structures, and $\underline{\hat{\sigma}}$ the deviatoric Cauchy stress; σ_{eqa} is the anisotropic equivalent stress defined by $\sqrt{(\underline{\hat{\sigma}} - \underline{\alpha}) : \underline{\underline{L}} : (\underline{\hat{\sigma}} - \underline{\alpha})}$.

For simplicity, a rigid plastic version of the model is presented and all the tensor derivatives are assumed to be objective rates. The plastic deformation rate is given by the associated flow rule :

$$\underline{\dot{\varepsilon}}^p = \dot{\lambda} \frac{\partial F_p}{\partial \underline{\sigma}} = \frac{\dot{\lambda}}{\sigma_{eqa}} \underline{\underline{L}} : (\underline{\hat{\sigma}} - \underline{\alpha}) \tag{3-45}$$

where $\dot{\lambda}$ is the plastic multiplier and a superposed dot denotes time differentiation. $\dot{\lambda}$ is zero within the rigid region or during rigid unloading. During a plastic loading process, $\dot{\lambda}$ is positive and determined by the consistency condition. The anisotropic equivalent strain rate $\dot{\varepsilon}^p_{eqa}$ is defined as the term conjugated with σ_{eqa} to produce the dissipation power :

$$\sigma_{eqa} \dot{\varepsilon}^p_{eqa} = (\underline{\hat{\sigma}} - \underline{\alpha}) : \underline{\dot{\varepsilon}}^p \tag{3-46}$$

Using preceeding relations, one can check that $\dot{\lambda} = \dot{\varepsilon}^p_{eqa}$. Using (3-45) and (3-46), the anisotropic equivalent strain rate can be expressed by :

$$\dot{\varepsilon}^p_{eqa} = \dot{\lambda} = \sqrt{\underline{\dot{\varepsilon}}^p : \underline{\underline{L}}^{-1} : \underline{\dot{\varepsilon}}^p} \tag{3-47}$$

Finally relations (3-47) and (3-45) yield :

$$\underline{\hat{\sigma}} - \underline{\alpha} = \sigma_{eqa} \frac{\underline{\underline{L}}^{-1} : \underline{\dot{\varepsilon}}^p}{\sqrt{\underline{\dot{\varepsilon}}^p : \underline{\underline{L}}^{-1} : \underline{\dot{\varepsilon}}^p}} = \sigma_{eqa} \frac{\underline{\underline{L}}^{-1} : \underline{N}_{\dot{\varepsilon}^p}}{\sqrt{\underline{N}_{\dot{\varepsilon}^p} : \underline{\underline{L}}^{-1} : \underline{N}_{\dot{\varepsilon}^p}}} = \sigma_{eqa} \underline{n} \tag{3-48}$$

which defines tensor $\underline{n}$.

The evolution laws of the internal variables are written in a work-hardening recovery format which takes into account the mechanisms of formation and dissolution of dislocation structures. For sufficiently large, monotonic strains, all internal variables are supposed to reach some saturation values, which correspond to the balance between work-hardening and recovery.

The evolution of the polarity tensor $\underline{P}$ is described by the evolution equation :

$$\overset{\nabla}{\underline{P}} = C_P (\underline{N}_{\dot{\varepsilon}^p} - \underline{P}) \quad \dot{\varepsilon}^p_{eqa} \tag{3-49}$$

where C_P characterizes the polarization rate of the persistent dislocation structures

and $\underline{N}_{\dot{\varepsilon}^p}$ denotes the current direction of the strain rate tensor. Whatever the initial value of $\underline{P}$, $|\underline{P}|$ will approach unity and $\underline{P}$ will tend to $\underline{N}_{\dot{\varepsilon}^p}$, whenever the strain rate direction $\underline{N}_{\dot{\varepsilon}^p}$ remains unchanged for an amount of deformation which is sufficiently large with respect to $1/C_p$.

In the case of cyclic plasticity at small strain amplitudes, Chaboche and Rousselier, 1983 have used a kinematic hardening law of the form :

$$\overset{\nabla}{\underline{\alpha}} = C_\alpha (\alpha_{sat} \underline{N}_{\dot{\varepsilon}^p} - \underline{\alpha}) \dot{\varepsilon}^p_{eqa} \tag{3-50}$$

where C_α characterizes the saturation rate of $\underline{\alpha}$, and α_{sat} is a material parameter characterizing the saturation value of $|\underline{\alpha}|$. In the present model, however, α_{sat} will be considered as a function of the persistent dislocation structures, via the internal variable $\underline{\underline{S}}$. Thus, the backstress $\underline{\alpha}$ will describe not only the rapid variations of the flow stress following a change in the strain path, but also the new stationary states that are asymptotically approached after the changes in the strain path.

C_α has a higher value than C_p and $\underline{\alpha}$ approaches its saturation value faster than $\underline{P}$ and $\underline{S}$ after a few percents of strain increment, provided the strain rate tensor remains self-coaxial.

In the anisotropic case, equation (3-50) is generalized to

$$\overset{\nabla}{\underline{\alpha}} = C_\alpha (\alpha_{sat} \underline{n} - \underline{\alpha}) \dot{\varepsilon}^p_{eqa} \tag{3-51}$$

Taking (3-48) into account, this equation can be rewritten in the form :

$$\overset{\nabla}{\underline{\alpha}} = C_\alpha \left[\frac{\alpha_{sat}}{\sigma_{eqa}} (\underline{\hat{\sigma}} - \underline{\alpha}) - \underline{\alpha} \right] \dot{\varepsilon}^p_{eqa} \tag{3-52}$$

which shows that, in the present setting, $\underline{\alpha}$ becomes asymptotically coaxial with $\underline{\hat{\sigma}}$. α_{sat} is assumed to be given by :

$$\alpha_{sat} = \alpha^o_{sat} + (1-m) \sqrt{S_D^2 + q S_L^2} \tag{3-53}$$

where α^o_{sat} is the initial value of α_{sat} and the second term corresponds to the effect of the planar persistent dislocation structure. *(1-m)* denotes the contribution of the intergranular structure to kinematic hardening. S_D and S_L are given by the decomposition :

$$\underline{\underline{S}} = S_D \underline{N}_{\dot{\varepsilon}^p} \otimes \underline{N}_{\dot{\varepsilon}^p} + \underline{\underline{S}}_L \tag{3-54}$$

$$S_L = \left| \underline{\underline{S}}_L \right| \text{ and } S_D = \underline{N}_{\dot{\varepsilon}^p} : \underline{\underline{S}} : \underline{N}_{\dot{\varepsilon}^p} \tag{3-55}$$

So S_D is the strength of the dislocation structure associated with the currently active slip systems whereas $\underline{S}_L$ is related to the persistent dislocation structure. It is called a latent part of directional strength. q is a material parameter introduced to describe the fact that S_L, the latent dislocation term, has a stronger contribution than S_D, the currently active dislocation term ($q > 1$).

The physical argument for decomposing $\underline{S}$ is explained hereafter. When a metal is deformed from a well-annealed initial state, dislocation sheets or cells develop roughly parallel to the active slip planes. On the other hand, for a severely cold-deformed material subject to a subsequent orthogonal deformation, the strain rate is highly localized. The microbands are parallel to the newly active slip planes and, between them, new dislocation sheets are gradually formed. This experimental evidence strongly suggests that dislocation structures associated with the current direction of the strain rate evolve quite differently from the rest of the persistent dislocation structures.

In order to describe the evolution of S_D, Teodosiu and Hu propose :

$$\dot{S}_D = C_S\left[g\left(S_{sat} - S_D\right) - hS_D\right]\dot{\varepsilon}^P_{eqa} \tag{3-56}$$

where C_S characterizes the saturation rate of S_D, S_{sat} denotes the saturation value of S_D. h is a function of $\underline{\alpha} : \underline{N}_{\dot{\varepsilon}^P}$ and g is a function of S_D and $\underline{P} : \underline{N}_{\dot{\varepsilon}^P}$ describing the influence of the polarity. Neglecting the influence of g and h, i.e. setting $g=1$, $h=0$, the above equation describes a gradual saturation of S_D towards S_{sat}, corresponding to the formation and saturation of planar persistent dislocation structures associated with $\underline{N}_{\dot{\varepsilon}^P}$. In order to form dislocation sheets or cell walls, the amount of deformation along which $\underline{N}_{\dot{\varepsilon}^P}$ remains unchanged, should be larger than $1/C_S$.
The function h is defined as :

$$h = \frac{1}{2}\left(1 - \frac{\underline{\alpha} : \underline{N}_{\dot{\varepsilon}^P}}{\alpha_{\text{sat}}\,\underline{n} : \underline{N}_{\dot{\varepsilon}^P}}\right) \tag{3-57}$$

Experimental evidence shows that, for a severely prestrained material under a subsequent reversed deformation, there exists a work-hardening stagnation, followed by a resumption of work-hardening. This phenomenon is described via function g. Specifically, denoting :

$$P_D = \underline{P} : \underline{N}_{\dot{\varepsilon}^P} \tag{3-58}$$

it is assumed that :

$$g = \begin{cases} 1 - \dfrac{C_P}{C_S + C_P}\left|\dfrac{S_D}{S_{sat}} - P_D\right| & \text{if} \quad P_D \geq 0 \\ (1+P_D)^{n_P}\left(1 - \dfrac{C_P S_D}{C_S + C_P S_{sat}}\right) & \text{otherwise} \end{cases} \tag{3-59}$$

Clearly, g is continuous with respect to P_D. Assume that a material is first severely

deformed at a constant strain rate with direction $\underline{N_1}$; then, according to (3-49), at the end of this deformation, the polarity tensor $\underline{P}$ will be practically equal to $\underline{N_1}$. If the material is subsequently subject to a reversed deformation, i.e. $\underline{N_2} = -\underline{N_1}$, then, by (3-58) and (3-59), P_D=-1 and g=0. Considering also (3-56), it may be shown that the latter condition corresponds to a stagnation of work-hardening.

Teodosiu and Hu finally discuss the evolution of S_L, which results from the interaction between microbands and preformed microstructures. Two physical mechanisms are possible : the annihilation of dislocations in the preformed structures and the softening of the preformed structure after being sheared by microbands. Both mechanisms reduce the strength of the preformed structures, represented by S_L. Hence the following evolution equation is proposed to describe these phenomena :

$$\dot{\underline{\underline{S}}}_L = -C_S \left(\frac{S_L}{S_{sat}} \right)^{n_L} \underline{\underline{S}}_L \dot{\varepsilon}^P_{eqa} \tag{3-60}$$

where n_L is a positive material parameter.

The factor $(S_L / S_{sat})^{n_L}$ is introduced in order to explain the influence of the amount of prestrain ε_{ps}. For a severely deformed material under a subsequent orthogonal deformation, the percentage of grains containing microbands increases with the prestrain ε_{ps}. Since the decrease of S_L is mainly due to the interaction between microbands and preformed microstructures, the decreasing rate of $|S_L|$ should increase with ε_{ps}. When ε_{ps} is very small, $S_L << S_{sat}$, hence the evolution of $\underline{\underline{S}}_L$ is negligible, whereas when ε_{ps} is large, S_L approaches S_{sat}, and the evolution of $\underline{\underline{S}}_L$ is speeded up.

The identification of the model parameters is described in Hu 1992. Only mechanical tests with 3 strain paths are needed to find the 9 parameters :

- monotonic tensile or shear tests allow to fit α_o, S_{sat}, C_S ($C_P = C_S$ at low homologous temperature), C_α;
- stress reversal tests are used to reach m, n_p;
- orthogonal sequences in strain path are needed to get q, n_L.

The validation of the model is checked by comparison of predictions and experiments. Figure 3-17 presents the behavior of a sheet under a monotonic shear until 53 % and a subsequent reversed shear, in the rolling direction. Figure 3-18 shows the shear-plastic work curve for one monotonic shear (first curve), then for 2 cases where the monotonic shear is stopped, unloaded and subsequently followed by a shear test in an orthogonal direction.

The implementation of this model in a Marciniak Kuczynski's model to predict Forming Limit Diagrams has produced results which agree with well-known effects

of strain path modification (Hiwatashi *et al.*, 1998). The coupling of this model with a yield locus described by a texture approach (Hoferlin *et al.*, 1999) has been implemented into a FEM code.

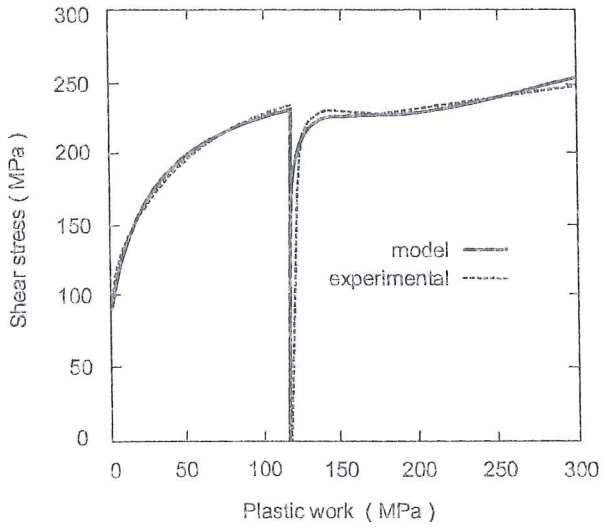

Figure 3-17 Experimental results and model correlation for AKDQ mild steel under reversed shear. The amount of preshear is 53%, from Teodosiu & Hu 1998.

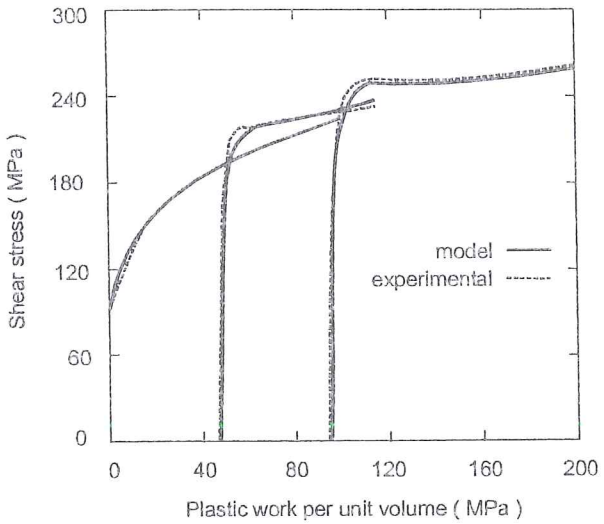

Figure 3-18 Experimental results and model correlation for AKDQ mild steel under orthogonal shear tests, from Teodosiu & Hu 1998.

3.6. Conclusion

The previous hardening models are only a few of those available in the prolific literature on this topic. The choice of one hardening model depends on different factors such as :

- significant strain rate effect or not,
- significant temperature effect or not,
- needed accuracy,
- the model use: description of monotonic loading, or cycles or complex strain paths such as initial shear followed by tension or followed by shear in an orthogonal direction or both...,
- the available tests to identify the model parameters.

The microscopic roots for models such as Teodosiu & Hu's model help to choose physical internal variables. This approach avoids a too high number of variables, as could happen if, starting from a classical isotropic, kinematic hardening model, one tried to improve it in order to describe complex strain paths.

Let us note that according to Vegter *et al.* 1999, Bergström-van Liempt-Vegter's model needs only the identification of 4 parameters, if similar materials have already been identified.

This chapter has presented both hardening types :
- the geometrical one, related to texture evolution, described with more details in chapter 4;
- the material one, related to dislocation density, dislocation cells, which can again be subdivided into direct and latent hardening as these substructures change with deformation.

The respective weight of geometrical and material hardening components depends on the material state, as studied by Winther *et al.* 1997.

Chapters 5 and 6, dealing with behavior models implemented in FEM codes, will show some choices made by scientists working in sheet metal forming simulation.

References

Bergstrom, Y. (1969/70) A dislocation model for the stress strain behaviour of polycrystalline α-Fe with special emphasis on the variation of the densities of mobile and immobile dislocations, *Mat. Sci. Eng.*, **5**, 179-192.

Bunge, H.J. (1982) Texture Analysis in Materials Science, Butterworths Publishers, London.

Chaboche, J.L., Rousselier, G. (1983) On the plastic and viscoplastic constitutive equations, Parts I and II, *ASME, J. Pressure Vessel Technol.*, **105**, 153-165.

Dafalias, Y.F., Popov, E.P. (1975) A model of nonlinearly hardening materials for complex loading, *Acta Mech.*, **21**, 173.

Estrin Y., Mecking, H., (1984) *Acta Metall.*, **32**, 57.

Ewing, J.A., Rosenhain, W. (1900) The crystalline structure of metals; *Phil. Trans. R. Soc.*, London, **193**, 353.

Follansbee, P.S., Kocks, U.F. (1988) A constitutive description of the deformation of copper based on the use of the mechanical threshold stress as an internal state

variable, *Acta Metall.*, 36/1, 81-93.
Frenckel J. (1926) Zur Theorie der Tlastizitätsgrenze und dert gestigheit kristallinischer Körper, *Z. Phys.*, 37, 572-609.
Hiwatashi, S., Van Bael, A., Van Houtte, P., Teodosiu, C. (1998) Prediction of forming limit strains under strain-path changes : application of anisotropic model based on texture and dislocation structure. *Int. J. of Plasticity*, 14/7, 647-669.
Hoferlin, E., Van Bael, A., Hiwatashi, S., Van Houtte, P. (1998) Influence of texture and microstructure on the prediction of forming limit diagram, 19th RISO *Symposium on Materials Science*, 7-11 Sept. 1998.
Hoferlin, E., Van Bael A., Van Houtte P., Teodosiu C. (1999) An accurate model of texture and strain-path induced anisotropy, Numisheet'99, 13-17 September 1999, Besançon, France, 91.
Hoferlin, E. (2001) Incorporation of an accurate model of texture and strain-path induced anisotropy in simulations of sheet metal forming, Ph.D thesis , Katholieke universiteit Leuven.
Holt, D.L. (1970) Dislocation cell formation in metals, *J. Appl. Phys.*, 41, 3197-3201.
Hu, Z. (1992) Lois de comportement des métaux en grandes transformations tenant compte de l'évolution de la microstructure, Institut National Polytechnique de Grenoble et Université de Paris-Nord, thèse de doctorat.
Huétink, J., Streppel, A.H., Vreede, P.T. (1995) Development and experimental verification of constitutive equations for anisotropic sheet metal, *Computational Plasticity – Fundamentals and applications*, Proceedings of the fourth international conference held in Barcelona, Spain, 3-6 April 1995, Owen and Onate Eds, Pineridge Press.
Khan A.S., Huang S. (1995) Continuum theory of plasticity, Wiley & Sons Eds.
Krabiell, A., Dahl, W. (1982) Zum Einfluss von Temperatur und Dehngeschwindigkeit auf die Streckgrenze von Baustahlen unterschiedlicher Festigkeit. *Arch. Eisenhüttenwesen*, 52, 429-436.
Krieg, R.D. (1975) A practical two surface plasticity theory. *Journal of applied mechanics*, 641-646.
Magnée, A. (1994) Physique du solide, notes de cours de la Faculté des Sciences Appliquées, Université de Liège.
Mandel, J. (1971) Plasticité classique et viscoplasticité (Courses and Lectures 97), CISM, Udine, Springer,New York.
Maudlin, P.J., Bingert J.F., House J.W., Chen S.R. (1999) On the modeling of the Taylor cylinder impact test for orthotropic textured materials : experiments and simulations, *Int. J. Plasticity*, 15, 139-166.
Miller, M.P., Mc Dowell, D.L. (1994) Stress State Dependent Deformation Behaviour of FCC Polycrystals, in *Numerical Predictions of Deformation Processes and the Behaviour of Real Materials*, Andersen, Bilde-Sorensen, Lorentzen, Pedersen, Sorensen Eds, Riso National Labs, Roskilde, Denmar, 421.
Miller, M.P., Dawson P.R., Bammann, D.J. (1995) Reflecting microstructural evolution in hardening models for polycrystalline metals, *Simulation of*

Materials Processing : Theory, Methods and Applications, Shend&Dawson Eds, 1995, Balkema.

Miller, M.P., Mc Dowell, D.L. (1996) Modeling large strain multiaxial effects in FCC polycrystals, *Int. J. of Plasticity*, **12/7**, 875-902.

Mroz, Z. (1967) On the description of anisotropic work-hardening. *J. Mech. Phys. Solids*, **15**, 163.

Pijlman, H.H., Huétink, J., Carleer, B.D., Vegter, H. (1998) Application of the Vegter yield criterion and a physically based hardening rule on simulation of sheet forming, *Simulation of Materials Processing : Theory, Methods and Applications*, Balkema, Huétink & Baaijens Eds.

Phillips, A., Lee, C.W. (1979) Yield surfaces and loading surfaces. Experiments and recommendations, *Int. J. Solids & Structures*, **15**, 715-729.

Prager, W. (1955) The theory of plasticity : a survey of recent achievements. *Proc. Inst. Mech. Eng.*, **169**, 41.

Rietman, A.D., Van Liempt, P., Huétink, H. (1997) The modeling of compression tests with a physically based material model using finite elements, *Computational plasticity – fundamentals and applications*, Owen, Onate & Hinton Eds.

Schmitz A. (1995) Development and experimental validation of a coupled thermal, mechanical and textural model for ferritic hot-rolling of steel, Faculty of Engineering of the Catholic University of Leuven.

Teodosiu, C., Hu, Z. (1998) Microstructure in the continuum modelling of plastic anisotropy, *Proceedings of the 19th Riso Int. Symp. on Materials Science : Modelling of Structure and Mechanics of Materials from Microscale to Products*, Carstensen, J.V., Leffers, T. Eds.

Van Bael, A. (1994) Anisotropic yield loci derived from crystallographic data and their application in finite element simulations of plastic forming processes, proefschrift voorgedragen tot het behalen van het doctoraat in de toegepaste wetenschappen, Katholieke Universiteit Leuven.

Van Houtte, P. (1985) Development of textures by slip and twinning, *Preferred orientation in deformed metals and rocks : an introduction to modern texture analysis*, H.R. Wenk Ed., Academic Press, New-York, 233-258.

Van Houtte, P. (1988) A comprehensive mathematical formulation of an extended Taylor-Bishop-Hill model featuring relaxed constraints, the Renouard-Wintenberger theory and a strain rate sensitivity model, *Textures and Microstructures*, **8-9**, 313-350.

Van Houtte, P. (1995) Micromechanics of polycrystalline materials, Chaire Francqui, Université de Liège.

Van Liempt, P. (1994) Workhardening and substructural geometry of metals, *J. Mater. Process. Technol.*, **45**, 459-464.

Vegter, H. (1991), On the plastic behaviour of steel during sheet forming, Dissertation, University of Twente.

Vegter, H., An Y., Pijlman H.H., Huétink J. (1999), Different approaches to describe the plastic material behaviour of steel and aluminium-alloys in sheet forming, *2nd ESAFORM Conference on Material Forming*, Guimaraes, Portugal, Covas J.A. Ed.

Winther, G., Jensen D.J., Hansen N. (1997) Modelling flow stress anisotropy caused by deformation induced dislocation boundaries, *Acta Mater.*, **45/6**, 2455-2465.

Ziegler, H. (1959) A modification of Prager's hardening rule. *Quart. Appl. Math.*, **17**, 55.

4. MICROSCOPIC MODELS AND MICRO-MACRO APPROACHES

4.1. Taylor's single crystal plasticity model

4.1.1. Description

At the crystal level, the plastic microscopic velocity gradient generated by a particular slip system s is given by:

$$L_{ij}^{s} = K_{ij}^{s}\dot{\gamma}^{s} \tag{4-1}$$

where Schmid's tensor K_{ij}^{s} is defined by relation (3-1) and $\dot{\gamma}^{s}$ is the slip rate acting on this slip system s. In practice, multiple slips occur together. Hence the microscopic velocity gradient applied on a crystal $\underline{L}^{micro}$ is given by :

$$\underline{L}^{micro} = \sum_{s} \underline{L}^{s} + \underline{\Omega}^{L} \tag{4-2}$$

where $\underline{\Omega}^{L}$ is the *rate of crystal lattice rotation.*
The establishment of this well-known relation is recalled in van Houtte 1995. Its link with the classical formalism of Continuum Mechanics will be summarized in Section 4.4.

Assuming for simplicity that elastic strains are small and can be neglected, as in Asaro & Needleman 1985, Becker 1990, Neale 1993 or Dawson 1997, this microscopic velocity gradient can be split into a microscopic plastic deviatoric strain rate $\underline{\dot{\varepsilon}}^{p\,micro}$ and a microscopic spin $\underline{\Omega}^{micro}$:

$$\underline{\dot{\varepsilon}}^{p\,micro} = sym(\underline{L}^{micro}) = \sum_{s} \underline{A}^{s}\dot{\gamma}^{s} \tag{4-3a}$$

$$\underline{\Omega}^{micro} = skw(\underline{L}^{micro}) = \sum_{s} \underline{Z}^{s}\dot{\gamma}^{s} + \underline{\Omega}^{L} \tag{4-3b}$$

where $\underline{A}^{s}$ and $\underline{Z}^{s}$ are respectively the symmetric and skew-symmetric parts of Schmid's tensor $\underline{K}^{s}$. The 2 components of the microscopic spin $\underline{\Omega}^{micro}$ are symbolically represented on Figure 4-1. The first term of (4-3b), $\sum_{s} \underline{Z}^{s}\dot{\gamma}^{s}$, is called plastic spin $\underline{\Omega}^{p}$.

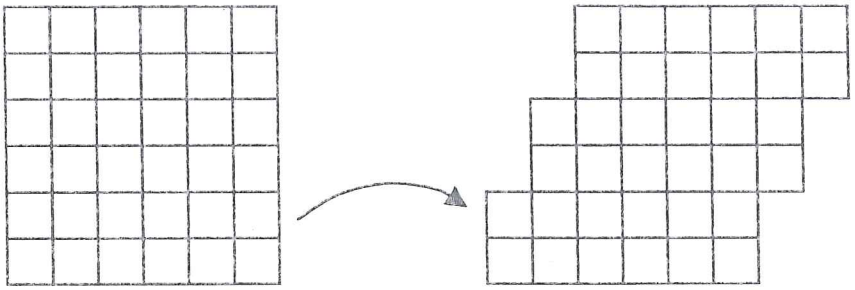

(a) $\underline{\Omega}^p = \sum_s \underline{Z}^s \dot{\gamma}^s$ = plastic spin or slip induced spin;

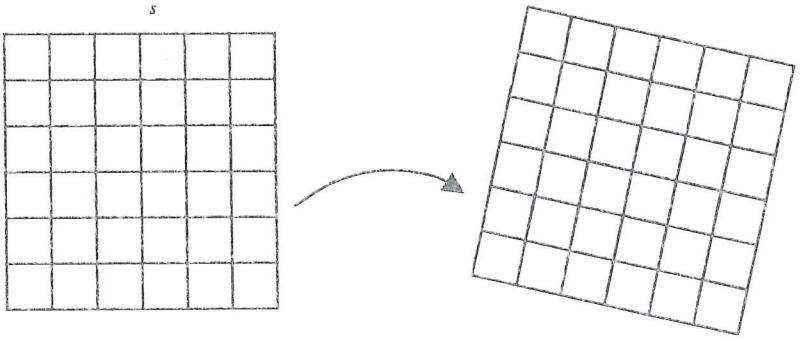

(b) Ω^L = rate of crystal lattice rotation as a rigid body, used to update texture.

Figure 4-1 Representation of the 2 terms of the crystal microscopic spin, from the slides presented at NUMISHEET 1999, (Duchêne *et al.* 1999).

Several different combinations of slip rates may achieve the prescribed strain rate. According to Taylor 1938, the one which minimizes the power dissipation is chosen:

$$\dot{W}^p = \sum_s \tau_c^s \left| \dot{\gamma}^s \right| = min \tag{4-4}$$

Taylor roughly assumes that all slip systems have a common value τ_c of their *Critical Resolved Shear Stress* τ_c^s. The CRSS concept has been introduced in section 3.1. This common value τ_c is reasonable for annealed condition. A weaker hypothesis, proposed by van Bael 1994, consists in using proportional CRSS τ_c^s inside a particular crystallite. It is expressed by constant ratios to a *common reference CRSS* τ_c:

$$\alpha^{\pm s} = \tau_c^{\pm s} / \tau_c \tag{4-5}$$

For instance, for b.c.c crystal, van Bael 1994 has :

$$\alpha^{\pm\{110\}\langle 111\rangle} = 1 \qquad \alpha^{\pm\{112\}\langle 111\rangle} = 0.95 \tag{4-6}$$

where Miller's indices describe the slip system s. The sign $\pm$ appears because the slip system can be extended to pseudo-slip systems representing twinning. In this

case, slip in anti-twinning direction must be prohibited : $\tau_c^{-s} = \infty$ (van Houtte & Wagner 1985).

The prescribed strain rate $\underline{\dot{\varepsilon}}^{p\,micro}$ can be split into a scalar magnitude $\dot{\varepsilon}_{eq}^{p}$ computed by the classical von Mises' formula and a *strain rate mode* $\underline{U}_{\dot{\varepsilon}^p}$ very close to the $\underline{N}_{\dot{\varepsilon}^p}$ direction of the plastic strain rate in Teodosiu's model (Section 3.5.5) :

$$\underline{U}_{\dot{\varepsilon}^p} = \underline{\dot{\varepsilon}}^{p\,micro} / \dot{\varepsilon}_{eq}^{p\,micro} \tag{4-7}$$

Introducing also the slip rate $\dot{\gamma}_{scaled}^{s}$ per unit equivalent strain rate :

$$\dot{\gamma}_{scaled}^{s} = \dot{\gamma}^{s} / \dot{\varepsilon}_{eq}^{p\,micro} \tag{4-8}$$

advantage can be taken of the assumed strain-rate insensitivity to simplify the formulation. Indeed, dividing relation (4-4) by the strain rate magnitude and the reference CRSS τ_c leads to :

$$\frac{\dot{W}^{p}}{\dot{\varepsilon}_{eq}^{p\,micro}\tau_c} = \sum_s \alpha_s \left|\dot{\gamma}_{scaled}^{s}\right| = minimum \tag{4-9}$$

with, according to equation (4-3a), the minimization constraint :

$$\underline{U}_{\dot{\varepsilon}^p} = \sum_s \underline{A}^{s} \dot{\gamma}_{scaled}^{s} \tag{4-10}$$

These two equations are called Taylor's equations and may be solved efficiently by means of linear programming (Simplex Method) as explained by van Houtte 1988. This approach has been implemented in the LAGAMINE code by Munhoven 1997. The solution $\dot{\gamma}_{scaled}^{s}$ depends only on the prescribed strain mode $\underline{U}_{\dot{\varepsilon}^p}$ and it does not depend on the magnitude $\dot{\varepsilon}_{eq}$ or on the value of the reference CRSS τ_c.

In the Simplex Method, relation (4-9) is called the cost function, to be minimized under the constraint (4-10). This primal problem in the space of slip rates is transformed into a dual problem where the stresses are now the independent variables. In the stress space, the value $\dot{W}^{p} / \dot{\varepsilon}_{eq}^{p\,micro}\tau_c$ (4-9) represents a maximum :

$$\frac{\dot{W}^{p}}{\dot{\varepsilon}_{eq}^{p\,micro}\tau_c} = \underline{U}_{\dot{\varepsilon}^p} : \frac{\underline{\sigma}^{micro}}{\tau_c} = maximum \tag{4-11}$$

This retrieves the approach proposed by Bishop-Hill, which assumes that the admissible stress states satisfy the yield locus constraints expressed by relation (3-3) (see section 3.1) and that the real stress state maximizes the external plastic work. Taylor's and Bishop-Hill's methods are strictly equivalent, that is why they are very often referred to as the *Taylor-Bishop-Hill (TBH) crystal model.*

The Simplex Method produces both slip rates and microscopic stresses at the crystal level. In practice, using the same CRSS τ_c for all slip systems leads to multiple solutions (set of activated slip systems). Each set achieves the prescribed strain rate (4-3a) with the same minimum power dissipation (4-9). Van Houtte 1988 proposes different methods to choose one particular solution. The approach implemented by Munhoven 1997 just stops at the first computed solution. From an energy point of view, all the solutions are equivalent. However, they produce different slip rates, microscopic stresses and hence different crystal lattice rotations. Once the set of active slip systems and the corresponding slip rates are known by the resolution of equations (4-9), (4-10), the crystal rotation $\underline{\Omega}^L$ produced by one imposed velocity gradient can be reached using relation (4-3b). It is expressed by:

$$\underline{\Omega}^L = \underline{\Omega}^{micro} - \sum_s \underline{Z}^s \dot{\gamma}^s \tag{4-12}$$

If a texture is described by a set of representative crystals orientations (Tóth & van Houtte 1992), the rotation of each representative crystal leads to the up-dated texture. Taylor's assumption about an homogeneous velocity gradient:

$$\underline{L}^{macro} = \underline{L}^{micro} \tag{4-13}$$

allows to easily update texture with the help of the previous relations. This will be extensively used in the micro-macro approaches presented hereafter.

This Taylor's model is of common use in scientific works dedicated to micro-macro approaches (van Houtte *et al.* 1989, Hirsch 1991, Winther *et al.* 1997, Aukrust *et al.* 1997)

4.1.2. Taylor's factor

$M(g, \underline{U}_{\dot{\varepsilon}^p})$ is the Taylor's factor associated with a crystal of orientation g for a given strain mode $\underline{U}_{\dot{\varepsilon}^p}$. It is conventionally derived from the plastic power dissipation per unit volume $\dot{W}^p$ by the following relation:

$$M(g, \underline{U}_{\dot{\varepsilon}^p}) = \frac{\dot{W}^p}{\dot{\varepsilon}_{eq}^{p\,micro}\tau_c} = \sum_s \alpha_s \left|\dot{\gamma}^s_{scaled}\right| = \frac{1}{\tau_c}\sigma_{ij}^{micro}(U_{\dot{\varepsilon}^p})_{ij} \tag{4-14}$$

Physically, it represents a certain amount of dislocation glide rate associated to the crystal orientation and to the applied strain rate.

4.2. Strain rate sensitivity approach for single crystal plasticity model

Another approach issued from the theory of thermally activated dislocation glide consists in adopting a viscoplastic flow rule :

$$\dot{\gamma}^s = \dot{\gamma}_0 \left| \frac{\tau^s}{\tau_c^s} \right|^{1/n} sign(\tau_s) \qquad (4\text{-}15)$$

where $\dot{\gamma}^s$ is the slip rate on the slip system s, $\dot{\gamma}_0$ is a reference slip rate defined so that $|\dot{\gamma}^s| = \dot{\gamma}_0$ when $|\tau^s| = \tau_c^s$ and the parameter n characterizes the material rate-sensitivity. Under isothermal conditions and in a narrow range of strain rates, the hereabove simple power-law equation has proven its validity. For cold deformation, the rate sensitivity is rather low and the stress dependence on the slip rate can be reasonably approximated with n close to 0. The slip system shear rate $\dot{\gamma}^s$ does not vanish as long as the resolved shear stress τ^s on the corresponding slip system s is not identically zero. It keeps however a low value if τ^s is not close to τ_c^s. This equation applies a posteriori the activation condition defined by Schmid's law by filtering out the inactive systems. It has been widely used (Asaro & Needleman 1985, Anand *et al.*1997) to overcome the problem of non uniqueness in selecting a set of active systems by the TBH approach.

For cold rolling and biaxial sheet stretching, Neale 1993 asymptotically sets $n \to 0$ in relation (4-15) to recover the rate independent response. His comparison with the TBH results reveals that:
-the plastic work and active slip systems are identical;
-the unique stress derived from (4-15) and (3-2) corresponds to the average of the active yield surface vertices involved in the Bishop-Hill solutions;
-the active shear rates and lattice spins are identical for situations where no slip system ambiguity results from the TBH analysis.

Anand & Kothari 1996 use FEM simulations of tensile and compression tests to check that both texture and stress results computed by the viscoplastic approach with $n \to 0$ or by the TBH method are very close to each other.

4.3. Evolution rule for CRSS value

Whatever the solution chosen to model single crystal behavior (TBH model or viscoplastic flow rule), the CRSS τ_c^s appears and evolves in a different way for each individual slip system s. This implies the knowledge of the initial value of τ_c^s as well as its evolution equation. Slip on any slip system generally induces hardening for all slip systems. This is taken into account by adopting an evolution equation of the CRSS of the form :

$$\dot{\tau}_c^s = \sum_u h^{su} \dot{\gamma}^u \qquad (4\text{-}16)$$

where h^{su} is the so called hardening matrix. Diagonal components of this matrix correspond to the self-hardening effect, while off-diagonal components describe

cross-hardening effects. Franciosi 1988 proposes an evolution rule for the components of this matrix. This rule depends on the pair of slip systems, their shearing rates and their temperature. This approach could seem sophisticated. However, it is still not accurate enough. The fact that hardening defined by one fixed structure of dislocations is affected by structure modification is not taken into account.

Of course, the macroscopic hardening concept, which links the flow stress to the dislocation density and the microstructure (see chapter 3), applies to the CRSS. So, as presented by Anand 1977, the CRSS can be decomposed into two additive components:

- $(\tau_c^s)_t$ representing the resistance to slip due to "thermal" obstacles. This means obstacles that thermal activation can overcome such as solute atoms, forest dislocations, Peierls' resistance;
- $(\tau_c^s)_a$ representing the resistance to slip due to "athermal" obstacles (that thermal energy is unable to overcome) such as dislocation walls and large incoherent precipitates.

Since, for pure b.c.c materials, $(\tau_c^s)_t$ is controlled by the interactions with the Peierls' lattice resistance, it is reasonable to assume that this term is constant. For f.c.c materials, the magnitude of both $(\tau_c^s)_t$ and $(\tau_c^s)_a$ is controlled by the interactions of glide dislocations with forest dislocations, consequently it is difficult to separate the observed strain hardening between $(\tau_c^s)_t$ and $(\tau_c^s)_a$. Nevertheless the variation in $(\tau_c^s)_a$ is expected to be much smaller than that in $(\tau_c^s)_t$. Thus, for b.c.c materials, it is reasonable to assume that:

$$\dot{\tau}_c^s = \left(\dot{\tau}_c^s\right)_a = \sum_u h^{su}\,\dot{\gamma}^u \tag{4-17}$$

and for f.c.c:

$$\dot{\tau}_c^s = \left(\dot{\tau}_c^s\right)_t = \sum_u h^{su}\,\dot{\gamma}^u \tag{4-18}$$

The choice for h^{su} constitutes a distinction between the micro-macro approaches implemented in FEM codes. Khan & Cheng 1996 and Teodosiu 1997 review the different proposals. Some of them will be presented in Chapter 5.

4.4. Mechanical frame for single crystal plasticity

In the frame of Continuum Mechanics, researchers as Asaro 1983, Anand & Kothari 1996 use an *isoclinic* configuration, which is an intermediate conceptual local configuration defined by Figure 4-2, to decompose the deformation gradient tensor:

$$\underline{F} = \frac{\partial \underline{x}}{\partial \underline{X}} = \frac{\partial \underline{x}}{\partial \underline{x}*} . \frac{\partial \underline{x}*}{\partial \underline{X}} = \underline{F}^* . \underline{F}^p \tag{4-19}$$

$\underline{X}$ coordinates in the initial configuration expressed in axes $\underline{X}_i$;

$\underline{x}$ coordinates in the deformed configuration expressed in axes $\underline{x}_i$;

$\underline{x}*$ coordinates in the isoclinic configuration expressed in axes $\underline{X}_i$;

$\underline{F}*$ sum of an overall "elastic" distortion of the lattice and the rigid rotation of the lattice;

$\underline{F}^p$ "plastic" simple shears that do not disturb the geometry of the lattice.

The lattice in the isoclinic relaxed configuration has the same orientation as the lattice in the reference configuration. The incremental deformation of a crystal is taken as the result of the contributions from two independent atomic mechanisms:

- the sum of an overall "elastic" distortion of the lattice and a rigid rotation of the lattice ($\underline{F}^*$);
- "plastic" simple shears that do not disturb the lattice geometry ($\underline{F}^p$).

The microscopic velocity gradient is linked to the deformation gradient tensor:

$$\underline{L}^{micro} = \frac{\partial \dot{\underline{x}}}{\partial \underline{x}} = \frac{\partial \dot{\underline{x}}}{\partial \underline{X}} . \frac{\partial \underline{X}}{\partial \underline{x}} = \dot{\underline{F}} . \underline{F}^{-1} \tag{4-20}$$

$$\underline{L}^{micro} = \dot{\underline{F}}* . \underline{F}*^{-1} + \underline{F}* . \dot{\underline{F}}^p . \underline{F}^{p-1} . \underline{F}*^{-1} \tag{4-21}$$

The plastic shear rate is expressed through a certain number of slip systems s (the active ones in the TBH model and all slip systems in the rate sensitive approach):

$$\underline{L}^{micro} = \dot{\underline{F}}* . \underline{F}*^{-1} + \sum_s \dot{\gamma}^s \underline{K}*^s \tag{4-22}$$

Schmid's tensor $\underline{K}*^s$ is expressed in deformed configuration, but as the crystal lattice is not affected by $\underline{F}^p$, one has:

$$\underline{K}*^s = \underline{F}* . \underline{K}^s . \underline{F}*^{-1} \tag{4-23}$$

So in the micro-mechanical frame, one gets (4-22) which can be compared to relation (4-2) of Taylor's model presented in section 4.1 :

$$\underline{L}^{micro} = \underline{\Omega}^L + \sum_s \underline{L}^s \tag{4-2}$$

Since in (4-2), the elastic part of $\underline{F}*$ has been neglected, the strain rates deduced from (4-22) and (4-2) are different:

$$(4\text{-}22) \rightarrow \underline{\dot{\varepsilon}} = sym(\underline{L}^{micro}) = \underline{\dot{\varepsilon}}^{elastic} + \underline{\dot{\varepsilon}}^{p\,micro} = \underline{\dot{\varepsilon}}^{elastic} + \sum_s \underline{A}*^s \dot{\gamma}^s \tag{4-24}$$

$$(4\text{-}2) \rightarrow \underline{\dot{\varepsilon}} = sym(\underline{L}^{micro}) = \underline{\dot{\varepsilon}}^{p\,micro} = \sum_s \underline{A}^{*s}\,\dot{\gamma}^s \tag{4-25}$$

The skew-symmetric parts of both velocity gradients are identical and are called the spin:

$$\underline{\Omega}^{micro} = \underline{\Omega}^{L} + \underline{\Omega}^{p} = \underline{\Omega}^{L} + \sum_s \underline{Z}^{*s}\,\dot{\gamma}^s \tag{4-26}$$

where $\underline{\Omega}^{L}$ is the crystal lattice rotation due to both the global rigid body rotation of the macroscopic body and the particular crystal rotation due to texture updating.

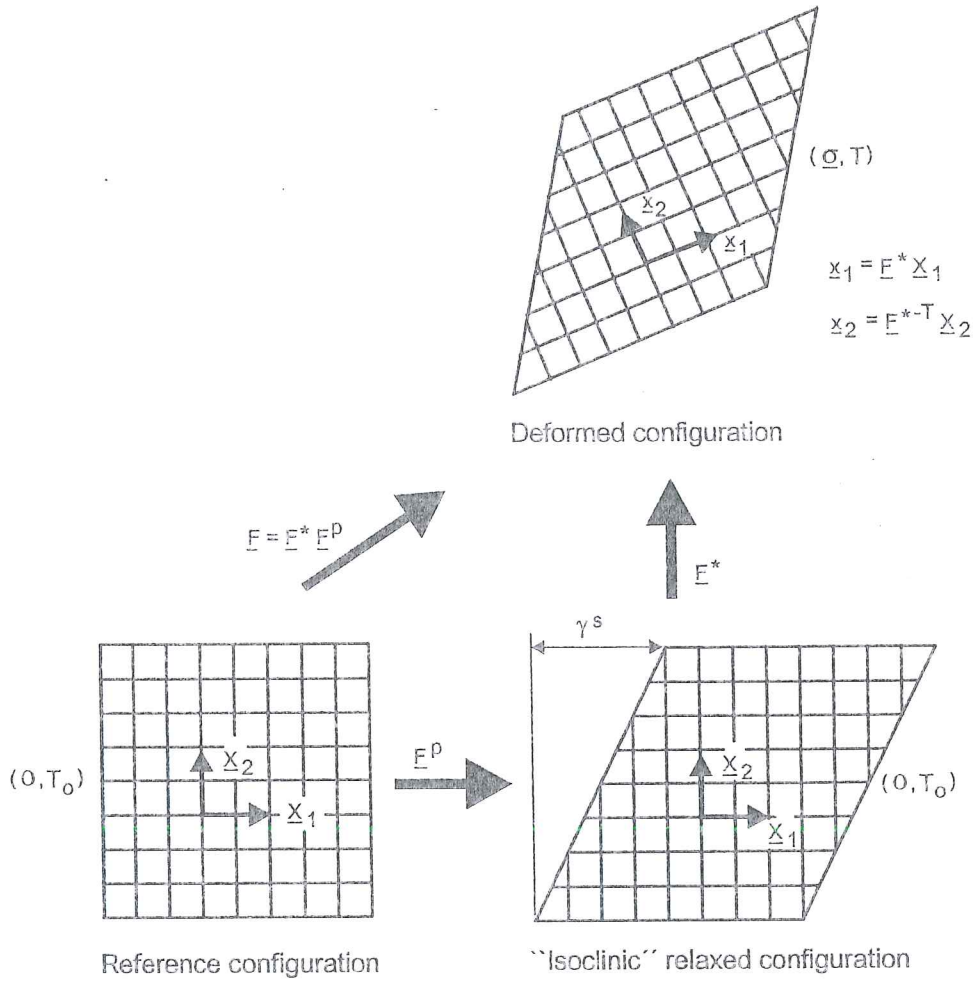

Figure 4-2 Schematic diagram showing the multiplicative decomposition of the deformation gradient tensor $F = F^* F^p$
(adapted from Aasro 1983, Anand & Kothari 1996).

4.5. Polycrystal plasticity models

4.5.1. Description

Starting from the state of individual crystallites, different assumptions have been proposed to deduce the state of the corresponding polycrystal characterized by the macroscopic strain rate tensor $\underline{\dot{\varepsilon}}^{macro}$ and the stress tensor $\underline{\sigma}^{macro}$. The most logical approach is a volume average weighted by the ODF function $f(g)$ defined by relation (3-4):

$$\underline{\dot{\varepsilon}}^{macro} = \oint \underline{\dot{\varepsilon}}^{micro}(g) f(g) dg \tag{4-27}$$

$$\underline{\sigma}^{macro} = \oint \underline{\sigma}^{micro}(g) f(g) dg \tag{4-28}$$

Although the assumption of homogeneous microscopic stress tensor $\underline{\sigma}^{micro}$ and strain rate tensor $\underline{\dot{\varepsilon}}^{micro}$ in one single crystal is already a simplification, most macroscopic models are bound by stronger assumptions :

Sachs (1928) applies the loading state (uniaxial tension for instance) at each individual crystallite as if it were a free-standing single crystal, assumed to have only one slip system (van Houtte 1995) This leads to more or less severe violations of geometric compatibility at the grain boundaries and, in general, quite unsatisfactory results (Gil-Sevillano *et al.* 1980). In particular, the predictions of texture evolutions due to deformation do generally not compare favorably with the experimental results.

- ***Full Constraint Taylor*** (1938) (FC) assumes an homogeneous plastic strain rate distribution:

$$\underline{\dot{\varepsilon}}^{p\,macro} = \underline{\dot{\varepsilon}}^{p\,micro} \tag{4-27}$$

This assumption leads to equilibrium violations at grain boundaries. However this model often computes, for many practical applications, more acceptable results than the previous one. The assumption (4-29) provides an upper bound solution.

- The Full Constraint Taylor's model enforces rigorous geometric compatibility at the expense of stress equilibrium. The so-called ***Relaxed Constraint Taylor's (RC)*** model drops this strict assumption by relaxing the compatibility of well chosen components of the velocity gradient tensor. In the ***lath model*** for rolling $L_{(RD)(ND)}$ is not prescribed and the ***pancake model*** does not enforce the component $L_{(TD)(ND)}$ either, where RD, TD and ND are the rolling, transverse

and normal directions. As shown by van Houtte 1988, these kinds of relaxations can be implemented in an elegant way using pseudo-slip system.

As compared to FC models, RC models sometimes produce better and more detailed results, especially for rolling texture predictions, although their justification is still under debate. The problem of accommodating the strain misfits inherent to RC models leads scientists like Wagner, Lücke, Arminjon, Imbault, van Houtte to propose several more advanced models which try to take these misfits into account. The summary presented in van Houtte 1996 confirms that such models lie between TBH and self-consistent approaches and yield improved results compared to classical FC or RC models.

In general, Taylor type models are quite successful for f.c.c and b.c.c metals where a large number of slip systems ensures that individual crystals can accommodate an arbitrary deformation. However, these types of models are not valid for materials whose crystals have an insufficient number of deformation modes to sustain an arbitrary strain. Such kinematically rank deficient materials are not rare: semi-crystalline polymers, minerals and other geological materials, superconducting ceramics, metals of hexagonal close-packed crystal structure such as zinc, zirconium and titanium. Two proposals adapted to such cases are described in Prantil, Dawson and Chastel 1995. The first one due to Parks & Ashi 1990 is shortly summarized hereafter and the other one due to Chastel is a modified Sachs approach.

- ***Taylor hybrid approach*** (Parks & Ashi 1990) has been specifically proposed to handle kinematically rank deficient crystals. The crystal strain rate is the macroscopic one from which the components that available slip systems cannot accommodate have been removed. The crystal strain rate computation takes into account an average part from which one can find that the average crystal deformation rate is equal to the macroscopic one. The crystal stress is determined from the active slip systems and by a projection of the macroscopic stress.

- ***Self-consistent models*** (Berveiller & Zaoui 1979, Canova & Lebensohn 1995 Molinari 1997, Masson & Zaoui 1999) consider a grain as a solid inhomogeneity embedded in a homogeneous infinite matrix subjected to macroscopic loading. All the grains are treated that way one after the other, the matrix behavior results from the weighted average of the individual contributions of all the grains. Both strain rate and stress heterogeneities are allowed, but they are linked by an interaction formula based on Eshelby's 1957 work. For elastic cases, Kröner 1961 uses the interaction formula at the grain level:

$$(\underline{\sigma}^{micro} - \underline{\sigma}^{macro}) = -\underline{\underline{L}}^{*} : (\underline{\varepsilon}^{micro} - \underline{\varepsilon}^{macro}) \qquad (4\text{-}28)$$

where $\underline{\underline{L}}^{*}$ is a 4^{th} rank tensor called the "interaction tensor". The interested reader can find the method to identify $\underline{\underline{L}}^{*}$ in Van Houtte 1995.

This approach has been extended to elastoplastic states. However, an incremental linearization proposed by Hill 1965 seems to be better adapted:

$$\dot{\underline{\sigma}}^{micro} - \dot{\underline{\sigma}}^{macro} = -\underline{\underline{L}}^{H} : (\dot{\underline{\varepsilon}}^{micro} - \dot{\underline{\varepsilon}}^{macro}) \qquad (4\text{-}29)$$

where $\underline{\underline{L}}^{H}$ is called the Hill's constraint tensor. It depends on the elastoplastic modulus, on the shape and orientation of the crystals.

Masson & Zaoui 1999 summarizes the scientific controversies on this topic and demonstrates that Hill's conception could be adopted even for elastoviscoplasticity.

Whatever self-consistent approach is used, a rather long iterative solution procedure is required. This is mainly due to the fact that, at the end of the iterative process, the macroscopic values must coincide with the average of the grain response. However, unlike the Taylor's models, the self-consistent models allow to take into account both effects of texture and grain morphology on the mechanical response of the material.

- ***Homogenization technique,*** used by Smit *et al.* 1998, Miehe *et al.* 1999 or Geers *et al.* 2000, is directly based on a mathematical procedure already applied to find micro-macro links in composite materials. Two levels of finite element models are used: a mesh of the entire structure and a mesh of the Representative Volume Element (RVE). At each interpolation point of the macroscopic mesh, the finite element model of the RVE is called to provide the stress-strain behavior of the material.

The interested reader can find general information on these topics in the course written by van Houtte 1995, except for the Taylor hybrid approach and the homogenization technique. Chapter 5 presents finite element applications of the above micro-macro hypotheses.

4.5.2. Average Taylor's factor

The TBH theory described in section 4.1 for one crystal can directly be applied to polycrystals with Taylor's assumption (4-29). So, plastic strain rate tensors $\dot{\underline{\varepsilon}}^{p}$ are supposed to be homogeneous throughout the polycrystal. In addition, Taylor assumes that the common reference CRSS τ_c (common reference value for all the slip systems in one crystal) is the same for all crystallites in the polycrystal in one representative volume element. It is called the *average common reference CRSS* $\bar{\tau}_c$:

$$\tau_c = \bar{\tau}_c \qquad (4\text{-}30)$$

This assumption seems acceptable for materials in their annealed state, though it becomes questionable after accumulation of a certain deformation (Bunge *et al.*

1985). With relations (4-29) and (4-32), the average plastic power dissipation in a polycrystal is easily computed from its expression for a single crystal (4-14) and the ODF (3-4):

$$\overline{\dot{W}^p}(\underline{\dot{\varepsilon}}^{p\,macro}) = \oint \dot{W}^p(\underline{\dot{\varepsilon}}^{p\,micro}, g) f(g) dg = \dot{\varepsilon}_{eq}^{p\,macro} \overline{\tau}_c \overline{M}(\underline{U}_{\dot{\varepsilon}^p}) = \sigma_{eq}^{macro} \dot{\varepsilon}_{eq}^{p\,macro} \qquad (4\text{-}31)$$

with the average Taylor's factor :

$$\overline{M}(\underline{U}_{\dot{\varepsilon}^p}) = \oint M(\underline{U}_{\dot{\varepsilon}^p}, g) f(g) dg \qquad (4\text{-}32)$$

Hereafter any over-lined $\overline{\text{variable}}$ indicates a value which is assumed to be an average for all crystallites belonging to the same elementary volume considered in the macroscopic approach.

The average Taylor's factor only depends on the texture of the polycrystalline material $f(g)$ and on the given strain rate mode $\underline{U}_{\dot{\varepsilon}^p}$ but not on the strain rate magnitude $\dot{\varepsilon}_{eq}^{p\,macro}$.

Relation (4-33) yields the important **micro-macro link**:

$$\sigma_{eq}^{macro} = \overline{\tau}_c \, \overline{M}(\underline{U}_{\dot{\varepsilon}^p}) \qquad (4\text{-}33)$$

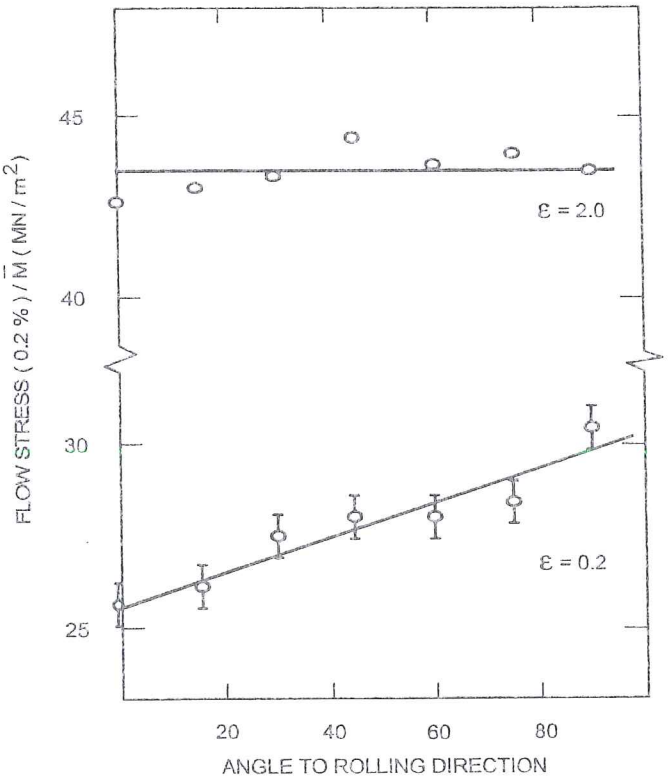

Figure 4-3 Ratio between the tensile yield stress and the corresponding Taylor's factor according to the angle α with the rolling direction (after Jensen & Hansen 1987).

This relation retrieves the physical considerations of Chapter 3 on hardening. Both geometric (textural) hardening related to $\overline{M}$ and material (strain) hardening related to $\overline{\tau}_c$ coexist and appear in a micro-macro approach. Experimental works also demonstrate that the anisotropic behavior cannot be attributed to only one of these factors. For instance, Jensen & Hansen 1987 measured the 0.2% tensile yield stress on specimens cut at different angles α to the Rolling Direction. Their material was a sheet of commercially pure aluminum, which was previously cold-rolled at an equivalent true strain of up to 200%. Textures of the rolled sheet were determined and the average Taylor's factors $\overline{M}$ were computed for different levels of deformation. Figure 4-3 shows the evolution of the ratio $\sigma_{eq}^{macro} / \overline{M}$ corresponding to $\overline{\tau}_c$ according to (4-35), versus the angle α to the rolling direction. At very large strains, $\overline{\tau}_c$ is almost constant, indicating that the observed plastic anisotropy can mainly be attributed to the crystallographic texture. On the contrary, after moderately large monotonic strains, $\overline{\tau}_c$ increases with α, showing a strong influence of the intragranular microstructure on the plastic anisotropy. According to Teodosiu's 1997 review, this conclusion seems true for polycrystalline f.c.c:

- for moderately cold-rolled sheet, plastic anisotropy seems due to the orientation of the dislocation structures (sheets of high dislocation densities more or less parallel to the {111} slip planes);
- for heavily cold-rolled sheets, plastic anisotropy mainly seems due to the crystallographic texture, because dislocations are arranged in thick-walled, equiaxed cells, providing an almost isotropic hardening.

Let us note that the further work of Winther, Jensen and Hansen 1997 studies the combined effect of texture and microstructure on the flow stress anisotropy of metals containing dislocation boundaries with a macroscopic orientation with respect to the sample axes. Assuming that dense dislocation walls and micro-bands resist like ordinary grain boundaries, a value of the CRSS depending on a Petch-Hall equation is adopted. In their approach, Taylor's or Sachs' polycrystal assumption is used on a set of 1152 crystals, representative of the texture. It has been proved that the presence of dislocation boundaries has a significant effect on anisotropic yield.

4.6. Link between the evolution of the reference CRSS and macroscopic strain hardening

Taylor 1938 proposes that the common reference CRSS τ_c evolves as a function of the total slip Γ in each crystal:

$$\Gamma(g) = \int_0^t \dot{\Gamma}(g)dt \tag{4-34}$$

where g defines the crystal orientation. In a similar way, van Bael 1996, assuming constant CRSS-ratios α_s, defines the total slip rate $\dot{\Gamma}$ as :

$$\dot{\Gamma}(g, \underline{\dot{\varepsilon}}^{p\,micro}) = \sum_s \alpha_s |\dot{\gamma}_s| = \dot{\varepsilon}_{eq}^{p\,micro} M(g, \underline{U}_{\dot{\varepsilon}^p}) \tag{4-35}$$

where g defines a crystal orientation, $\underline{\dot{\varepsilon}}^p$ is a strain rate tensor represented by its mode $\underline{U}_{\dot{\varepsilon}^p}$ and magnitude $\dot{\varepsilon}_{eq}^{p\,micro}$.

Using Taylor's assumptions:

- $\underline{\dot{\bar{\varepsilon}}} = \underline{\dot{\varepsilon}}^{p\,micro} = \underline{\dot{\varepsilon}}^{p\,macro}$
- $\bar{\tau}_c = \tau_c$

the *total polycrystal slip rate* $\dot{\bar{\Gamma}}$ is defined by:

$$\dot{\bar{\Gamma}}(\underline{\dot{\bar{\varepsilon}}}^p) = \oint \dot{\Gamma}(g, \underline{\dot{\bar{\varepsilon}}}^p) f(g) dg = \dot{\bar{\varepsilon}}_{eq} \bar{M}(\underline{U}_{\dot{\varepsilon}^p}) \tag{4-36}$$

The *total polycrystal slip* $\bar{\Gamma}$ *is* then computed by integration of the slip rate and an important **micro-macro link** appears:

$$d\bar{\Gamma} = d\bar{\varepsilon}_{eq}^p \bar{M} \tag{4-37}$$

If one works with a uniaxial test where $\varepsilon_{eq}^{p\,macro} = \varepsilon$ and $\sigma_{eq}^{macro} = \sigma$, the macroscopic work hardening can easily be deduced from relations (4-35) and (4-39):

$$\frac{d\sigma}{d\varepsilon} = \bar{M}^2 \frac{d\tau_c}{d\bar{\Gamma}} + \tau_c \frac{d\bar{M}}{d\varepsilon} \tag{4-38}$$

The first term (material hardening) on the right side of equation (4-40) indicates an isotropic hardening at the polycrystal level, since an average is done whatever slip system is activated and for all crystals. The second term (geometrical hardening) is due to the evolution of texture resulting from plastic deformation. It is often neglected in macroscopic models or even in simple micro-macro models (Schmitz 1995, Winters 1996). Relation (4-40) is well known and comments can be found in Aernoudt *et al.* 1987.

4.7. Summary

This chapter has introduced the single crystal plasticity as well as the assumptions to develop a macroscopic plastic model from microscopic models. The physical mechanisms and their models were implemented in finite element codes for validation purpose. They also allow accurate simulations of deep drawing or rolling. Chapters 5 and 6 summarize some applications of this type.

References

Aernoudt, E., Gil-Sevillano J. & Van Houtte, P. (1987) Constitutive Relations and Their Physical Basis, S.I. Andersen et al. Eds, RisØ National Laboratory, Roskilde, Denmark, 1-38.

Anand, L., Kothari, M. (1996) A Computational Procedure for Rate-Independent crystal plasticity, *J. Mech. Phys. Solids,* **44/4**, 525-558.

Anand, L., Balasubramanian S., Kothari, M. (1997) Constitutive Modeling of Polycrystalline Metals at Large Strains : Application to Deformation Processing, *Large plastic deformation of crystalline aggregates*, International Centre for Mechanical Sciences, Courses and Lectures n° 376, Springer Ed, 109-172.

Asaro, R.J. (1983) Micromechanics of crystals and polycrystals, *Advances in Applied Mechanics*, **23**, 1-115.

Asaro, R.J., Needleman, A. (1985) Texture development and strain hardening in rate dependent polycrystals, *Acta Metallurgica*, **33**, 923-953.

Aukrust, I., Tjotta, S., Vatne, H.E., Van Houtte, P. (1997) Coupled FEM and texture modelling of plane strain extrusion of an Aluminium alloy, *Int. J. of Plasticity*, **13, 1/2**.

Becker (1990) An analysis of shear localization during bending of a polycrystalline sheet, *Microstructural Evolution in Metal Processing*, **46**.

Berveiller, M., Zaoui, A. (1979) An extension of the self-consistent scheme to plastically-flowing polycrystals, *J. Mech. Phys. Solids*, **26**, 325-344.

Bunge, H.J. (1982) Texture Analysis in Materials Science, Butterworths Publishers, London.

Canova, G.R., Lebensohn, R. (1995) Micro-macro modelling, *Computer Simulation in Materials Science, NATO ASI,* Ile d'Oleron, France, June 6-16.

Dawson, P.R. & Kumar, A. (1997) Deformation Process Simulations Using Polycrystal Plasticity, *Large plastic deformation of crystalline aggregates*, International Centre for Mechanical Sciences, Courses and Lectures n° 376, Springer Ed, 247.

Duchêne L., Godinas A., Habraken, A.M.(1999) Metal Plastic Behaviour linked to Texture Analysis and FEM Method, *NUMISHEET '99, 4th Int. Conf. and Workshop on Numerical Simulation of 3D Sheet Forming Processes*, Besançon, France, 13-17 September 1999, Edité par J.C. Gélin, P. Picart, Université de Franche-Comté et ENSMM, 97-102.

Eshelby, J.D. (1957) The determination of the elastic field of an ellipsoïdal inclusion and related problems. *Proc. Roy. Soc. London,* **A241**, 376-396.

Franciosi, P. (1988) On flow and a work hardening expression correlation in metallic single crystal plasticity, Revue Phys. Appl., **23**, 383-394.

Geers, M.G.D., Kouznetsova, V., Brekelmans, W.A.M. (2000) Constitutive approaches for the multi-level analysis of the mechanics of microstructures, 5th National Congress on Theoretical and Applied Mechanics, Louvain-La-Neuve, May 23-24, 2000.

Hill, R. (1965) Continuum micro-mechanics of elastoplastic polycrystals, *J. Mech. Phys. Solids*, **13**, 89-101.

Hirsch, J.R. (1990) Correlation of deformation texture and microstructure, *Materials Science and Technology*, **6**, 1048.

Jensen J., Hansen D.&N. (1987) Relations Between Texture and Flow Stress in Commercially Pure Aluminium, *Constitutive Relations and their Physical Basis, 8th Riso Int. Symp. on Metallurgy and Mat. Sci.*, Andersen S.I. et al. Eds, Riso Nat. Lab., Roskilde, 353-360.

Kalidindi, S.R., Bronkhorst, C.A., Anand, L. (1992) Crystallographic texture evolution during bulk deformation processing of FCC metals, *J. Mech. Phys. Solids*, **40**, 537-579.

Kalidindi, S.R., Anand, L. (1994) Macroscopic shape change and evolution of crystallographic texture in pre-textured FCC metals, *J. Mech. Phys. Solids*, **42/3**, 459-490.

Kallend, J.S., Kocks, U.F., Rollett, A.D., Wenk, H.R. (1991) popLA – an integrated software system for texture analysis. *Text. microstruct.*, **14-18**, 1203-1208.

Khan, A.S., Cheng, P. (1996) An anisotropic elastic-plastic constitutive model for single and polycrystalline metals. I – theoretical developments, *Int. J. Plasticity*, **12/2**, 147-162.

Kröner, E. (1961) Zur plastischen Verformung des Vielkristalls, *Acta Metall.*, **9**, 155-161.

Laszlo Tóth, L.S., Van Houtte, P. (1992) Discretization techniques for orientation distribution functions, *Textures and Microstructures*, 1992, 229-244.

Masson, R., Zaoui, A. (1999) Self-consistent estimates for the rate-dependent elastoplastic behaviour of polycrystalline materials, *J. of Mechanics and Physics of Solids*, **47**, 1543-1568.

Miehe C., Schröder J., Schotte J. (1999) Computational homogenization analysis in finite plasticity, simulation of texture development in polycrystalline materials, *Computer methods in applied mechanics and engineering*, **171**, 387-418.

Molinari, A. (1997) Deformation Process Simulations Using Polycrystal Plasticity, *Large plastic deformation of crystalline aggregates*, International Centre for Mechanical Sciences, Courses and Lectures n° 376, Springer Ed, 173-246.

Munhoven, S. (1997) Taylor ULg A, rapport intermédiaire n° 4, Convention Micro-Macro 2748.

Neale, K.W. (1993) Use of Crystal Plasticity in Metal Forming Simulations, *Int. J. Mech. Sci.*, **35/12**, 1053-1063.

Parks, D.M. & Ahzi S. (1990) Polycrystalline plastic deformation and texture evolution for cyrstals lacking five independent slip systems, *J. Mech. Phys. Solids*, **38/5**, 701-724.

Prantil, V.C., Dawson, P.R., Chastel, Y.B. (1995) Comparison of equilibrium-based plasticity models and a Taylor-like hybrid formulation for deformations of constrained crystal systems, *Modelling Simul. Mater. Sci. Eng.*, **3**, 215-234.

Sachs, G. (1928) Zur Ableitung einer Fliessbedingung, *Z. Verein Deutscher Ing*, **72**, 734-736.

Sarma, G.B., Dawson, P.R. (1996) Texture Predictions Using a Polycrystal Plasticity Model Incorporating Neighbor Interactions, *Int. J. of Plasticity*, **12/8**, 1023-1054.

Schmitz A. (1995) Development and experimental validation of a coupled thermal, mechanical and textural model for ferritic hot-rolling of steel, Faculty of Engineering of the Catholic University of Leuven.

Sevillano, G., Van Houtte, P., Aernoudt, E. (1980), Large strain work hardening and textures, *Progress in Materials Science*, **25**, 111.

Smit, R.J.M., Brekelmans, W.A.M., Meijer, H.E.H. (1998) Prediction of the mechanical behavior of nonlinear heterogeneous systems by multi-level finite element modeling, *Comp. Meth. Appl. Mech. Eng.*, **155**, 181-192.

Taylor, G.I. (1938) Plastic strains in metals, *J. Inst. Metals*, **62**, 307-324.

Teodosiu, C. (1997) Dislocation modelling of crystal plasticity, *Large plastic deformation of crystalline aggregates*, International Centre for Mechanical Sciences, Courses and Lectures n° 376, Springer Ed, 21-80

Tóth, L.S., Van Houtte, P. (1992) Discretization techniques for orientation distribution functions, *Textures and Microstructures*, 1992, **19**, 229-244.

Van Bael, A. (1994) Anisotropic yield loci derived from crystallographic data and their application in finite element simulations of plastic forming processes, proefschrift voorgedragen tot het behalen van het doctoraat in de toegepaste wetenschappen, Katholieke Universiteit Leuven.

Van Houtte, P. (1988) A comprehensive mathematical formulation of an extended Taylor-Bishop-Hill model featuring relaxed constraints, the Renouard-Wintenberger theory and a strain rate sensitivity model, *Textures and Microstructures*, **8-9**, 313-350.

Van Houtte, P., Mols, K., Van Bael, A., Aernoudt, E. (1989) Application of yield loci calculated from texture data, *Textures and microstructures*, **11**, 23-39.

Van Houtte, P. (1995) Micromechanics of polycrystalline materials, Chaire Francqui, Université de Liège.

Van Houtte, P. (1996) Microscopic strain heterogeneity and deformation texture prediction, *Textures of Materials*, Proceedings of the 11th Int. Conf. on Textures of Materials, vol. 1, ICOTOM-11, Liang Z., Zuo L., Chu Y. Eds.

Winters, J. (1996) Implementation of a texture-based yield locus into an elastoplastic finite element code. Application to sheet forming. Katholieke Universiteit Leuven, proefschrift voorgedragen tot het behalen van het doctoraat in de toegepaste wetenschappen, Katholieke Universiteit Leuven.

Winther, G., Jensen D.J., Hansen N. (1997) Modelling flow stress anisotropy caused by deformation induced dislocation boundaries, *Acta Mater.*, **45/6**, 2455-2465.